Using live cell imaging to study interactions between *Listeria monocytogenes* and host cells during infection

A thesis submitted to The University of Manchester for the degree of Doctor of Philosophy in the Faculty of Biology, Medicine and Health

2022

Liam T. Feltham

School of Biological Sciences

Division of Immunology, Immunity to Infection and Respiratory Medicine

Table of Contents

Final word count: 31,720

Table of Figures

Table of Tables

Abbreviations

(p)pGpp	guanosine tri- tetra- penta- phosphate
AA	Amino Acid
ABC	adenosine triphosphate binding casette
actA/ActA	actin assembly inducing protein
AP2	adaptor protein 2
Arp2/3	actin-related protein 2/3
Bcr	benzalkonium chloride resistance
BetL	glycine betanine transpoter
bp	base pair
BSA	bovine serum albumin
Bsh	bile salt hydrolase
Buk	butyrate kinase
CD4/8	cluster of differentiation 4/8
CFU	colony forming units
Cm	chloramphenicol
CSF-1	colony stimulating factor 1
Csp	cold shock protein
DAPI	4’,6-diamidino-2-phenylindole
DC	dendritic cell
DhaM	dihydroxyacetone kinase
DltA/B/C/D	D-alanine-D-alanyl carrier protein ligase
DMEM	Dulbecco’s modified Eagle media
DNA	deoxyribonucleic acid

dNTP	deoxynucleoside triphosphate
dsRed	*Discosoma* red fluorescent protein
EDTA	ethylenediaminetetraacetic acid
Ena	protein enabled
Erm	erythromycin
eSLAP	epithelial spacious *Listeria*-containing phagosomes
EU	European Union
FCS	fetal calf serum
FepD	ferric enterobactin transport system permease
FIJI	Fiji is Just ImageJ
Gad	glutamic acid decarboxylase
Gbu	gamma-butyrobetaine utilization
gDNA	genomic deoxyribonucleic acid
GFP	green fluorescent protein
GSR	general stress response
GTP	guanosine triphosphate
Hbp2	haemin/haemoglobin binding protein 2
HeLa	Henrietta Lacks
HEPES	hydroxyethyl piperazineethanesulfonic acid
HGFR	human growth factor receptor
HIV	human immunodeficiency viruses
LLO	listeriolysin O
Hsp60	heat shock protein 60
HUVEC	human umbilical vein endothelial cells

HLVCM	human large vessel endothelial cell basal medium
IgA	immunoglobulin A
IL-12	interleukin 12
IL-6	interleukin 6
InlA/B/C/F/P	Internalin A/B/C/F/P
IsdC/E	iron regulated surface determinant protein
LAP	*Listeria* adhesion protein
LB	lysogeny broth
LIPI-1	*Listeria* pathogenicity island 1
LLS	listeriolysin S
Lpd	lamellipodin
lpdA	dihydrolipoyl dehydrogenase
LRR	leucine rich repeat
MAPK	mitogen-activated protein kinases
MCP-1	monocyte chemoattractant protein-1
MCS	multiple cloning site
MES	2-(N-morpholino)ethanesulfonic acid
Met/c-Met	tyrosine-protein kinase Met
MLCK	Myosin light-chain kinase
MogR	motility gene repressor
MOI	multiplicity of infection
Mpl	metalloprotease
MprF	multipeptide resistance factor
mRNA	messenger ribonucleic acid

NadA/B	quinolinate synthase
NF-κB	nuclear factor kappa B
NOD2	nucleotide Binding Oligomerization Domain Containing 2
PBS	phosphate buffered saline
PCR	polymerase chain reaction
PdxT/S	pyridoxal 5'-phosphate synthase subunit
PG	peptidoglycan
PlcA/B	phospholipase A/B
PrfA	positive regulatory factor A
PstC/A	phosphate transport system permease
qPCR	quantitative polymerase chain reaction
RNA	ribonucleic acid
RTE	ready to eat
SDS	sodium dodecyl sulphate
SigB	alternative sigma factor B
SLAP	spacious *Listeria*-containing phagosomes
SrtB	sortase B
TatA/C	twin arginine transporter
Tif	tagged image file
TLR	toll-like receptor
TNF-α	tumour necrosis factor alpha
TSA	tryptone soya agar
TSB	tryptone soya broth
VASP	vasodilator-stimulated phosphoprotein

Abstract

Listeria monocytogenes is a Gram-positive bacterium that is found ubiquitously throughout the world. It is a major foodborne intracellular pathogen and can cause a range of human diseases. It invades the cells of mammalian hosts, escapes the intracellular vacuole, replicates in the cytosol and spreads to neighbouring cells using actin-based motility. After breaching the intestinal barrier *L. monocytogenes* causes systemic infections in immunocompromised people.

The intracellular lifecycle of *L. monocytogenes* is under the control of the regulator PrfA which regulates major virulence genes. It is widely characterised and well-studied. However, many studies on *L. monocytogenes* have used population level snapshot data which masks the kinetics of single cell interactions. Individual host cells and individual *L. monocytogenes* cells are heterogenous and infection outcomes depend on these heterogenous interactions.

By designing a live cell imaging model, designed to specifically study single-cell interactions between bacteria and host cells, this study revealed novel host-pathogen interactions during infection. Successful replicative invasions are a rare event, only 9.1% (±1.2%) of host cells are susceptible to infection and only 0.4% (±0.05%) of the bacterial population can successfully form replicative invasions. *L. monocytogenes* forms aggregates in response to a proteinaceous host factor >10 kDa with the aggregates being PrfA regulated and ActA mediated. This is a novel strategy the bacteria use to increase invasion success rate through multiple invasion events. Aggregating bacteria were 3.5-fold more invasive than a non-aggregating mutant, formed 4-fold more replicative invasions in HeLa and 10-fold more in primary HUVEC cells. Additionally, in a competition assay the wildtype outcompeted the non-aggregating mutant by 10-fold.

Aggregates were also shown to preferentially interact with and invade cells in the G2/M phase and this was due to InlB-Met interactions, as Met is upregulated during the G2/M phase. Host cells depleted of Met showed a 2.5-fold reduction in the number of associated bacteria.

RNA-Seq analysis of *L. monocytogenes* treated with the causative host factor upregulated PrfA regulated virulence genes, and genes involved in iron uptake and glycerol metabolism. Analysis of gene expression between the wildtype and the non-aggregating mutant showed that aggregation downregulates genes involved in cationic peptide resistance. However, the process of aggregation did not upregulate the PrfA virulence regulon.

Overall, this study has demonstrated the value of live imaging single cell interactions between human cells and pathogens and how this can uncover novel interactions that lead to a greater understanding of the biology of infection.

Declaration

No portion of the work referred to in the thesis has been submitted in support of an application for another degree or qualification of this or any other university or other institute of learning.

Copyright statement

Acknowledgements

I would like to express my deepest gratitude to my supervisors: Dr Pawel Paszek, Professor Ian Roberts and Dr Mark Muldoon for their outstanding mentorship over the last 4 years. Their guidance and advice have been invaluable in helping me grow as a scientist and as a person. I am grateful to the Paszek lab associates, Dr David Spiller for teaching me how to capture the imaging data in this thesis and Dr James Bagnall for his expertise and advice. Thanks to the BBSRC for funding this project.

I am thankful to all members of the Roberts lab group. Dr Josephine Moran and Dr Melissa Lawson who have acted as my role-models and mentors. Marie Goldrick and Elizabeth Lord whose technical expertise, friendliness and patience meant I always had somewhere to turn when I needed help. My fellow PhD students Ömer Faruk Bay, Emma Layton, Lamis Alnakhli and Emmanuel Akabuogo whose camaraderie has left me with delightful memories. "*Queen's head, down your pint."*

Thank you to Alexander Hallam and Mary Smith (and Bobby) for their friendship and compassion, but mostly for the Friday nights in The Red Lion – "*three best friends just having a laugh."* Thanks to the rest of Team Waste for their friendship and boisterousness which provided a welcome distraction on many weekends.

I would like to thank my family. My parents Jayne and Mark Feltham for their financial support, love and their unerring faith that I would achieve this one day, even when I didn't believe it myself. My grandma Patricia McDonough for her love and being my biggest supporter, and for *always* listening to me talk about science. My brother Kieran Feltham for his companionship, particularly during the dark days of lockdown, and for being a consistent source of joy and laughter in my life.

Thank you to my wife-to-be Holly Deakin for her love, kindness and support. You're my inspiration and drive, I couldn't have finished this without you. You didn't carry it for me, but you carried me. "*Up from the ashes grow the roses of success.*"

And finally, I would like to thank Manchester United Football Club for consistently reminding me that no matter how bad things get, it can always get worse.

Preface

The author graduated from Manchester Metropolitan University in July 2013 with a Bachelor of Science in Biology. He graduated with distinction from the University of Birmingham in December 2014 with a Master of Science in Microbiology and Infection. He worked as a Research Technician at the University of Manchester until 2016, and a Biological Scientist at point-of-care diagnostics company Microbiosensor Ltd until 2018. In 2018, he was offered a place as a PhD student on the BBSRC Doctoral Training Partnership under the supervision of Dr Pawel Paszek, Professor Ian Roberts and Dr Mark Muldoon. The results of his PhD work are presented in this thesis.

"*There is nothing like looking, if you want to find something. You certainly usually find something, if you look, but it is not always quite the something you were after.*"

-Thorin Oakenshield, 2941 of the Third Age

1. Introduction

1.1 *Listeria monocytogenes*

The genus *Listeria* includes 21 species of Gram-positive rod-shaped bacteria that are found ubiquitously throughout the world, mostly as soil-borne saprophytic bacteria. Two species, *L. monocytogenes* and *L. ivanovii,* are mammalian pathogens and the causative agents of the human disease listeriosis (Quereda, Moron-Garcia, Palacios-Gorba et al., 2021). *L. monocytogenes* is most commonly found in water, soil and decaying vegetation (Rolhion and Cossart, 2017). It is a resilient species that is able to grow in a range of temperatures with growth reported at temperatures as low as -0.4°C (Chan and Wiedmann, 2009) and as high as 45°C (Bayles, Annous and Wilkinson, 1996), high salt concentrations of up to 10% salinity, and a pH range of 4.5-10 (Arizcun, Vasseur and Labadie, 1998). This capacity for stress tolerance allows *L. monocytogenes* to contaminate man-made niches such as farms (infected crops and livestock) and food processing environments, transmit to and contaminate food and subsequently colonise the gastrointestinal tract of human hosts (Figure 1.1). Once inside the host *L. monocytogenes* has a variety of mechanisms that allow it to invade eukaryotic host cells, establish an intracellular niche, evade the immune system, and disseminate throughout the hosts body (NicAogain and O'Byrne, 2016). This can cause severe complications and outcomes such as meningitis and pre-term abortions, as *L. monocytogenes* is able to cross both the blood-brain barrier and the placental barrier (Radoshevich and Cossart, 2018).

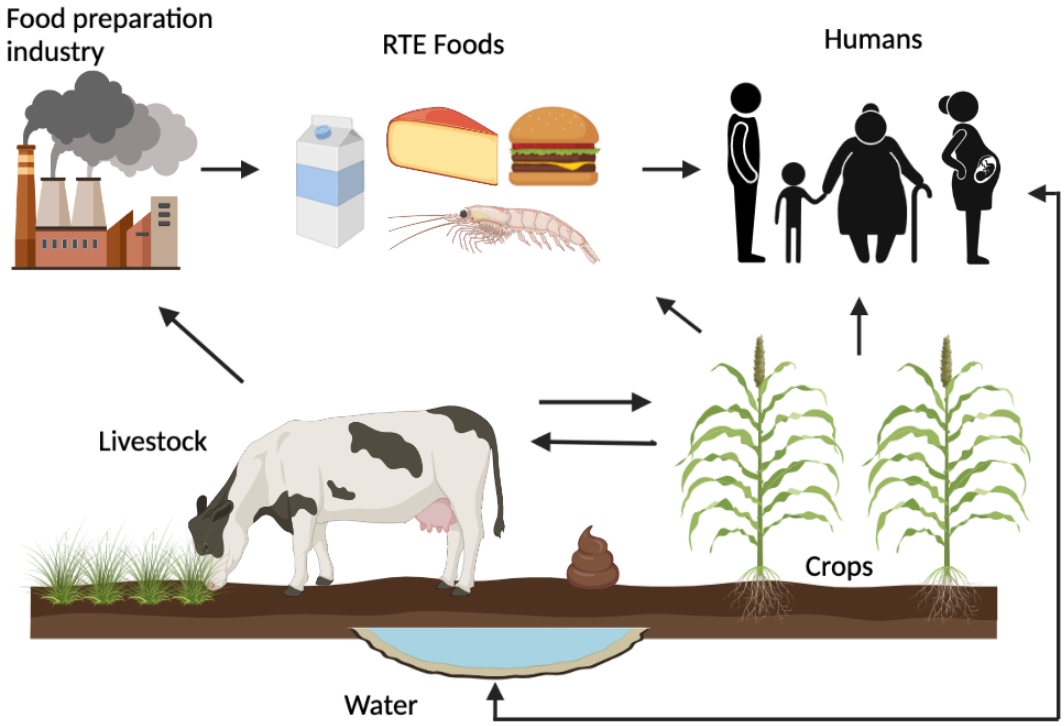

Figure 1. 1. *L. monocytogenes* routes to infection in humans. Transmission routes for *L. monocytogenes* between soil, water, farms, industry, food products and humans. Transmission routes of *L. monocytogenes* hosts are shown by the arrows. (Adapted from Quereda, Moron-Garcia, Palacios-Gorba et al., 2021)

1.2 Listeriosis

L. monocytogenes was first identified by E.G.D. Murray in 1926 as the bacteria responsible for an outbreak of mononucleosis of rabbits in Cambridge (Murray, Webb and Swann, 1926). It was later shown to be responsible for meningitis outbreaks in humans, eventually being recognised as an important food-borne pathogen affecting humans, livestock and wild animals (Gray and Killinger, 1966). The disease has a variety of clinical symptoms. In immunocompetent individuals it is usually a self-limiting disease that causes acute febrile gastroenteritis after the ingestion of heavily contaminated foods. However, ingestion of contaminated foods by immunocompromised individuals can cause invasive listeriosis as the bacteria

crosses the intestinal barrier and infects other organs in the body (D'Orazio, 2019) (Figure 1.2).

The minimum infectious dose of *L. monocytogenes* is unclear and to date no epidemiological data has been able to establish the levels of contamination in food associated with listeriosis cases. It is estimated that an infectious dose for healthy individuals is $1.0 \times 10^7 – 1.0 \times 10^9$ CFUs and $1.0 \times 10^5 – 1.0 \times 10^7$ CFUs in high risk individuals (Pouillot, Klontz, Chen et al., 2016; Quereda, Moron-Garcia, Palacios-Gorba et al., 2021).

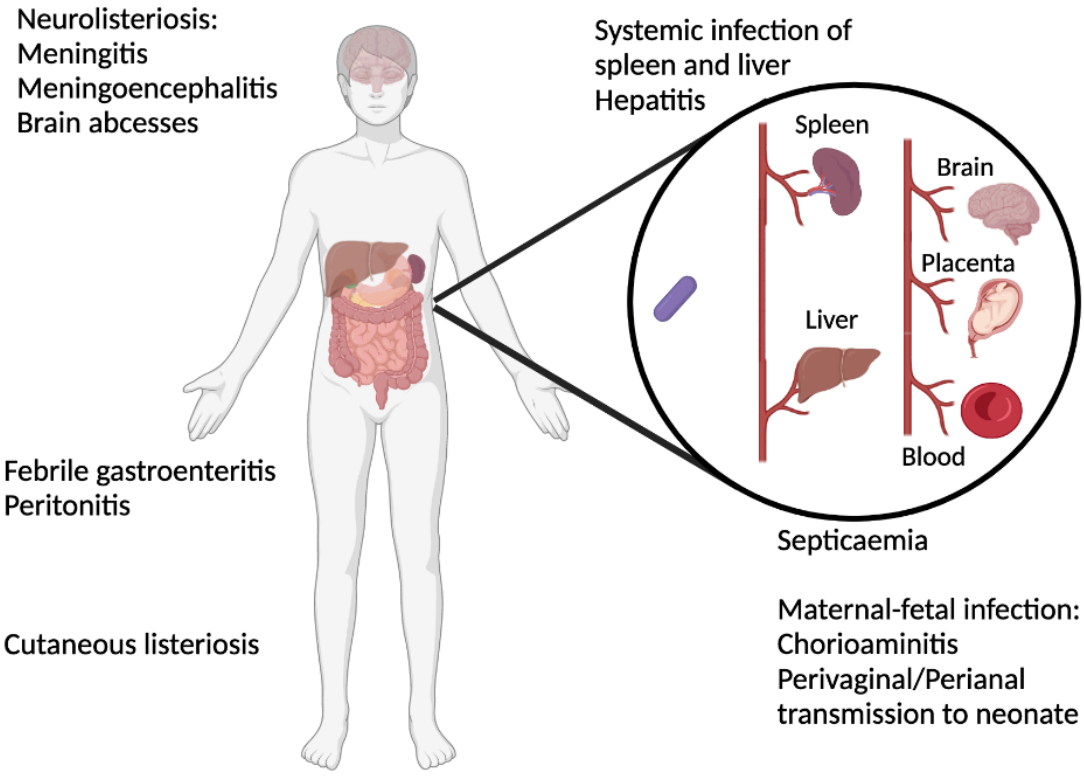

Figure 1. 2. Clinical presentations of listeriosis in humans. Schematic showing the various clinical presentations of listeriosis and where in the body they occur. Once *L. monocytogenes* crosses the intestinal barrier it can cause systemic infections of the spleen and liver, and these can develop further into septicaemia and neurolisteriosis. In pregnant women it can spread to the unborn fetus through and colonise the neonate upon birth. (Adapted from Quereda, Moron-Garcia, Palacios-Gorba et al., 2021)

1.2.1 Febrile gastroenteritis

Febrile gastroenteritis occurs when immunocompetent individuals ingest heavily contaminated foods, in most cases the foods are contaminated with >1.0 x 10^9 CFU/ml of *L. monocytogenes* (Quereda, Moron-Garcia, Palacios-Gorba et al., 2021). The disease has an average incubation time of 24 hours with a range of 6 to 240 hours (Goulet, King, Vaillant et al., 2013). It usually passes without any severe complications in healthy individuals. Febrile gastroenteritis caused by *L. monocytogenes* is characterised by the primary symptoms of diarrhoea, fever, headache and muscular or joint pain (Ooi and Lorber, 2005).

1.2.2 Invasive listeriosis

The most common outcomes of invasive infections are: septicaemia, neurolisteriosis and pregnancy-associated infections. Between 2009 and 2013 the largest study to date on listeriosis outcomes – the **M**ulticentric **O**bservational **Na**tional study on **LIS**teriosis and *Listeri**A*** (MONALISA) – was performed in France. This study examined: 107 maternal-neonatal cases, 427 bacteraemia cases and 252 neurolisteriosis cases. Listeriosis was shown to be a severe disease with a very poor prognosis. Over 80% of infected mothers experienced severe neonatal complications, and only 39% of patients with neurolisteriosis survived and made a full recovery. The mean incubation period of listeriosis is eight days but is variable depending on the clinical type (Charlier, Perrodeau, Leclercq et al., 2017).

Septicaemia listeriosis symptoms are similar to other bacterial septicaemia infections: vomiting, nausea, fever, chills and malaise. It has a mortality rate of 46% within 3 months (Doganay, 2003). Neurolisteriosis presents clinically in several ways, the 2 most common are meningitis and meningoencephalitis. Common clinical symptoms include fever, seizures, tremors and ataxia. It can also present as brain abscesses and brain stem infections which cause fever, headache, nausea and vomiting (Mylonakis, Hohmann and Calderwood, 1998). Pregnancy associated

listeriosis has non-typical symptoms that vary case-to-case but typically presents with flu-like symptoms or similar symptoms to a urinary tract infection. Contracting *L. monocytogenes* during pregnancy can cause fetal complications from infection of placental tissue or infection of the fetus through chorioamnitis. These can cause fetal loss or a high neonate mortality rate after birth. Post-birth complications also occur from *L. monocytogenes* neonatal colonisation via the birth canal, causing neonatal meningitis seven to fourteen days after birth (Schlech, 2019).

1.2.3 Localised infections

Localised listeriosis infections represent only 10% of all cases. The majority of these are cutaneous and are an occupational hazard for farmers and veterinarians who are exposed to infected animal tissue. Cutaneous infections present as pustular non-painful, self-limiting eruptions from the skin from which *L. monocytogenes* can be isolated. They are generally mild and easily treatable (McLauchlin and Low, 1994). Other rare forms of localised listeriosis include, hepatitis, peritonitis, endocarditis, bile-tract infections, eye infections and musculoskeletal infections (Badar, Bhuiyan and Nabeel, 2022; Charlier, Fevre, Travier et al., 2014; Charlier, Leclercq, Cazenave et al., 2012; Hof, 2017; Samant, Uyemura, Sarbagya et al., 2022).

1.2.4 Incidence rates of listeriosis

L. monocytogenes has the highest mortality rate of all foodborne pathogens in the western hemisphere. In 2019 the mortality rate in the EU was 17.6%, with an estimated incidence rate of two to five cases per million people per year (European Food Safety, European Centre for Disease and Control, 2021). Due to the COVID-19 pandemic monitoring of *L. monocytogenes* case and fatality rates were interrupted. The latest analysed five-year period (2015-2019) showed a stabilisation in case numbers in the EU and European Economic Area, after many years of a trend of increasing cases. However case fatality rate increased from 2018 (European Food

Safety, European Centre for Disease and Control, 2021). The biggest risk factors for contracting invasive listeriosis are: age (elderly or neonate), pregnancy, alcoholism, HIV, cancer, diabetes, immunity defects, drug immunosuppression (e.g. steroids), liver and kidney disease (Goulet, Hebert, Hedberg et al., 2012). In the elderly most cases are reported in individuals over the age of 64 (European Food Safety, European Centre for Disease and Control, 2021). In pregnancy cases the incidence rate of listeriosis is 13-fold higher than in the general population (Silk, Date, Jackson et al., 2012).

In EU-regulated food supply chains, incidence of unsatisfactory *L. monocytogenes* testing at retail sites is low (European Food Safety, European Centre for Disease and Control, 2021). *L. monocytogenes* was not detected in hard cheeses and only 2.1% of meat products when monitored against the criteria set out by the EU in Regulation (EC) No 2073/2005. However, during food processing the unsatisfactory result rate is higher for all ready-to-eat (RTE) products – with the highest unsatisfactory rate being fish products, *L. monocytogenes* was detected in 5.8% of these (European Food Safety, European Centre for Disease and Control, 2021). Humans are frequently exposed to subclinical exposures of *L. monocytogenes* – healthy adults will have on average two incidence cases of *L. monocytogenes* carriage per year, however this is short lived as faecal shedding of *L. monocytogenes* in these cases lasts for four days (Grif, Patscheider, Dierich et al., 2003). These points demonstrate the need for robust and careful monitoring of *L. monocytogenes* in the food supply chain and the population to manage cases of listeriosis.

1.3 *L. monocytogenes* as a tool for studying cell biology

As well as being a human pathogen – *L. monocytogenes* has been utilised as a model for studying biological processes due to its remarkable ability to invade, survive and replicate in both professional phagocytes and a variety of non-phagocytic cells. *L. monocytogenes* has also been used as a model system for

understanding pathogenicity of other cytosolic pathogens such as *Salmonella enterica* and *Shigella flexneri* (Hamon, Bierne and Cossart, 2006). There are many examples where studying *L. monocytogenes* has led to new insights in cellular biology (Rolhion and Cossart, 2017).

Studying the intracellular motility of *L. monocytogenes* led to the discovery of the Arp2/3 complex, the first actin nucleator discovered in eukaryotic cells (Welch, Iwamatsu and Mitchison, 1997). Studying the interactions between host cells *and L. monocytogenes* during bacterial invasion discovered that clathrin-dependent endocytic machinery is key for actin polymerisation and bacterial entry. Previously it was thought to only be involved in endocytosis of small molecules and objects <150 nm in size (Conner and Schmid, 2003; Veiga and Cossart, 2005). Studying the main virulence regulon of *L. monocytogenes* led to the discovery of the first RNA thermo-sensor for regulating virulence in bacteria. Since its discovery several of these have been discovered in other bacteria such as *Escherichia coli* and *Yersinia pseudotuberculosis* (Bohme, Steinmann, Kortmann et al., 2012; Johansson, 2009; Johansson, Mandin, Renzoni et al., 2002). MicroRNA studies in mice have shown an interplay between *L. monocytogenes* interactions with gut microbiota and the host - host microRNA expression triggered by *L. monocytogenes* infection is downregulated by intestinal microbiota (Archambaud, Sismeiro, Toedling et al., 2013).

Due to being a wide-spread pathogenic organism and its usefulness as a cell biology tool, the biology of *L. monocytogenes* infection is widely studied and well characterised.

1.4 *L. monocytogenes* pathogenesis and virulence

1.4.1 SigB and environmental stress tolerance

L. monocytogenes success as a food-borne pathogen begins with the colonisation of RTE foods. It has a range of mechanisms that allow it to survive and proliferate in most of the processes used for food preservation and protection. Salting of food is a common preservation method but *L. monocytogenes* can survive high salt conditions – once exposed to osmotic shock it upregulates *gbu* (glycine-betaine transporter) and *betL* (carnitine ABC transporter) and uses these transporters to adapt to the high-salt environment (Burgess, Gianotti, Gruzdev et al., 2016). Refrigeration is another common food preservation method as many bacteria do not grow at these low temperatures because biological membranes fluidity is reduced and gene expression is slowed or halted due to stabilised secondary structures in nucleic acids. *L. monocytogenes* has a cold shock response whereby it severely reduces its growth rate, upregulates the production of branched chain fatty acids and transporters that help to retain membrane fluidity and induces RNA helicases and cold-shock proteins that melt RNA secondary structures and allow protein synthesis to continue at low temperatures (Hingston, Chen, Allen et al., 2017). *L. monocytogenes* also carries genes for efflux pumps that help it resist many of the common disinfectants used in the food processing pipeline such as benzalkonium chloride. *L. monocytogenes* can tolerate the presence of benzalkonium chloride by utilising the efflux pump from the benzalkonium chloride resistance locus (*bcrACB)* (Dutta, Elhanafi and Kathariou, 2013). Many of these stress-related regulatory responses are under the control of alternative sigma factor B (SigB) – a regulon containing up to 300 genes that fall under the General Stress Response (GSR) of *L. monocytogenes* and are involved in a range of stress-tolerance mechanisms such as metabolism, flagella synthesis, pH homeostasis, osmolarity regulation, antimicrobial resistance and quorum sensing (Guerreiro, Arcari and O'Byrne, 2020; Liu, Orsi, Gaballa et al., 2019).

1.4.2 Pathogenesis – SigB and stress tolerance in the host

Upon ingestion of contaminated foods *L. monocytogenes* is exposed to the low pH of the stomach acid (pH 1-2) (Smith, Liu and Paoli, 2013). SigB plays a crucial role in *L. monocytogenes* survival in this condition as it upregulates the transcription of *gad* genes which encode a glutamate decarboxylase (GAD) system, which transports an electron from a molecule of glutamate and converts it into γ-aminobutyrate. This reaction modulates intracellular pH of the bacteria by electron transfer (Gahan and Hill, 2014). A second SigB regulated response to stomach acid pH is upregulation of the arginine deaminase pathway (*arcABC)* which exports ornithine from the cell and imports arginine. This generates ammonia, which associates with a proton in the cytoplasm and modulates cytoplasmic pH (Gahan and Hill, 2014).

Bile is another host defence in the gastrointestinal tract, it acts as a natural antimicrobial containing a mixture of acids, cholesterol, phospholipids and biliverdin. It causes bacterial protein unfolding/aggregation, cell membrane degradation and oxidation of the bacterial cytosol (Cremers, Knoefler, Vitvitsky et al., 2014). *L. monocytogenes* utilises a bile salt hydrolase (Bsh) which deconjugates bile salts and the membrane transporter BilE which acts as a bile exclusion system, allowing it to tolerate and survive the secretion of host bile (Begley, Gahan and Hill, 2005; Sleator, Wemekamp-Kamphuis, Gahan et al., 2005).

Exposure to bile salts induces another transcriptional change in *L. monocytogenes* – the activation of the positive regulatory factor A (PrfA) regulon. PrfA is the main virulence regulator in *L. monocytogenes* (Gahan and Hill, 2014). Both *bsh* and *bilE* are also under the control of PrfA, and exposure to bile salts induces a transcriptional upregulation of PrfA but not of SigB (Guariglia-Oropeza, Orsi, Guldimann et al., 2018). This suggests that bile acts as a signal for *L. monocytogenes* to switch from SigB transcriptional profile to the virulent PrfA transcriptional profile and subsequent upregulation of the *Listeria* Pathogenicity Island 1 (LIPI-1) genes,

preparing it for host intracellular invasion (Toledo-Arana, Dussurget, Nikitas et al., 2009) (Figure 1.3).

L. monocytogenes reaches the intestinal lumen where it is exposed to further environmental stresses and the presence of the host microbiota. The host resident microbiota provides colonisation resistance against invading pathogenic organisms through a number of interactions such as inhibiting growth to outcompete the invading pathogen and production of antimicrobial peptides and synthesis of short chain fatty acids to help maintain the intestinal barrier (Rolhion and Chassaing, 2016). However, *L. monocytogenes* has evolved factors that allow it to combat and evade the defence mechanisms of the host microbiota. It can utilise alternative metabolic sources such as ethanolamine to bypass the competition of the microbiota (Archambaud, Nahori, Soubigou et al., 2012). It can also produce bacteriocins such as listeriolysin S (LLS) which is bactericidal, killing competing bacteria from the host microbiota such as species of the *Allobaculum* and *Alloprevotella* genus (Cotter, Draper, Lawton et al., 2008). By reducing the presence of these *L. monocytogenes* alters the gut microbiota to promote intestinal colonisation, as LLS deficient strains are impaired in their capacity to compete with intestinal microbiota and survive in the intestinal lumen (Quereda, Dussurget, Nahori et al., 2016).

SigB regulated genes also aid survival in the host intestinal lumen as it deals with a high osmolarity environment (Becattini and Pamer, 2017). Similar to its response to osmotic shock in the food preparation pipeline, the genes for membrane transporters *betL*, *gbu* and *opuC* are upregulated by SigB (Becattini and Pamer, 2017) . Other SigB GSR factors induced at this stage include proline synthetase (ProAB) which promotes accumulation of the osmo-protectant proline, the serine protease HtrA that degrades misfolded proteins and RelA which is a guanosine tetra- penta- phosphate ((p)ppGpp) synthesase. Intracellular modulation of (p)ppGpp is essential for osmotolerance (Burgess, Gianotti, Gruzdev et al., 2016).

1.4.3 Pathogenesis - activation of the PrfA regulon

In addition to regulating the GSR, SigB also regulates key virulence genes. PrfA, the master virulence regulator is encoded on LIPI-1 and has three transcriptional promoters (discussed further in section 1.5), one of which is positively regulated by SigB. SigB also regulates the Internalin genes *inlA* and *inlB* which are essential for eukaryotic cell invasion and crossing the intestinal barrier (Liu, Orsi, Gaballa et al., 2019). Therefore, the exposure of *L. monocytogenes* to the stresses involved in reaching the intestinal lumen primes its gene expression to prepare to switch to an intracellular lifestyle. Inside of the host cell PrfA and PrfA-regulated virulence gene expression upregulation allows the bacteria invade eukaryotic cells, survive and replicate intracellularly and to spread from cell-to-cell (de las Heras, Cain, Bielecka et al., 2011).

LIPI-1 contains the *prfA* gene itself and many PrfA regulated virulence genes: listeriolysin (hly), phospholipases (*plcA* and *plcB*), actin-assembly inducing protein (*actA*), zinc metalloprotease (*mpl*) and a nucelomodulin (*orfX*). Outside of LIPI-1 PrfA also regulates bile salt hydrolase (*bsh*) a range of internalins (*inlA*, *inlB*, *inlC*) (de las Heras, Cain, Bielecka et al., 2011) These genes are integral for *L. monocytogenes* infection and intracellular life cycle (Figure 1.3).

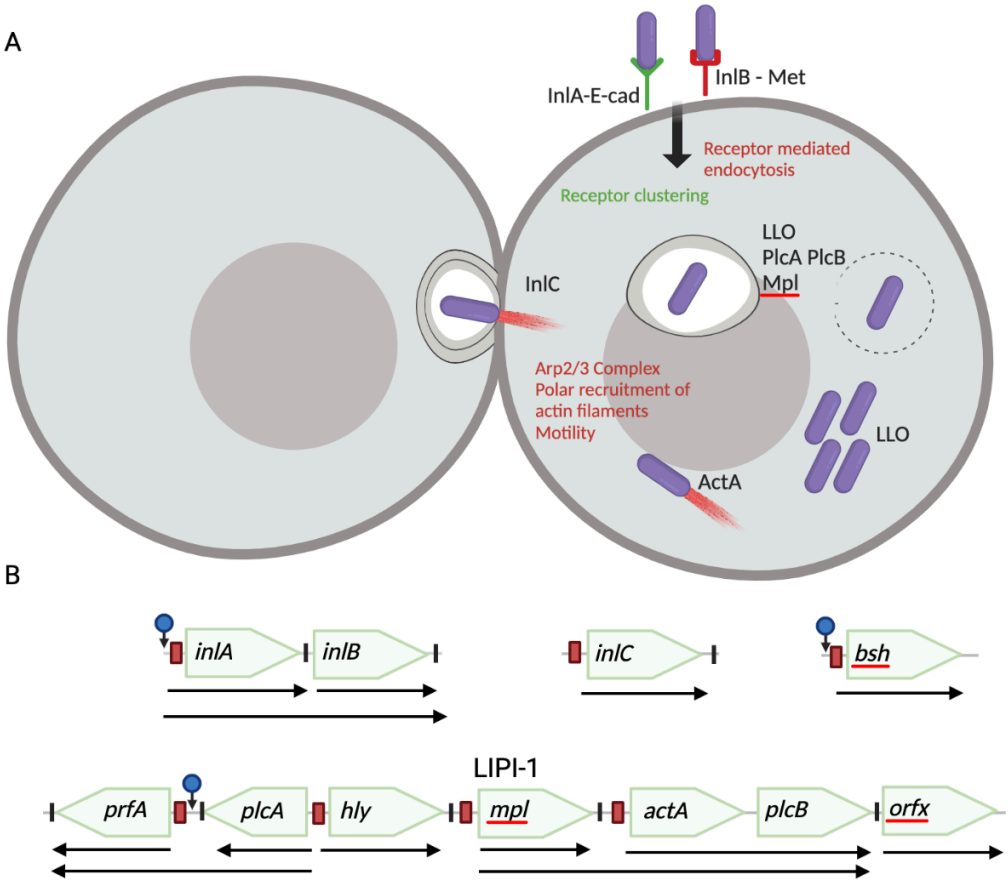

Figure 1. 3. The PrfA regulon and gene functions in *L. monocytogenes* intracellular lifecycle. A) Schematic of *L. monocytogenes* intenalin-mediated invasion of a non-phagocytic cells. Internalisation occurs either through Internalin A (InlA) binds to E-cadherin which induces receptor clustering and internalisation or by InlB which binds to Met, which induces receptor mediated endocytosis. *L. monocytogenes* is internalised into a vacuole which is lysed by LLO, phospholipases and metalloprotease (Mpl). LLO modulates the host environment allowing. *L. monocytogenes* cytosolic replication. ActA promotes actin polymerisation by mimicking the Arp2/3 complex to recruit actin filaments to the polar end of the bacterial cells. This propels *L. monocytogenes* through the host cytoplasm and forms protrusions into neighbouring cells where InlC weakens the apical junctions facilitating cell-to-cell spread. **B)** Schematic of PrfA virulence cluster in *L. monocytogenes*. Green arrows represent open reading frames and black vertical lines show transcriptional terminators. Black arrows show transcriptional units. PrfA boxes are shown in red and blue circles show SigB-regulated genes.

1.4.4 Crossing the intestinal barrier – InlA, InlB and LAP

In order to establish a successful infection *L. monocytogenes* must cross the host intestinal epithelial barrier. *L. monocytogenes* has 3 main strategies for achieving this: Transcytosis through goblet cells, translocation involving *Listeria* adhesion protein (LAP) or invasion of M-cells and Peyers patches (Quereda, Moron-Garcia, Palacios-Gorba et al., 2021).

Transcytosis of goblet cells is achieved through Internalin A (InlA) mediated invasion. InlA is one member of the internalin family, a group of 25 genes in *L. monocytogenes*. The internalins are composed of signal peptide sequence, followed by a leucine-rich repeat (LRR) region responsible for protein-protein interactions, a conserved inter-repeat domain and variable C-terminal regions. InlA has a LPXTG motif that covalently binds it to the cell wall (Camejo, Carvalho, Reis et al., 2011). The host receptor for InlA is E-cadherin (E-cad), a transmembrane adherent junction protein. Once InlA binds to E-cad it triggers a cascade that leads to clustering of E-cad, recruitment of clathrin endosomal machinery and cytoskeletal rearrangement driven by the Arp2/3 complex – eventually leading to internalisation of *L. monocytogenes.* InlB plays a role in this process *in vivo* but it is dispensable with little to no invasive loss (Nikitas, Deschamps, Disson et al., 2011).

LAP is an alcohol acetaldehyde that promotes adhesion of *L. monocytogenes* to intestinal epithelial cells through interaction with heat shock protein 60 (Hsp60), a chaperonin that has a secondary function as a receptor (Wampler, Kim, Jaradat et al., 2004). Translocation involving LAP occurs at the tip of intestinal villi and this induces an immune response, invoking activation of the Nuclear Factor κB (NF-κB), secretion of pro-inflammatory cytokines and activation of the myosin light chain kinase (MLCK) (Drolia, Tenguria, Durkes et al., 2018). MLCK disrupts the epithelial cell tight junctions, weakening the epithelial layer and allowing the bacteria to pass through to the *lamina propria* (Drolia, Tenguria, Durkes et al., 2018).

Peyer's patches are found in regions of the intestinal epithelium where there are many Microfold cells (M-cells). M-cells are highly specialised epithelial cells that sample from the intestinal lumen and pass them to the antigen presenting cells of the Peyer's patches – this mechanism allows specific immune monitoring and response against invading pathogens (Chiba, Nagai, Hayashi et al., 2011). *L. monocytogenes* hijacks this system by utilising Internalin B (InlB). InlB is another member of the internalin family, and its variable C-terminal region has glycine and tryptophan (GW) repeats that are involved in non-covalent cell wall interactions (Jonquieres, Bierne, Fiedler et al., 1999). The host receptor for InlB is the tyrosine-protein kinase Met (Met) receptor, sometimes called human growth factor receptor (HGFR) or c-Met (Bottaro, Rubin, Faletto et al., 1991). Met has a much wider tissue distribution than E-cad and thus InlB is important for invasion into several cell types including hepatocytes, fibroblasts and endothelial cells (Braun, Ohayon and Cossart, 1998). M-cell and Peyer's patch invasion has been shown to be reliant on InlB in mouse models (Chiba, Nagai, Hayashi et al., 2011). Similar to InlA, InlB binding induces phosphorylation, ubiquitination and clathrin mediated endocytosis of the bacteria into the host cell. After M cell invasion *L. monocytogenes* can either pass through the intestinal barrier by transcytosis or spread to adjacent enterocytes (Rey, Chang, Latour-Lambert et al., 2020). These points demonstrate that *L. monocytogenes* has several strategies for invading several different types of host cells.

1.4.5 Entry and proliferation in eukaryotic cells – LLO, PlcAB, Mpl

L. monocytogenes is able to invade and proliferate within both phagocytic and non-phagocytic cells. Once inside these cells (either through one of the previously described methods or by phagocytosis by immune cells) the bacteria become internalised into the cell in a membrane bound compartment called the endosome or phagosome. *L. monocytogenes* has a number of virulence factors, enabling escape of this vacuole and escape into the cytosol – where it can proliferate and spread to neighbouring cells (Camejo, Carvalho, Reis et al., 2011) (Figure 1.3).

Listeriolysin O (LLO) - encoded by the *hly* gene - is a cholesterol dependent cytolysin that binds to cholesterol and forms large pores on the membrane. LLO activity is mostly restricted to the endosomal environment to stop host cell lysis after the bacteria has escaped the vacuole into the cytosol by two mechanisms. Firstly, it is pH sensitive and most active in the low pH present in the endosome/phagosome (Bavdek, Kostanjsek, Antonini et al., 2012). Secondly, it has a PEST-like (rich in proline (P), glutamic acid (E), serine (S) and threonine (T)) sequence – a collection of 26 amino acids at the N-terminal of the protein – that interacts with adaptor protein 2 (AP2) of the host cell endocytosis machinery which promotes LLO removal and thereby preserves plasma membrane integrity in the host cell preventing premature host cell lysis (Chen, Nguyen, Mitchell et al., 2018). The PEST-like sequence also undergoes a cysteine glutathionylation in the cytosol that is inhibitory to LLO activity (Portman, Huang, Reniere et al., 2017). In endosomes and phagosomes, the presence of oxidoreductases prevents cysteine glutathionylation and preserves LLO activity (Portman, Huang, Reniere et al., 2017). This tight regulation of LLO is important to *L. monocytogenes* virulence as damaging the host cell would expose the bacteria to immune system recognition. At the transcriptional level LLO mRNA expression is restricted in the cytosol by codon-restriction in the PEST-encoding region and the formation of a ribosomal blocking secondary structure (Chen, Nguyen, Mitchell et al., 2018; Peterson, Portman, Feng et al., 2020).

LLO also has many secondary functions both inside and outside of the host cell. It participates in dampening of the DNA damage response through degradation of the sensor Mre11 (Samba-Louaka, Pereira, Nahori et al., 2014). It can induce histone modifications that lead to increased expression of cytokines and drives inflammation (Nguyen, Peterson and Portnoy, 2019). LLO can modulate the immune response through mechanisms such as mitogen-activated protein kinase (MAPK) activation (Witte, Archer, Rae et al., 2012). The MAPK signalling transduction pathway is essential for the host immune response. LLO is implicated in activation of the pathway by phosphorylation to promote entry into epithelial cells (Weiglein, Goebel, Troppmair et al., 1997). LLO also modulates the adaptive

immune response, it can induce $CD4^+$ T lymphocyte unresponsiveness by triggering a transcriptional response that drives the expression of negative regulators of T-cell receptor signalling (Gekara, Zietara, Geffers et al., 2010). LLO interacts with mitochondria and leads to mitochondrial fragmentation, breaking of the mitochondrial network into visually punctate structures (Stavru, Palmer, Wang et al., 2013). It may also play a role in controlling the phagocytosis rate of bacteria by host macrophages. Treating macrophages with recombinant LLO compromised phagocytosis of *L. monocytogenes.* One hypothesis is that the bacterial population uses LLO to coordinate host cell uptake and reduce internalisation at high multiplicities of infection. This reduces the probability of replicative invasions in macrophages (Moran, Feltham, Bagnall et al., 2022).

LLO has been implicated in *L. monocytogenes* utilisation of vacuole-bound intracellular niches in certain cell types. In macrophages *L. monocytogenes* expressing lower levels of LLO may enter a slow-growing state inside spacious *Listeria* containing phagosomes (SLAPs) (Birmingham, Canadien, Kaniuk et al., 2008). In epithelial cells similar structures called epithelial *Listeria* containing phagosomes (eSLAPS) have been observed – but a key difference is that inside of the eSLAPS *L. monocytogenes* was able to proliferate just as fast as in the cytosol (Peron-Cane, Fernandez, Leblanc et al., 2020). This constituted alternative intracellular niches for *L. monocytogenes* that might promote long term colonisation of host tissue.

Other virulence factors are involved in assisting vacuole escape include Phospholipase A (PlcA) and Phospholipase B (PlcB) that cleave the phosphate-glycerol bond of the hydrophilic head of phospholipids to aid in vacuole escape (de las Heras, Cain, Bielecka et al., 2011). They also subvert the hosts autophagic defences by stalling pre-autophagosomal structures and thus prevent clearance of *L. monocytogenes* in infected cells (Tattoli, Sorbara, Yang et al., 2013). Metalloprotease (Mpl) activates the proenzyme forms of the phospholipases in the acidified vacuole environment (Alvarez and Agaisse, 2016).

Overall, vacuole escape is an integral step in the intracellular life cycle of *L. monocytogenes* and LLO is integral to *L. monocytogenes* virulence, both inside and outside of the host cell.

1.4.6 Cell-to-cell spread: ActA

Once in the host cytosol *L. monocytogenes* become motile via actin polymerisation. The *actA* gene is upregulated and expresses the actin-assembly inducing protein ActA. ActA enables *L. monocytogenes* to nucleate and polymerise actin directly and constitutively (Kocks, Gouin, Tabouret et al., 1992). It does this by imitating the host cells natural actin machinery and binding to the actin-nucleation complex Arp2/3 (May, Hall, Higgs et al., 1999). This drives actin recruitment, branching of actin filaments and these propel the bacteria through the host cytosol. The recruitment of Arp2/3 and Enabled/vasodilator-stimulated phosphoprotein (Ena/VASP) proteins also disguises the bacteria from autophagic recognition and avoid degradation (Cheng, Chen, Engstrom et al., 2018). The “actin comet tails” (named for their appearance in microscopy images) also allow the bacteria to form membrane protrusions and spread to neighbouring cells (Dowd, Mortuza, Bhalla et al., 2020) (Figure 1.3).

ActA is composed of 640 amino acids (AA) (Figure 1.4) (Pillich, Puri and Chakraborty, 2017). It harbours a signal peptide at AA1-30 that is required for direct transport of ActA to the bacterial membrane and a transmembrane domain at AA589-610 (Travier and Lecuit, 2014). It has 3 distinct regions, the N-region, P-region and C-region. The N-region of ActA (AA30-264) is essential for host actin polymerisation, especially the region AA117-126 (Pistor, Chakraborty, Walter et al., 1995). The N region does not directly stimulate actin polymerisation, it mediates actin nucleation with the Arp2/3 complex which is bound by region AA126-158 (Welch, Iwamatsu and Mitchison, 1997). ActA is located on the poles of the bacterial cells so that actin is recruited locally to these areas, facilitating intracellular movement. The P region contains 4 proline rich repeats in the region

AA264-387 that bind to Ena/VASP proteins which in turn bind to actin filaments and the actin binding protein profilin (Theriot, Rosenblatt, Portnoy et al., 1994). This region is important in modulating the length of actin comet tails (Lasa, Gouin, Goethals et al., 1997). The C region is not implicated in actin tail formation and forms a hydrophobic region. ActA has also been shown to have important secondary functions. ActA mediated aggregation and biofilm formation, which is driven by direct ActA-ActA interactions, has been shown to be critical in the lumen to promote persistence in the colon and the cecum and fecal shedding (Travier and Lecuit, 2014). Removal of the C-region of ActA inhibited this aggregation (Travier, Guadagnini, Gouin et al., 2013). ActA is also implicated in invasion of host cells through actin cytoskeleton rearrangement and the formation of pseudopods that facilitate effective invasion of host cells (Suarez, Gonzalez-Zorn, Vega et al., 2001).

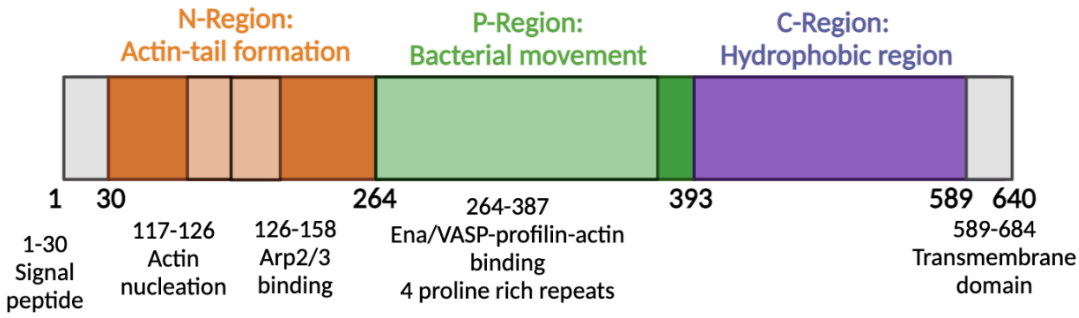

Figure 1. 4. Structure of the ActA protein. Schematic showing the 3 regions of ActA. Highlighted areas are involved in actin tail formation and intracellular motility. Numbers show the amino acid (AA) location of these regions (Adapted from Travier and Lecuit, 2014).

Other virulence factors are involved in *L. monocytogenes* ability to spread cell-to-cell. Internalin C (InlC) helps to weaken cortical tension between host cells and is involved in elongating membrane protrusions (Rajabian, Gavicherla, Heisig et al., 2009). Host cell lamellipodin (Lpd) is important to *L. monocytogenes* intracellular

motility, it interacts with phosphatidylinositol (3,4)-bisphosphate [PI(3,4)P2] and VASP recruited to the bacterial cell surface via ActA. This recruitment is essential for intracellular motility and altering host levels of Lpd affected protrusion formation and intracellular velocity (Wang, King, Goldrick et al., 2015). Once the bacteria reach the new uninfected host cell they must escape the double membrane vacuole caused by protruding through the membranes. It uses PlcA, PlcB and LLO in the mechanisms previously described to achieve this. LLO is dispensable in escaping double membrane vacuoles in epithelial cells suggesting it may not be required for *L. monocytogenes* systemic spread after the initial stages of infection (Alberti-Segui, Goeden and Higgins, 2007). Overall, several virulence genes contribute to the cell-to-cell spread of *L. monocytogenes*, with *actA* being the most important gene for intracellular motility.

1.4.7 *L. monocytogenes* and the host immune response

Infection with *L. monocytogenes* invokes a strong immune response in the host (Zenewicz and Shen, 2007). The innate immune response is critical for early control of *L. monocytogenes* infection (Zenewicz and Shen, 2007). Neutrophils are rapidly recruited to the site of infection by IL-6 secretion. They engulf and kill bacteria and secrete chemokine colony stimulating factor 1 (CSF-1) and monocyte chemoattractant protein 1 (MCP-1). These recruit macrophages which are essential for bacterial clearance (Guleria and Pollard, 2001). *L. monocytogenes* can infect macrophages, inducing secretion of Tumour necrosis factor α (TNF-α) and Interleukin 12 (IL-12). These drive natural killer cells to secrete Interferon γ (IFNγ), activating macrophages and increasing their bactericidal activity (Tripp, Wolf and Unanue, 1993).

Macrophages are activated through toll-like receptors (TLR) which recognise ligands such as peptidoglycan, flagellin and bacterial DNA (Zenewicz and Shen, 2007). In *L. monocytogenes* infection, TLR2 is the most important TLR, *in vitro* studies have shown that TLR2 deficient macrophages secrete less cytokines in response to *L.*

monocytogenes infection (Seki, Tsutsui, Tsuji et al., 2002). Binding of a recognised ligand to its TLR initiates a signalling cascade which results in the activation of the transcription factor NF-κB. This results in expression of different cytokine and antigen-presentation related genes (Zenewicz and Shen, 2007).

The host recognises intracellular bacteria, transcriptional changes occur in macrophages and dendritic cells infected with *L. monocytogenes*, they present greater levels of antigenic surface molecules (such as LLO which has been shown to confer resistance to *L. monocytogenes* infections) for T cell activation and secrete higher amounts of pro-inflammatory cytokines (Brzoza, Rockel and Hiltbold, 2004). A protein that has been shown to detect cytosolic *L. monocytogenes* is NOD2, a cytosolic nucleotide-binding oligomerization domain protein. Its ligand is muramyl dipeptide which is a component of bacterial peptidoglycan and recognition of cytosolic *L. monocytogenes* initiates a signalling cascade that is distinct from the TLR signalling (Inohara, Ogura, Fontalba et al., 2003).

TLR activation and signalling drive the adaptive immune response by activation of dendritic cells (DCs) which in turn stimulate T cells which are required for final clearance of bacteria (Bhardwaj, Kanagawa, Swanson et al., 1998). CD4 and CD8 T cells compromise most of the adaptive immune response to *L. monocytogenes* due to its intracellular niche (Zenewicz and Shen, 2007). Infected cells and antigen presenting cells present *L. monocytogenes* antigens to the CD4 and CD8 T cells. T cells mediate anti-*Listeria* immunity by targeting and lysing infected cells with perforin to expose intracellular bacteria to nearby activated macrophages (Harty and Badovinac, 2002). Primary T cell response peaks at 7-9 days and then contracts to a smaller population of memory T cells which have a lower stimulation threshold for activation and upon secondary infection can quickly control of and eliminate the bacteria (Busch, Pilip, Vijh et al., 1998).

L. monocytogenes has evolved several mechanisms that allow it to survive the host immunes response. InlC is secreted in infected cells to facilitate cell-to-cell spread and prevents NF-κB activation, dampening cytokine expression and neutrophil

recruitment (Gouin, Adib-Conquy, Balestrino et al., 2010). *L. monocytogenes* also secretes nucelomodulins that induce epigenetic changes in host cells. For example, *Listeria* virulence factor OrfX targets RybP in the host cell nucleus that dampens macrophage oxidative response to infection (Prokop, Gouin, Villiers et al., 2017). *L. monocytogenes* is also capable of modifying its cell wall by N-deacelytation of its peptidoglycan (PG) (Boneca, Dussurget, Cabanes et al., 2007). PG is an important target for the innate immune system, and modification of PG by N-deacelytation has been shown to be key to avoiding optimal immune system recognition by NOD2 detection and conferring resistance to lysozyme (Boneca, Dussurget, Cabanes et al., 2007). The control of *L. monocytogenes* by the host immune response is vital in preventing systemic infections.

1.4.8 Systemic infections: Septicaemia

In immunocompromised people *L. monocytogenes* breaches the intestinal barrier and spreads to the *lamina propria*. From here it enters the blood and spread to other organs, the central nervous system and the brain. It does this by circulating in the host blood stream, intracellularly in mononuclear phagocytes and polymorphonuclear leukocytes but also freely in the blood plasma as extracellular bacteria (Drevets, 1999). During blood infection *L. monocytogenes* remodels its cell surface, increasing the amount of InlA and LAP to increase host cell invasions (Quereda, Moron-Garcia, Palacios-Gorba et al., 2021). *L. monocytogenes* can also incorporate D-alanine residues into its cell wall lipotechoic acids through D-alanine-D-alanyl carrier protein ligase operon (*dltABCD*) which reduces susceptibility to cationic antimicrobial peptides and a Δ*dltA* mutant was shown to have reduced numbers of bacteria in the blood of infected mice (Abachin, Poyart, Pellegrini et al., 2002).

1.4.9 Liver and Spleen infection

Once in the bloodstream *L. monocytogenes* can colonise the spleen and liver via the portal vein as early as 4 hours after infection (Melton-Witt, Rafelski, Portnoy et al., 2012). *L. monocytogenes* can also colonise these organs by travelling from the intestine via the mesenteric lymph nodes into the bloodstream (Bou Ghanem, Jones, Myers-Morales et al., 2012). InlB is critical to invasion of these organs, *L. monocytogenes* without a functional *inlB* gene has reduced invasion in a range of cell types including JEG-3 and HeLa and a reduced burden in both the spleen and liver of orally infected mice (Quereda, Rodriguez-Gomez, Meza-Torres et al., 2019).

When *L. monocytogenes* infects the liver, it leads to death of Kupffer cells – a type of professional phagocyte in the liver – and this drives an inflammatory response leading to monocyte recruitment to the liver (Bleriot, Dupuis, Jouvion et al., 2015). When *L. monocytogenes* infects the spleen the early stages of infection are controlled by neutrophils, dendritic cells and macrophages. CD8α+ dendritic cells are recruited to the spleen and these have been identified as a potential reservoir for *L. monocytogenes* to enter the reticuloendothelial system (Edelson, Bradstreet, Hildner et al., 2011). They are intrinsically susceptible to *L. monocytogenes* due to their delayed phagosomal acidification and are an entry point for *L. monocytogenes* to establish invasive infections (Edelson, Bradstreet, Hildner et al., 2011; Witter, Okunnu and Berg, 2016).

1.4.10 Brain infection

Compared to the other forms of invasive listeriosis, neurolisteriosis remains poorly understood. *L. monocytogenes* invades the central nervous through two main pathways: retrograde axonal transport and crossing of the blood-brain barrier (Oevermann, Zurbriggen and Vandevelde, 2010). Retrograde axonal transport occurs through either the oral or the olfactory epitheliums. This most commonly occurs in either ruminants or neonates during birth when *L. monocytogenes* may be

exposed to these areas in large numbers (Pagelow, Chhatbar, Beineke et al., 2018). Crossing of the blood-brain barrier (or the blood-cerebrospinal fluid barrier) can occur when *L. monocytogeenes* that are carried extracellularly in the bloodstream adhere to and invade/cross the surface of the barrier (Grundler, Quednau, Stump et al., 2013). Intracellular *L. monocytogenes* may also be carried across the barrier by infected leukocytes (Greiffenberg, Goebel, Kim et al., 1998).

The key virulence factors involved in brain infection are the internalins and LLO (Banovic, Schroten and Schwerk, 2020). InlA and InlB are required in *in vitro* models for invasion of human choroid plexus papilloma cells – deletion of either of these genes causes a reduction in invasion of these cells (Grundler, Quednau, Stump et al., 2013). InlB specifically may be important for crossing the blood brain barrier – *in vitro* studies in brain microvascular endothelium cell line HBMEC have shown that an InlB-deficient mutant has the greatest drop in invasion capacity (Greiffenberg, Goebel, Kim et al., 1998). The recently discovered Internalin F (InlF) may also play a role in bacterial invasion of the brain, InlF deficient mutants have a reduced entry into human brain microvascular endothelial cell line as well as decreased load in the brain in infected mice (Ghosh, Halvorsen, Ammendolia et al., 2018). LLO-mediated cytotoxicity against HBMEC cells enables *L. monocytogenes* to penetrate the brain microvascular endothelial layer (Zhang, Bae and Wang, 2015). Neurolisteriosis is the most poorly understood of *L. monocytogenes* invasive infections, future research will elucidate its pathogenesis and provide a greater understanding of the disease.

1.4.11 Placental and neo-natal infection

L. monocytogenes can cross the placental barrier in pregnant women either through extracellular bacteria in the blood infecting trophoblasts or by cell-to-cell spread from the maternal phagocytes (Bakardjiev, Theriot and Portnoy, 2006). The route and infection outcomes are dependent on the infectious dose (Vazquez-Boland, Krypotou and Scortti, 2017). InlA and InlB facilitate placental barrier crossing through a co-operative mechanism (Gessain, Tsai, Travier et al., 2015).

Syncytiotrophoblasts are the placental cell type that are in direct contact with maternal blood. These express both E-cad and Met on the surface and thus InlA and InlB are used by *L. monocytogenes* to enter these cells (Charlier, Disson and Lecuit, 2020). However, these cells do not have intrinsic PI3K activity that is required for internalisation of *L. monocytogenes*. InlB activation of the Met pathway promotes PI3K activity and cytoskeletal rearrangement facilitating bacterial internalisation (Disson, Grayo, Huillet et al., 2008). Another internalin – Internalin P (InlP) – has also been implicated in placental invasion. InlP binds to afadin and promotes bacterial transcytosis through the placental epithelial layer (Faralla, Rizzuto, Lowe et al., 2016). These examples demonstrate the adaptability of *L. monocytogenes* to invade a range of tissues due to its array of virulence factors.

1.5 Regulation of virulence factors

The ability of *L. monocytogenes* to infect hosts and form these systemic infections is due to the regulation of its virulence genes. The two main regulons *L. monocytogenes* uses for mammalian infection – SigB and PrfA – are tightly regulated to promote efficient infection. There are a number of regulatory mechanisms for each (Toledo-Arana, Dussurget, Nikitas et al., 2009).

1.5.1 SigB regulation

Stress tolerance and stress response are vital for *L. monocytogenes* to infiltrate the food production pipeline and survive the journey from food to the gastrointestinal tract and beyond. The GSR in *L. monocytogenes* is driven by SigB which is responsible for the regulation of approximately 300 genes. SigB binds directly to the RNA polymerase core which induces the transcriptional changes in this collection of genes.

1.5.2 Regulation of SigB by the stressosome

The activity of SigB is regulated by the anti-sigma factor RsbW and anti-anti-sigma factor RsbV, proteins at the center of a complex regulatory system in *L. monocytogenes* known as the stressosome (Guerreiro, Pucciarelli, Tiensuu et al., 2022). In unstressed conditions RsbV is in a phosphorylated state. However, a complex of proteins made of RsbR, RsbS, RsbL and RsbT senses osmotic stress, acidic stress, or blue light and release RsbT. RsbT activates RsbU phosphatase, which dephosphorylates RsbV. RsbV binds to RsbW and releases SigB which binds to RNA polymerase (Guerreiro, Arcari and O'Byrne, 2020) (Figure 1.5).

Two component systems are also responsible for SigB regulation. Two component systems are sensor/signal transduction systems that are widespread in many species of bacteria (Chan, Hu, Chaturongakul et al., 2008). Currently 16 systems are described in *L. monocytogenes* (Chan, Hu, Chaturongakul et al., 2008). One of these is the LisR/LisK system which has been shown to regulate genes involved in remodelling of the cell envelope (Nielsen, Andersen, Mols et al., 2012). The molecular mechanisms behind these two component systems are currently unclear, but LisRK has been implicated in activating SigB in various conditions such as cold temperatures, low pH and the presence of antibiotics (Cotter, Emerson, Gahan et al., 1999). Treating *L. monocytogenes* with cefuroxime, an antibiotic that targets the cell wall and which activates cell-envelope related genes activates LisRK. LisRK responds to changes in membrane fluidity through an unknown mechanism (Kallipolitis, Ingmer, Gahan et al., 2003)

There is evidence to suggest a regulatory crosstalk between the PrfA and SigB regulons (Gaballa, Guariglia-Oropeza, Wiedmann et al., 2019). However, the role that SigB plays in the activation and modulation of virulence is still an open question. SigB is vital for the bacteria to reach and survive in the gastrointestinal tract, and it also regulates *inlA* and *inlB* for crossing the intestinal barrier (Ollinger, Wiedmann and Boor, 2008). But the mechanisms by which *L. monocytogenes*

establishes systemic infections and an intracellular niche are mostly under the control of the PrfA regulon (Tiensuu, Guerreiro, Oliveira et al., 2019).

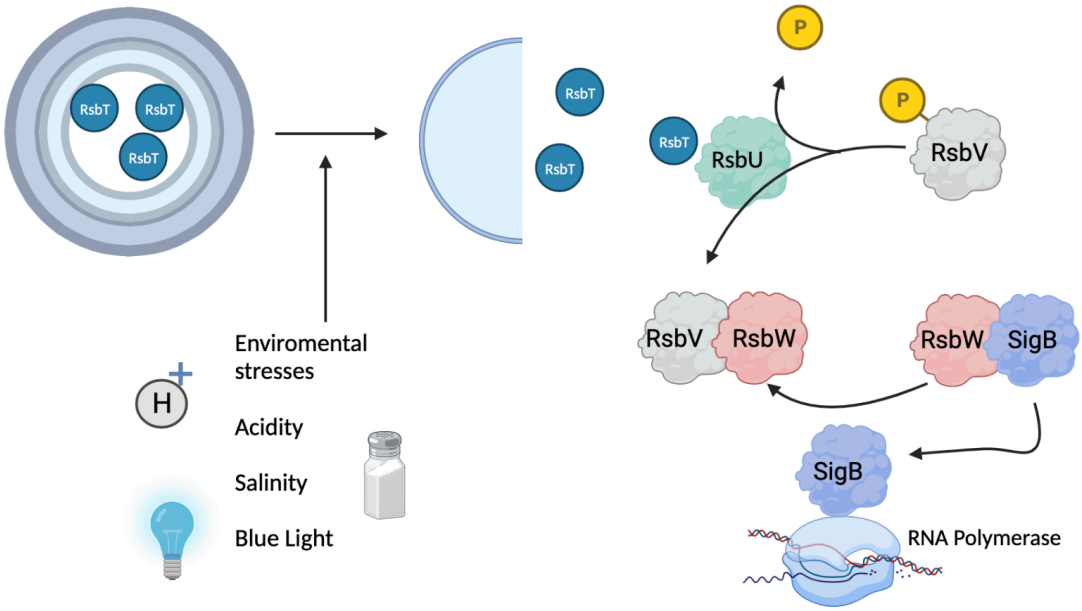

Figure 1. 5. Regulation of SigB in response to stress in *L. monocytogenes.* The stressosome is a complex of proteins containing RsbT. In unstressed conditions RsbT remains in the core of this structure. Stress conditions lead to phosphorylation of the complex and the core of RsbT is released. This initiates a cascade that activates SigB downstream. RsbU dephosphorylates RsbV which couples with RsbW. RsbW is normally bound to SigB – so this binding releases SigB which then binds to RNA polymerase (Adapted from Guerreiro, Arcari and O'Byrne, 2020).

1.5.3 PrfA regulation

PrfA is a 237 residue 27 kDa protein. It belongs to a family of transcription factors termed cAMP receptor proteins/fumarate nitrate reductase regulators (Crp/Fnr) (Wang, Feng, Zhu et al., 2017). PrfA is a homodimer that consists of a N-terminal β-barrel domain, an α-helix linker region that links the N- and C-terminal domains, and a DNA binding domain at the C-terminal, utilising a “winged” helix-turn-helix (HTH) motif, with the HTH domain being complimented with β-strands and loops

(Eiting, Hageluken, Schubert et al., 2005). HTH domains are found in many transcriptional factors as the α-helices are capable of binding to the major groove of DNA (Brennan and Matthews, 1989). PrfA activates transcription of its regulon by binding to a palindromic promoter region (PrfA box) of canonical sequence t**TAAC**annt**GT**t**A**a, which contains seven conserved nucleotides (bold capital letters) and a tolerance of two mismatches. The PrfA box is located at -41bp or -42bp in the target promoters (Scortti, Monzo, Lacharme-Lora et al., 2007). The PrfA regulon contains the core virulence genes: the LIPI-1 genes (Figure 1.3), *inlA* and *inlB*, *bsh* as well as many as 145 other genes that may be indirectly influenced by PrfA including transporters, metabolic enzymes, regulators and proteins of unknown function (Milohanic, Glaser, Coppee et al., 2003). Interestingly many of these genes also fall under SigB regulation – demonstrating the close link between these regulons (Ollinger, Wiedmann and Boor, 2008).

1.5.4 PrfA transcriptional regulation

Variation in sequences of the PrfA boxes in the promoters of genes alter its affinity for PrfA. For example, P*hly* promoter is perfectly symmetrical and has a high affinity for PrfA whereas P*actA* has two nucleotide mismatches and has a lower affinity (Williams, Thayyullathil and Freitag, 2000) (Figure 1.6). The promoter sites upstream of *prfA* play an important role in controlling transcription of the gene. P1 and P2 are regulated by Sigma factor A (SigA) and both SigA/ SigB respectively and produce monocistronic transcripts of *prfA* (de las Heras, Cain, Bielecka et al., 2011). This highlights the close link between the stress response and transition into a virulent pathogenic state. The P2 region has a PrfA box that allows PrfA to negatively regulate itself, however this has been shown to not affect virulence in mice (Tiensuu, Guerreiro, Oliveira et al., 2019). The P3 promoter is PrfA regulated and produces bicistronic transcripts of *plcA* and *prfA*. This is dependent on PrfA activation at temperatures above 30°C, and constitutes a positive feedback loop (Leimeister-Wachter, Domann and Chakraborty, 1992) (Figure 1.6).

1.5.5 PrfA post-transcriptional regulation

The 5' end of the *prfA* mRNA acts as an RNA thermosensor. At temperatures below 37°C a stem-loop blocks the ribosomal binding site. However, at temperatures 37°C or higher, such as in the host, the stem-loop melts and allows ribosomal binding to the Shine-Dalgarno site permitting efficient translation (Johansson, Mandin, Renzoni et al., 2002). S-adenosylmethionine (SAM) riboswitches also play a key role in post transcriptional regulation. Two key ones, SreA and SreB are involved in *prfA* regulation. Binding of SAM to a riboswitch causes early transcriptional termination and the generation of small RNAs 100-250 nucleotides long. Through an unknown mechanism, these bind to the 5' end of the *prfA* mRNA where the thermosensor hairpin is located and inhibit *prfA* expression, however they only do so when the thermosensor is in a melted state and the ribosomal binding site is exposed (Loh, Dussurget, Gripenland et al., 2009) (Figure 1.6).

1.5.6 PrfA post-translational regulation

Crp transcriptional regulators typically have a co-factor that is required for full DNA binding affinity (Hall, Grundstrom, Begum et al., 2016). For a long time, it was hypothesised that PrfA had a co-factor but none had been identified. It was eventually identified as glutathione (GSH) - an antioxidant that protects cells from oxidative damage. GSH binds to PrfA directly and increases the DNA binding affinity of PrfA to the PrfA box. *L. monocytogenes* is able to synthesise its own glutathione and also transport exogenous GSH, which is found in high quantities in the host cell cytosol, and thus GSH acts as a signalling molecule that informs the bacterium that it in the intracellular environment and triggers upregulation of PrfA regulated virulence genes (Reniere, Whiteley, Hamilton et al., 2015) (Figure 1.6).

Carbon sources act as another layer of regulation. In its saprophytic *state L. monocytogene*s utilises environmental sugars such as cellobiose and glucose, which are taken up by the phosphoenolpyruvate phosphotransferase system (PTS) and

have been shown to inhibit virulence factor expression (Milenbachs, Brown, Moors et al., 1997). It is proposed that PTS-dependent sugars are transported trans-membrane and the phosphoryl group of Enzyme II A (EIIA) is transferred to Enzyme II B, leaving EIIA in an unphosphorylated state. In its unphosphorylated state EIIA sequesters PrfA activity through an unknown interaction with PrfA (Freitag, Port and Miner, 2009). However, when *L. monocytogenes* is grown in non-PTS sugars, in particular those that will act as carbon sources in the intracellular environment such as glycerol and glucose-1-phosphate, EIIA is in a phosphorylated state, does not act on PrfA and virulence gene expression is not inhibited (Chico-Calero, Suarez, Gonzalez-Zorn et al., 2002; Johansson and Freitag, 2019).

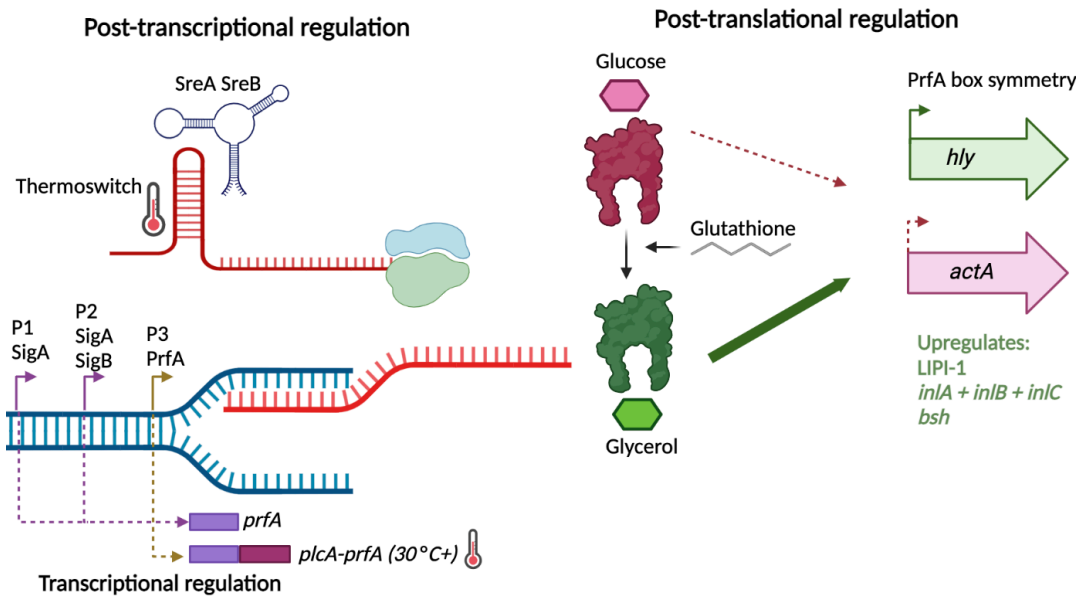

Figure 1. 6. Regulation of PrfA in *L. monocytogenes.* Transcription of *prfA* is regulated by the three promoters P1, P2 and P3 which are regulated by SigA, SigA/SigB and PrfA respectively. Post-transcriptional regulation involves an RNA thermoswitch that melts at 37°C and the SAM riboswitches SreA and SreB. The PrfA protein is regulated post-translationally by glutathione, when unbound (red protein) PrfA has weak DNA binding activity (red broken arrow). Glutathione couples to PrfA (green protein) and greatly increases the transcription of PrfA regulon (green arrow). PTS sugars such as glucose inhibit PrfA activity but host intracellular sugars such as glycerol do not. PrfA-box regulates virulence gene transcription by having variable symmetry and affinity for PrfA, for example P*hly* (green gene arrow) has a perfectly symmetrical PrfA box whereas P*actA* (red gene arrow) has 2 nucleotide mismatches and a lower affinity for PrfA binding.

1.5.7 CodY regulation of *prfA* and *sigB*

CodY acts as a virulence regulator that may be a key pivot in the SigB to PrfA switch that is essential in *L. monocytogenes* transition from saprophyte to pathogen. CodY plays a key role in sensing branched chain amino acids (BCAA) that act as a sensory cue for the bacteria. CodY binds to BCAA when they are in excess and acts as a transcriptional repressor of many genes involved in amino acid biosynthesis (Lobel,

Sigal, Borovok et al., 2012). However, when BCAA concentrations are low – such as in the host cytosol – CodY is freed and *prfA* expression is increased. The binding site for this is 15bp downstream of the *prfA* start codon and it has been suggested that DNA looping plays a role in CodY regulation of *prfA* transcription (Lobel, Sigal, Borovok et al., 2015). Additionally, CodY represses *sigB* transcription in conditions of nutrient excess while repressing genes involved in metabolism and motility (Bennett, Pearce, Glenn et al., 2007). The overlap in CodY regulation between these two regulons therefore plays a role in *L. monocytogenes* sensing the intracellular environment and fine-tuning gene expression to survive in the host (Bennett, Pearce, Glenn et al., 2007; Lobel and Herskovits, 2016).

1.5.8 VirR Regulation

A third regulon involved in *L. monocytogenes* virulence is VirR – the regulator from the two-component sensing system VirR/VirS. The VirR/VirS system has been shown to control genes involved in modification of the bacterial cell surface to combat cationic peptide and a strain of *L. monocytogenes* with a Δ*virR* mutation showed a 100-fold reduction in establishing systemic infections in mice (Mandin, Fsihi, Dussurget et al., 2005) Specifically, VirR/VirS has been shown to regulate the *dltABCD* operon and *mprF* (Mandin, Fsihi, Dussurget et al., 2005). These genes encode proteins that are involved in esterification of the bacterial cell surface with amino acids by lysinylation of phosphatidyl-glycerol by MprF and d-alanylation of cell wall teichoic acid by DltA. This lends resistance to cationic peptides by reducing the negative charge of the surface (Thedieck, Hain, Mohamed et al., 2006). Although it is less well studied than PrfA and SigB, it is thought that the VirR system works to protect *L. monocytogenes* from the environment and certain antimicrobial responses from the host immune system (such as defensins) or antimicrobial compounds (Kang, Wiedmann, Boor et al., 2015).

1.5.9 Other regulatory mechanisms

Several other regulators play an important role in *L. monocytogenes* switch to a pathogenic organism. MogR acts as a repressor for flagella genes and is controlled by a thermosensor antirepressor that releases MogR at 37°C (Shen and Higgins, 2006). This is important for *L. monocytogenes* as flagellins antigenicity are an important signal for the host immune response (Shen and Higgins, 2006). Cold shock proteins CspA, CspB and CspD which were originally thought to be involved in stress tolerance, aggregation and biofilm formation have recently been shown to play a role in virulence. Csp deficient mutants have lower transcript levels of *prfA* and PrfA-regulated virulence genes and impaired epithelial cell invasion (Eshwar, Guldimann, Oevermann et al., 2017).

1.6 Live-cell imaging of infection as a mechanism to study and understand the real time events involved in *L. monocytogenes* invasion of cells.

There is a large degree of complexity in interactions between *L. monocytogenes* and the host. The bacteria has a large array of virulence factors, many with secondary functions. This dynamic nature of the bacteria coupled with the complexity of infection outcomes means that there are potentially many host-cell interactions that are still undiscovered. Live cell imaging of infection has been widely used to study and discover novel interactions between pathogens and hosts. For example, in *Salmonella* live cell imaging was used to show the biogenesis and dynamics of *Salmonella*-induced filaments which are crucial for Salmonella to traffic nutrients into the *Salmonella*-containing vacuoles in which it establishes its intracellular niche (Drecktrah, Levine-Wilkinson, Dam et al., 2008). In *Mycobacterium tuberculosis* live cell imaging discovered members of the Ras superfamily of low molecular weight GTPase which are crucial in the phagosomal arrest that *M. tuberculosis* uses to avoid phagosome-lysosome fusion and maturation and providing it with a vacuole in which it persists (Kyei, Vergne, Chua et al., 2006). Live cell imaging has also

already been successfully deployed in studies of *L. monocytogenes* such as for studying clathrin-mediated uptake via the internalins, vacuole escape and phagosome interactions with LLO and the dynamics of cell-to-cell spread driven by a small population of pioneer bacteria (Henry, Shaughnessy, Loessner et al., 2006; Loessner, Kramer, Ebel et al., 2002; Ortega, Koslover and Theriot, 2019; Veiga, Guttman, Bonazzi et al., 2007).

"Seeing is believing" is a phrase that could not be truer when assessing the value of imaging interactions between human cells and pathogens. Advances in imaging technology means that it is feasible to image the entire infection process, from the exposure of bacteria to host cells up to the establishment of successful infections with excellent temporal resolution (Bain, Gow and Erwig, 2015). In addition, individual interactions can be followed over time to understand the relationship between the pathogen and host and monitor different outcomes. Previous studies have typically used snapshot data which masks the kinetics of these interactions, however these do not capture individual interactions between single host cells and bacteria.

Probabilistic infection outcomes during individual host pathogen interactions are the consequence of heterogeneity of host and pathogen at the single cell level. Only a subset of interactions results in replicative infections. At the single cell level the host has inherently noisy transcription factors and effector gene production, particularly in signalling pathways involved in the host control of *L. monocytogenes* infection, such as NF-κB activation (Adamson, Boddington, Downton et al., 2016), TLR2 and TLR4 signalling (Kellogg, Tian, Etzrodt et al., 2017) and cytokine production (Bagnall, Rowe, Alachkar et al., 2020).Host cells such as Caco-2 and JEG3 cells have also showed single cell heterogeneity with temporally transient susceptibility to *L. monocytogenes* replicative invasions (Costa, Pinheiro, Reis et al., 2020).These heterogenous factors means some host cells are more permissive than others at the time of infection and are a contributing factor for the rarity of replicative invasions.

Pathogens cell-to-cell variability allows rapid adaptability to environmental changes, and diversification of their phenotype across the population, enhancing their survivability in the host (Norman, Lord, Paulsson et al., 2015). Both the SigB and PrfA regulon in *L. monocytogenes* has been shown to be heterogenous at the single cell level in response to environmental triggers, demonstrating how virulence gene expression can vary between individual bacteria (Guldimann, Guariglia-Oropeza, Harrand et al., 2017). The numerous and complex transcriptional, post-transcriptional and post-translational regulatory systems that control the PrfA regulon may contribute to this cell-to-cell heterogeneity.

The single cell variability is also important during the intracellular lifecycle, for example during epithelial cell invasion, a small population of "pioneer" bacteria is present that promote cell-to-cell spread (Ortega, Koslover and Theriot, 2019). *L. monocytogenes* is able to switch from an active motile state to a persistent, non-replicative state in a subset of epithelial cells (Kortebi, Milohanic, Mitchell et al., 2017).

Because of this inherent variability in host and pathogen, interactions between two seemingly similar cells may result in different infection outcomes (Garcia-Del Portillo, 2008). Examples of this can be seen in other intracellular pathogens such as *Salmonella* where invasions of macrophages can result in either bacterial killing and clearance (McIntrye, Rowley and Jenkin, 1967) or persistence leading to systemic host invasions (Stapels, Hill, Westermann et al., 2018). Live cell imaging can capture, characterise and quantify these interactions and outcomes at the single cell level.

Thanks to the widely studied virulence mechanisms of *L. monocytogenes*, it should be possible for imaging experiments to uncover novel and undescribed interactions between host cells through a combination of long-term imaging, targeted manipulation of previously characterised key virulence factors and the development of an appropriate infection model. This could lead to a greater understanding of the infection process of *L. monocytogenes*, potentially providing

new therapeutic targets which can be used to help eradicate *L. monocytogenes* from the food processing pipeline and combat listeriosis on a global scale.

1.7 Aims

A live cell approach to study and quantify single cell interactions between *L. monocytogenes* and host cells, will lead to a greater understanding about the heterogenous host-pathogen interactions and how these affect the probabilistic infection outcomes. To do this, an experimental model that can be utilised to monitor single cell events is required, and these events will need to be quantified and characterised to understand their relevance to infection outcomes.

In order to achieve this, the aims of this study are to:

i) Use live-cell microscopy approaches to develop an *in vitro* infection model for monitoring single-cell host pathogen interactions of *L. monocytogenes*

ii) Characterise key interactions between *L. monocytogenes* and host cells and mechanistically understand regulation of probabilistic infection outcomes

iii) Use molecular microbiology and next-generation sequencing to characterise the role of PrfA regulon in controlling outcomes of single-cell host pathogen interactions of *L. monocytogenes*

2. Materials and Methods

2.1 Bacterial strains, media and growth conditions

L. monocytogenes were routinely grown at 37°C shaking 200 rpm in Tryptone Soya Broth (TSB) (Oxoid) or with additional 1.5% (w/v) agar (Oxoid) on a plate unless otherwise stated. Where required media was supplemented with antibiotic (Erythromycin 5 μg/ml, Chloramphenicol 7 μg/ml).

Escherichia coli were routinely cultured at 37°C shaking 200 rpm in Luria Bertani (LB) broth (1% (w/v) tryptone, 1% (w/v) NaCl, 0.5% (w/v) Yeast Extract) or with additional 1.5% (w/v) agar (Oxoid) on a plate unless otherwise stated. Where required media was supplemented with antibiotic (Erythromycin 300 μg/ml, Chloramphenicol 35 μg/ml).

Table 2. 1. Table of bacterial strains used in this study. Designated strain names used in the text are displayed in brackets.

Bacterial strain	**Features**	Source
Escherichia coli DH5α	*80dlacZΔM1*, *recA1*, *endA1*, *gyrA96*, *thi-1*, *hsdR17*, (rk-mk+), *supE44*, *relA1*, *deoR*, Δ(*lacYZA -argF*) U169, *phoA*	(Hanahan, 1983)
Listeria monocytogenes EGDe::InlA^{M}	Wildtype, serotype 1/2a. Murinised InlA protein. Used as background strain for all strains in this study	(Wollert, Pasche, Rochon et al., 2007)
Listeria monocytogenes EGDe::InlA^{m}::Δ*actA*	EGDe:InlA^{m} with *actA* deletion	Roberts (unpublished data)

Listeria monocytogenes EGDe::InlA^{m}:: *actA*-ΔC	EGDe::InlA^{m} with partial deletion of *actA* gene (C-terminal region) of EGDe, deletion of nucleotides 693-1179.	(Travier, Guadagnini, Gouin et al., 2013), This study
Listeria monocytogenes EGDe:: InlA$^{m::}$ Δ*inlB*	EGDe::InlA^{m} with *inlB* deletion	This study
Listeria monocytogenes EGDe:: InlA^{m}:: GFP (Lm-GFP)	EGDe::InlA^{m} with integrated pAD$_1$-cGFP	(Moran, Feltham, Bagnall et al., 2022)
Listeria monocytogenes EGDe:: InlA^{m} dsRed (Lm-dDsRed)	EGDe::InlA^{m} with pJEBAN6	(Moran, Feltham, Bagnall et al., 2022)
Listeria monocytogenes EGDe:: InlA^{m}:: P*actA*-GFP (Lm-P*actA*-GFP)	EGDe::InlA^{m} with integrated pAD$_3$-P*actA*-GFP	(Moran, Feltham, Bagnall et al., 2022)
Listeria monocytogenes EGDe:: InlA^{m}::dsRed::P*actA*-::GFP dsRed (Lm-dsRed-P*actA*-GFP)	EGDe::InlA^{m} with integrated pAD$_3$-P*actA*-GFP and pJEBAN6	(Moran, Feltham, Bagnall et al., 2022)
Listeria monocytogenes EGDe:: *actA*-ΔC ::dsRed *(*Lm-*actA*-ΔC-dsRed)	EGDe::InlA^{m}:: Δ*actA*-ΔC with pJEBAN6	This study
Listeria monocytogenes EGDe::*actA*-ΔC::dsRed::P*actA*-GFP dsRed *(*Lm-*actA*-ΔC-dsRed-P*actA*-GFP)	EGDe::InlA^{m}:: *actA*-ΔC integrated pAD$_3$-P*actA*-GFP and pJEBAN6	This study

Listeria monocytogenes EGDe::Δ*sigB*::dsRed::P*actA*-GFP dsRed	EGDe:: InlA^{m} with *sigB* deletion and integrated pAD$_3$-P*actA*-GFP and pJEBAN6	Roberts (Unpublished data)
Listeria monocytogenes EGDe::Δ*inlB*::GFP	EGDe::InlA^{m} Δ*inlB* with integrated pAD$_1$-cGFP	This study
Listeria monocytogenes EGDe::Δ*actA*::P*actA*-GFP	EGDe::InlA^{m} ::Δ*actA with* integrated pAD$_3$-P*actA*-GFP	This study

2.1.1 Preparation of bacterial inocula for infection assays

Bacterial inocula were prepared by taking a single colony of the bacteria from a TSB agar plate and placing in TSB (with antibiotics for plasmid strains see Table 2.2) and culturing overnight at 37°C shaking at 200 rpm. 5 ml of this overnight culture was sub-cultured into 100 ml fresh TSB media in a glass conical flask (with antibiotics for plasmid strains – see Table 2.1) and incubated at 37°C. After three hours the OD_{600} of the culture was measured by placing 1 ml into a cuvette and analysing the OD_{600} in a spectrophotometer (Jenway). Readings were taken every 30 minutes until OD_{600} reached a value between 0.5-0.6. The culture was then centrifuged in a benchtop centrifuge (Eppendorf) at 3500 x *g* for 15 mins at room temperature. The supernatant was then removed and the pellet was resuspended in an equivalent volume of room temperature PBS (Sigma). The sample was centrifuged again at 3500 x *g* for 15 mins at room temperature. This wash step was repeated until three washes were completed. After the third wash the pellet was resuspended in 2 ml of PBS with 15% (v/v) glycerol (Fisher). This solution was aliquoted into 70 µl aliquots and was snap frozen by placing into liquid nitrogen for a few seconds. The bacterial inocula were stored at -80°C in PBS with 15% (v/v) glycerol. The viable count for each inoculum batch was recorded by taking three of the frozen samples, serially diluting to a dilution factor of 1.0×10^{-8} and placing 20 µl of this sample onto a TSB agar plate. This was incubated overnight at 37°C and the average of the three samples was recorded as the CFU/ml for the batch of inocula for use in experiments.

2.2 Plasmids

Table 2. 2. List of plasmids used in this study. Cm = Chloramphenicol, Erm = Erythromycin.

Plasmid	Features	Antibiotic	Source
pAD_1-cGFP	Integrative plasmid with constitutive GFP expression	Cm	(Balestrino, Hamon, Dortet et al., 2010)
pAD_3-P*actA*-GFP	Integrative plasmid expressing GFP under control of P*actA*	Cm	(Balestrino, Hamon, Dortet et al., 2010)
pJEBAN6	Plasmid expressing constitutive dsRedExpress	Erm	(Andersen, Roldgaard, Lindner et al., 2006)
pAULA	Cloning vector, pJDC9 derivative, MCS inside *lacZ*, *ori* (Ts)	Erm	(Chakraborty, Leimeister-Wachter, Domann et al., 1992)
pAULA- Δ*inlB*	pAULA vector containing 300bp flanking each side of *inlB*	Erm	This study
pAULA-*actA-ΔC*	pAULA vector containing 300bp flanking each side of *actA* and *actA* gene with deletion of nucleotides 1324 – 1824	Erm	This study

The plasmids constructed for this study were designed in Snapgene. DNA strands were either synthesised externally by GeneArt (ThermoFisher) or obtained by PCR (Section 2.3).

2.3 DNA manipulation

2.3.1 DNA Extraction

Plasmid DNA was extracted from *E. coli* using the QIAprep Miniprep Kit (Qiagen) following the manufacturer's instructions. 5 ml of an overnight culture of *E. coli* was centrifuged at 3500 x *g* for 10 mins at 4°C. The supernatant was removed and the pellet was resuspended in 500 µl of P1 (RNAase A containing) buffer. The solution was transferred to a 1.5 ml Eppendorf tube and 500 µl of buffer P2 (NaOH and SDS-containing buffer, prewarmed to dissolve SDS) and the tube was inverted until the solution was clear and viscous. Neutralising buffer N3 was added and the tube was inverted 4-6 times and the tubes were centrifuged at 13000 x *g* for 10 mins in a benchtop centrifuge (Eppendorf). The supernatant was transferred to a provided spin column and this was centrifuged at 13000 x *g* for 1 min to bind the DNA to the column membrane. 750 µl of Ethanol-containing wash buffer was added to the column and this was centrifuged at 13000 x *g* for 1 min. This was step was repeated then the column was centrifuged a final time at 13000 x *g* for 1 min to remove all traces of wash buffer. 50 µl of pre-warmed (37°C) purified water (MilliQ) was added directly to the column membrane and left for up to 5 mins, the DNA was eluted by centrifuging the column at 13000 x *g* for 1 min. DNA quality and quantity was analysed using a Nanodrop spectrophotometer (ND-1000).

2.3.2 Restriction endonuclease digestion

All of the restriction enzymes and accompanying buffers were purchased from New England Biolabs and used according to the manufacturer's instruction. Table 2.3 lists the restriction enzymes that were used for specific DNA fragments to clone

into plasmid restriction sites. 1-2 µg of DNA fragment or plasmid to be digested was added to a 1.5 ml Eppendorf tube with 5 µl of 10x buffer, 1 µl of each restriction enzyme and the reaction was made up to 50 µl with water. Digestion was performed by placing the tubes in a 37°C water bath for 2 hours.

2.3.3 Purification of restriction digests and PCR products

Purification of restriction digests and PCR products was performed using the QIAQuick PCR Purification Kit (Qiagen) following the manufacturer's instructions. Five volumes of PB binding buffer were added to one volume of PCR/Digest product and mixed briefly. This was transferred to a Mini-Elute column and this column was placed in a 2 ml collection tube and centrifuged for 1 min to bind DNA. Flow-through was discarded and 750 µl of ethanol-containing PE buffer was added to the column to wash the sample and removed enzymes, buffers and nucleotides. The column was centrifuged at 13000 x *g* for 1 min, the flow-through was discarded and the column was centrifuged again to remove remaining traces of wash buffer. 50 µl of pre-warmed (37°C) purified water (MilliQ) was added directly to the column membrane and left for up to 5 mins, the DNA was eluted by centrifuging the column at 13000 x *g* for 1 min. DNA quality and quantity was analysed using a Nanodrop spectrophotometer (ND-1000).

2.3.4 Agarose gel electrophoresis

Agarose gels were prepared by adding 1% (w/v) agarose to TE buffer (0.5 M Tris, 5.7% acetic acid (v/v), 10 mM EDTA adjusted to pH 8.0). This solution was heated until agarose was fully dissolved then left to set in a gel mould with a gel comb to set the required number of sample wells. Samples were mixed with 6x DNA loading dye (Thermofisher) and applied to the wells. The gel was electrophoresed in TE buffer containing 5 µg/ml of ethidium bromide. DNA fragments were then visualised using an ultraviolet transilluminator (GelDoc).

2.3.5 Gel purification of DNA fragments

If DNA fragments were required to be separated by gel electrophoresis before purification then a QIAQuick Gel Extraction Kit (Qiagen) was used. The desired DNA fragment was cut from the gel under UV light using a razor blade. The gel fragment was placed into a 1.5 ml Eppendorf tube containing the manufacturer's recommended amount of buffer QG depending on the gel fragment size. The tube was warmed in a 65°C water bath and vortexed every 2 mins until the gel had fully dissolved into the buffer. The solution was transferred to a column and centrifuged at 13000 x *g* for 1 min to bind the DNA to the column. 750 µl of ethanol-containing PE buffer was added to the column.

2.3.6 Ligation

Ligation of digested plasmid vector and desired digested and purified DNA fragment. Ligations were mixed at ratios of 1:3, 1:5 and 1:10 (Vector:Insert) and the concentrations were determined by Nanodrop spectrophotometer readings (ND-1000). 1 µl of T4-ligase (400U) (New England Biolabs) and 1 µl of 10x ligation buffer (50mM Tris-HCl pH 7.5, 10mM $MgCl_2$ 1mM ATP, 10mM DTT) and the solution was made up to 10 µl total with purified water (MilliQ). The mixture was placed in a bath of room temperature water and transferred to a cold room to be incubated at 4°C overnight. Ligation reaction was analysed by gel electrophoresis (see section 2.3.4).

2.3.7 Polymerase Chain Reaction

PCR was performed in a thermal cycler (Techne) and each reaction was composed of 2 µl of 1 mM of both the required forward and reverse primer (Table 2.3), 5 µl of 10 x PCR Buffer (Roche Molecular Biochemicals) 5 µl of 2.5mM dNTPs (Bioline), 0.3

µl of Taq polymerase, 1 µl of the proof-reading polymerase Pwo and 1 µl of the template DNA. The solution was made up to 50 µl with distilled water (MilliQ). The thermal cycler was set to run: 1 cycle of 94°C for 1 min for initial denaturation, 30 cycles of: 94°C for 15 sec to denature, T_A °C for 30 sec to anneal (T_A is the annealing temperature – the lowest melting temperature of the two primers minus 5°C) and 72°C for 1 min+ to elongate (elongation step has a variable time limit depending on fragment size, 1 min was added for every kb of fragment length) and one final elongation step at 72 °C for 5 mins. All primers were synthesised and purchased from Sigma-Aldrich and are listed in Table 2.3 along with any details of restriction enzyme.

Table 2. 3. Primer list for PCR reactions. Underlining indicates restriction enzyme digestion sites

Primer	Sequence (5'-3')	Enzyme	Notes
dInlB-F1	ACA**GGATCC**AATACT ACACCACCTTCC	BamHI	Forward primer for amplification of 300bp 5' of *inlB* for pAULA- Δ*inlB*
dInlB-R1	TTA**GCATGC**ACTATCC TCTCCTTGATTC	SphI	Reverse primer for amplification of 300bp 5' of *inlB* for pAULA- Δ*inlB*
dInlB-F2	TTA**GCATGC**CTGAAA AAGACCTAAAAAAGA AG	SphI	Forward primer for amplification of 300bp 3' of *inlB* for pAULA- Δ*inlB*
dInlB-R2	AAC**GTCGAC**ATAAGT AAAAGTCCTCCG	SalI	Reverse primer for amplification of 300bp 3' of *inlB* for pAULA- Δ*inlB*
V-actAC-F	CAGAAGAAGAAATTG ATCGCCTAG	-	Primer flanking 5' end of deleted region in *actA-Δ*C used to screen and validate mutant
V-actA-C-R	AGAACACGCCAATAG CTAAC	-	Primer flanking 3' end of deleted region in *actA-Δ*C used to screen and validate mutant

2.3.8 DNA sequencing

Any plasmids or synthesised fragments that were used for downstream applications were validated by Sanger sequencing, performed externally by Eurofins. Samples were prepared by adding 4 µM of primer, 150-300 ng of plasmid DNA and distilled water (MilliQ) to a 1.5 ml Eppendorf. Once the results were received the sequences were analysed by BLAST (Boratyn, Camacho, Cooper et al., 2013) to check the sequence against a reference strain or if the DNA was mutated or novel the sequence was checked in Snapgene.

2.4 Strain constructions

2.4.1 Plasmid construction

Several plasmids were constructed for this study and a list of all plasmids is shown in Table 2.2. These plasmids were constructed by the DNA manipulation methods described in Section 2.3 whereby a fragment with compatible restriction endonucleases was either synthesised or generated through PCR, and this was ligated into a digested vector to form the new plasmid. Plasmids were used to generate new strains by first cloning into *E. coli* to produce a high number of plasmids and stable plasmid-producing strain for storage. These were then extracted, purified and transformed into *L. monocytogenes.*

2.4.2 Preparation of chemically competent DH5α *Escherichia coli*

Chemically competent *E. coli* were prepared by adding 2 ml of *E. coli* DH5α overnight culture into 200 ml LB media with 30 mM $MgCl_2$ and growing at 37°C 200rpm in a shaking incubator until mid-log phase. The culture was pelleted by centrifuging at 3500 x *g* 4°C for 15 min and resuspending in 60 ml of a solution of 10 mM $MgCl_2$, 50mM $CaCl_2$ and 10 mM MES. The solution was incubated on ice for 20

min and then pelleted again for 5 min at 3500 x *g* 4°C and resuspended in 12 ml of the same solution mixed 50% (v/v) with glycerol. The bacteria were aliquoted into 200 µl in 1.5 ml Eppendorf tubes, snap frozen in liquid nitrogen and stored at -80°C until required. The bacteria were gently thawed on ice when required.

2.4.3 Transformations with competent DH5α *E. coli*

Competent DH5α cells were retrieved from -80°C storage and placed on ice. 100 µl of DH5α was added to up to 100 ng of plasmid in a 1.5 ml Eppendorf tube. This mixture was left for ice for 30 mins then transferred to a 42°C water bath for 90 seconds. It was then placed on ice for 2 mins and 750 µl of LB broth was added to each tube and incubated at 37°C 200 rpm for 45 mins. 200 µl of the solution was placed onto and LB agar plate (with antibiotic for plasmid selection see Table 2.2) and incubated overnight at 37°C. Successful colonies were transferred to a fresh agar plate and screened for presence of desired plasmid using colony PCR (see section 2.4.6).

2.4.4 Preparation of electrocompetent *L. monocytogenes* cells

A single colony from a streaked agar plate of *L. monocytogenes* EGDe::InlA^{m} was added to 10 ml of TSB in a 50 ml conical tube (Falcon). The tube was incubated overnight at 37°C 200 rpm and 1 ml of this overnight culture was sub-cultured into 100 ml of TSB supplemented with 0.5M sucrose. This was incubated at 37°C and 200 rpm for 4 hours. 1 mg of penicillin G was then added to the culture and it was incubated at 37°C 200 rpm for a further 2 hours. The solution was centrifuged (Eppendorf) at 3000 x *g* for 2 mins at 4°C. The supernatant was removed and the pellet was resuspended in 50 ml of 0.5M sucrose with 1mM HEPES adjusted to pH 7.5. The solution was centrifuged again at 3500 x *g* for 20 mins and this process was repeated until three wash steps had been completed. After the third wash the final pellet was resuspended in 300 µl of the sucrose/HEPES solution for use in

transformations. These bacteria were viable for transformations for up to a week when kept at 4°C.

2.4.5 Transformations with electrocompetent *L. monocytogenes*

TSB was pre-warmed to 37°C and electroporation cuvettes were cooled in plastic packaging on ice. 2 µg of plasmids to be transformed were added to the cuvettes and 50 µl of competent *L. monocytogenes* cells were added to the cuvettes. The cuvettes were then placed in the electroporator (BioRad Gene Pulser II) which was set to 2.5 kV, 25 µF and 200 Ω. Sample was pulsed, and if a successful time constant of 3-5 ms was achieved the sample was transferred to 1 ml of the pre-warmed TSB. Samples were incubated at 37°C for 1 hour. 250 µl were then plated onto TSB-antibiotic (see Table 2.2) plates and grown overnight at 37°C. Colonies were patch plated onto TSB agar with appropriate antibiotic (Table 2.2). These were incubated at 37°C overnight.

2.4.6 Colony PCR

Colony PCR was performed using MyTaq Red Mix (Bioline). A single colony of the bacteria for desired screening was transferred by using a 2 µl pipette tip to a solution containing 25 µl of 2x MyTaq Red mix, 1 µl of 100 µM forward and reverse primers (final concentration of 20 µm) and 23 µl of distilled deionised water (MilliQ). The PCR cycling conditions were set to the manufacturer's recommendations. 1 cycle of 95°C for 1 min for initial denaturation, 30 cycles of 95°C for 15 sec to denature, primer specific annealing temperature for 15 sec to anneal and 72°C for 30 seconds for extension (increased for long template lengths), and 1 cycle of 72°C for 5 mins for a final extension. Colony PCR samples were checked on an agarose gel by electrophoresis (section 2.3.4) against a negative and positive control and positive samples were processed for plasmid extraction for a digestion and sequencing to confirm results.

2.4.7 Induced homologous recombination with pAULA

For the knockout and partial knockout strains (see Table 2.1) additional steps were required after transformation to drive the plasmid onto the genome and screen for recombinant bacteria. Colonies identified with a positive colony PCR were transferred onto a fresh TSB agar plate with 5 µg/ml erythromycin. These were incubated overnight at 42°C. The colonies were then transferred again to a fresh TSB agar plate with 5 µg/ml erythromycin and incubated overnight at 42°C. A colony PCR was performed (section 2.4.6) to identify positive colonies. These were then transferred to TSB and cultured overnight at 30°C and 200 rpm in a shaking incubator. The colonies were sub-cultured into fresh TSB every day by taking 1 ml of the overnight culture and pipetting it into 10 ml of fresh TSB and incubating at 30°C and 200 rpm in a shaking incubator. On day 6 each overnight culture was serially diluted in PBS to a dilution factor of 1.0×10^{-7}. Dilution factors 10^{-5} to 10^{-7} were transferred to TSA plates and quantified by spread plate method and incubated overnight at 42°C. The colonies from the lowest successful dilution factor were transferred to fresh TSB agar plates – one with 5 µg/ml antibiotic and one without. All colonies that grew on the control plate but were inhibited by the antibiotic on the erythromycin agar plate were screened with colony PCR to confirm the presence of the required gene.

2.4.8 Construction of individual mutant strains

All the strains constructed in this study were created using the methods described in Section 2.4. Mutant strains without fluorescent proteins, such *Listeria monocytogenes* EGDe::InlAm::Δ*inlB,* were constructed by PCR of the desired gene, insertion of the PCR product or synthesised strand of DNA into pAULA by restriction cloning, transformation into electrocompetent *L. monocytogenes* and induced homologous recombination. Strains with fluorescent proteins such as *Listeria monocytogenes* EGDe:: *actA*-ΔC dsRed (Lm-*actA*-ΔC-dsRed) were constructed by the same method, with an additional transformation of the fluorescent protein

plamid into the mutant background strain (See Table 2.2). All DNA strands for cloning were obtained by PCR except for *actA*-ΔC which was synthesised.

2.5 Mammalian Cell Culture

2.5.1 Culturing of HeLa Cells

HeLa cells were grown in Dulbecco's modified eagle media (DMEM, Sigma) supplemented with 10% (v/v) fetal calf serum (FCS, Gibco) and 1% (v/v) non-essential amino acids (Gibco) at 37°C 5% CO_2 (v/v). Cells were maintained by sub-cultivating at a ratio between 1:2 to 1:6 split 2-3 times a week depending on cell density. Passage number was maintained between passage 8-20. For use in infection assays the cells were counted using a 1:1 ratio of 4% (v/v) Sigma Trypan Blue:Cell Suspension on a haemocytometer and seeded at a density of 2.0 x 10^5 cells in either a 1-compartment imaging dish or a 4-comparment imaging dish (Greiner Bio One) the day before invasion assay and incubated at 37°C 5% CO_2 (v/v).

2.5.2 Culturing of HeLa cells transfected with E2F1-Venus

HeLa cells transfected with E2F1-Venus were obtained from Ankers et al. (2016), this cell line was constructed by transfection using a bacterial accessory chromosome (BAC), details of which can be found in their study. Transfected HeLa cells were cultured as described in 2.5.1 however the cell media was supplemented with 10 µg/ml of Geneticin (Gibco) during sub-cultivation.

2.5.3 Culturing of HUVEC cells

HUVEC cells (Thermo Fisher) were recovered from cryopreservation at a density of 2.5 x 10^3 viable cells / cm^3. Viable cells were counted from the cryopreservation vial by mixing 10 µl of defrosted cells with 10 µl of trypan blue solution and counting under a microscope on a haemocytometer. The contents of the cryopreservation vial were diluted to a concentration of 1.25 x 10^4 cells/ml in Human Large Vessel Endothelial Cell Basal Medium (HLVEM, Thermo Fisher) supplemented with Large Vessel Endothelial Supplement (Thermo Fisher). 15 ml of this suspension was transferred to a 75 cm^2 cell culture flask (Corning). The solution was swirled to distribute HUVEC cells evenly across the flask surface then incubated at 37°C and 5% CO_2 (v/v) for at least 24 hours. To subculture the HUVEC cells the culture medium was removed from the flask and replaced with 4 ml of Trypsin/EDTA solution (Thermo Fisher). The solution was spread over the surface of the flask then 3 ml of Trypsin/EDTA solution was removed. The flask was incubated at 37°C for 2 minutes. The cells were viewed under a microscope until rounded and the flask was gently tapped to loosen cells from flask surface. 3 ml of Trypsin Neutralizer Solution (Thermo Fisher) was added to the flask and the solution was transferred to a 15 ml conical tube (Corning). The tube was centrifuged (Eppendorf) at 180 x *g* for 7 mins. Supernatant was removed and the pellet was resuspended in 4 ml of HLVEM. Cells were mixed with a pipette to ensure homogenous resuspension and counted under a microscope using 1:1 trypan blue solution and a haemocytometer. The cells were diluted in the HLVEM and seeded in a fresh T75 flask (Corning) at a cell density of 2.5 x 10^3 cells/cm^2. These were incubated at 37°C 5% CO_2 (v/v) and not disturbed for at least 24 hours. Once cell density reached 80% confluency the subculture procedure was repeated again. The cells were not used for more than 16 population doublings after the initial recovery as per the providers recommendations.

2.5.4 Culturing of Caco-2 cells

Cryopreserved Caco-2 cells were thawed by agitation in a 37°C water bath. The contents were transferred to a 15 ml tube (Corning) with 9 ml of DMEM culture medium. The tube was centrifuged at 125 x *g* for 5 mins and the supernatant was discarded. The cells were resuspended in 15 ml DMEM and transferred to a 75 cm^2 culture flask (Corning) and incubated at 37°C 5% CO_2 (v/v). The media was refreshed every 2-3 days and sub-culturing was performed when cells reached 80% confluency. To subculture the cells culture medium was removed and discarded and the cell layer was washed with PBS. 3 ml of Trypsin-EDTA solution was added and the cells were incubated at 37°C for 2 mins. 8 ml of DMEM was added to neutralise Trypsin and cells were further removed from flask surface by gentle pipetting. Viable cell count was calculated by counting the cells under an inverted microscope in a 1:1 solution of Trypan Blue solution in a haemocytometer. The cells were diluted to a density of 1 x 10^4 cells / cm^2 and transferred to a fresh 75 cm^2 cell culture flask (Corning) and incubated at 37°C 5% CO_2 (v/v) until required for experiments or ready for sub-culturing.

2.6 Aggregation assay

2.6.1 Preparation of Spent Media

1 ml of host cells were seeded into an imaging dish in DMEM supplemented with FCS and L-glutamine at a cell density of 2.0 x 10^5 cells/ml and incubated overnight at 37°C 5% CO_2 (v/v). The next day the DMEM was aspirated off the cells, they were washed with PBS and the media was replaced with serum-free DMEM (no FCS). The cells were incubated overnight at 37°C 5% (v/v) CO2. The next day this “spent media” was removed from the host cells and kept at 37°C until ready for use.

2.6.2 Aggregation assay

1 ml of spent media was added to a 75 cm^2 imaging dish and the bacterial inoculum was added to a final bacterial cell density of 1.0 x 10^7 CFU/ml. In some experiments a control was also performed, this was the same serum free media that hadn't been incubated overnight on mammalian cells. The dish was sealed with parafilm and either incubated at 37°C 5% CO_2 (v/v) in a cell culture incubator or incubated at 37°C 5% CO_2 (v/v) on the incubation unit of LSM 880 while imaged. A time series was taken every 15 seconds in an individual tile with brightfield, 488nm and 561nm lasers using the z-stack function taking 4 slices with 12.24 µM distance between the first and last slice. In non-fluorescent strains the 488 nm laser and brightfield was used for analysis.

2.6.3 Denaturation of proteins in spent culture media.

1 ml of spent media was placed in a 1.5 ml Eppendorf tube and heated to 100°C in a heat block (Grant) for 2 mins. After heating the boiled spent media was transferred to an imaging dish and an aggregation assay was performed (Section 2.6.2) to analyse changes in bacterial response compared to spent media alone.

2.6.4 Protein fractionation by size on spent media

Fractionation of spent media was performed using a Microcon Centrifugal 10k Filter Device. Column was inserted into a tube and 0.5 ml of spent media was added to the column taking care not to touch membrane with pipette tip (spin was repeated multiple times to produce larger volumes). The device was transferred to a table top centrifuge (Eppendorf) and centrifuged at 14,000 x *g* for 30 mins to elute flow-through. A new 1.5 ml Eppendorf tube was placed over the top of the device and centrifuged at 1000 x *g* for 3 mins to retrieve concentrate. This process was repeated until enough concentrate and flow-through was isolated to perform the aggregation assay (Section 2.6.2).

2.6.5 GFP expression analysis

For analysing GFP expression in single cells by microscopy, the aggregation assay was performed as described in 2.6.2 and the images were analysed in FIJI (Schindelin, Arganda-Carreras, Frise et al., 2012). Endpoint images at 2 hours were analysed by using the freehand draw tool in FIJI to mark regions of interest pertaining to individual bacteria for both the spent media sample and the fresh media sample. These were then analysed in the GFP channel by using the mean Intensity function to determine GFP expression.

2.6.6 RNA extraction

RNA extraction was performed using Purelink RNA Extraction Kit (Invitrogen) and Lysing Matrix E tubes (MP Biomedicals. Fresh lysozyme solution (10 mM Tris-HCl, 0.1 mM EDTA, 10 mg/ml lysozyme), 10% SDS (v/v) in RNAse-free water and lysis buffer (supplemented with 10 µl of 2-mercaptoethanol per 1 ml of buffer) were prepared before extraction. Bacterial cells were pelleted by centrifuging at 13000 x *g* for 3 mins and the supernatant was discarded. 100 µl of lysozyme solution was added and the pellet was resuspended by vortex. 0.5 µl of 10% (v/v) SDS solution was added and mixed via vortex. 350 µl of lysis buffer was added and mixed by vortex. The lysate was transferred to a Lysing Matrix E tube and homogenised in a rotor stator homogeniser (FastPrep FP120) at 6.5 speed setting for 45 seconds. The tube was centrifuged at 2600 x *g* for 5 mins and the supernatant was transferred to a RNAse-free microcentrifuge tube. 250 µl of 100% (v/v) ethanol was added to the tube and mixed by vortex to remove precipitate. The sample was transferred to a kit spin cartridge and centrifuged at 12000 x *g* for 15 seconds to bind RNA to column. Flow-through was discarded and 700 µl of Wash Buffer 1 (was added to the column. The column was centrifuged at 12000 x *g* for 15 sec and both the flow through and collection tube were discarded. The column was placed in a new collection tube and 500 µl of Wash Buffer 2 was added to the column. This was centrifuged at 12000 x *g* for 15 sec, and flow-through was discarded. The wash step

with Wash Buffer 2 was repeated and after flow-through was discarded again the column was centrifuged at 12000 x *g* to remove any residual wash buffer. The collection tube was discarded and the column was transferred to a recovery tube (RNAse free 1.5ml tube provided by kit) and 50 µl of RNAse free water was carefully added directly to the column membrane. This was incubated for 1 min at room temperature to elute RNA and then centrifuged at 12000 x *g* for 2 mins. All downstream work with RNA after this point was performed on ice to help preserve samples. RNA quantity was analysed by placing 1 µl of sample into a Nanodrop spectrophotometer (ND-1000). Super RNAse Inhibitor (Invitrogen) was added to the samples at a concentration of 1U/µl to inhibit any potential RNAse activity.

2.6.7 Removing genomic DNA from RNA samples

Genomic DNA (gDNA) was removed using TURBO DNAse kit. 0.1 volume of 10x TURBO DNAse buffer and 1 µl of TURBO DNAse was added the RNA samples and gently mixed. The samples were incubated in a 37°C water bath for 30 mins. The solution was mixed by vortex and 2 µl of DNAse inactivation reagent was added. The sample was incubated for 5 mins at room temperature and flicked 2-3 times during incubation to keep inactivation reagent suspended throughout the mixture. Sample was centrifuged at 10,000 x *g* for 90 sec and the supernatant was transferred to a fresh RNAse free collection tube. Samples were frozen at -80°C until ready for sequencing.

2.6.8 Quality Control of RNA samples

A small aliquot of each sample was taken before storage at -80°C for analysis of RNA integrity, concentration and presence of gDNA using an Agilent Tapestation System. 5 µl of the gel supplied loading dye (Agilent) was added to 1 µl of RNA sample in a 0.2 ml PCR tube. This was briefly centrifuged and the samples were heated at 72°C for 3 mins then placed on ice for 3 mins. Once cooled they were briefly vortexed and centrifuged to remove condensation from tube lids. The

samples were transferred to the Agilent TapeStation System and analysed using the 'Prokaryotic RNA' and 'No Ladder' user setting. RIN values and gels were shared with the sequencing facility to ensure samples were high enough quality for RNA-Seq.

2.6.9 RNA-Seq

RNASeq was performed by the Genomic Technology Core Facility. A ribosomal depletion kit (Illumina) was used to deplete ribosomal RNA from the provided samples as per manufacturer's instructions. An RNA sample prep kit (Illumina Stranded Total RNA Prep) was used to fragment and denature RNA, synthesise first and second strands, adenylate 3' prime ends, ligate anchors, clean up fragments and amplify and clean up the library. Additional probes to efficiently deplete the rRNA from *L. monocytogenes*. were added during the probe hybridization step on recommendation from *in silico* analysis performed by Illumina. Libraries were added to an eqimolar pool which was quantified by qPCR (KAPA). The pool was then denatured and loaded onto one lane of an SP NovaSeq 6000 flowcell using the XP workflow, at 200pM with 1% (v/v) PhiX spiked in. The NovaSeq 6000 was run in XP mode with (sequencing lengths: Read 1: 59bp, i7 index: 10bp, i5 index: 10bp, Read 2: 59bp**).**

2.6.10 Analysis of RNA-Seq results

Unmapped paired-end sequences from an Illumina HiSeq4000 sequencer were tested by FastQC. Sequence adapters were removed, and reads were quality trimmed using Trimmomatic_0.39 (Bolger, Lohse and Usadel, 2014). The reads were mapped against the reference *Listeria monocytogenes* EGDe Genome and annotation. Counts per gene were calculated using featureCounts (subread_2.0.0) (Liao, Smyth and Shi, 2014). Normalisation, Principal Components Analysis, and differential expression was calculated with DESeq2_1.36.0 (Love, Huber and Anders, 2014).

2.7 Internalisation assay

2.7.1 Internalisation of bacteria by host cells

HeLa cells were cultured in an imaging dish to a density of 2.0 x 10^5 cells and incubated overnight as described in section 2.5.1. Bacterial inocula (section 2.1.1) of the constitutively dsRed expressing *L. monocytogenes* in both the wildtype (Lm-dsRed) and *actA*-ΔC mutant *(*Lm-*actA*-ΔC-dsRed) were defrosted on ice and then added to 3 ml of cell media with no FCS at 1.0 x 10^7 CFU/ml. Cell media was aspirated off of the host cells in the imaging dish, they were washed with PBS and 1 ml of the media containing bacteria was added to the imaging dish. This was incubated at 37°C 5% CO_2 (v/v) for 2 hours.

2.7.2 Fixing and Staining

DMEM was removed from the imaging dish and the cells were washed twice with PBS. 1 ml of 4% (v/v) paraformaldehyde suspended in PBS was added and the dishes were incubated at room temperature for 20 mins. The PFA was removed and the cells were washed 3x in PBS. The cells were incubated with blocking buffer (1% (v/v) BSA, 22.52 mg/ml glycine, 0.1% (v/v) tween-20) for 30 mins and washed with PBS three times to remove residual buffer. 300 µl of diluted (1:500 from supplier stock - 8 µg/ml) rabbit anti-Listeria antibody (Abcam, ab35132) and incubated at room temperature for 20 mins. They were washed 3x in PBS and then secondary antibody donkey anti-rabbit IgG Brilliant Violet 421 (Biolegend) was added and incubated at room temperature for 20 mins and then washed 3x in PBS.

2.7.3 Imaging

Images were taken with a Zeiss 880 confocal microscope with 40x objective (1.4 NA) immersion oil lens. Images were taken using the Zen Black software. For excitiation of dsRed a wavelength of 561 nm at 1% strength was used and for

Brilliant violet 421 a wavelength of 405nm at 0.2% was used. Z-stack images were taken with 5 slices and a distance of 12.24 µm between the first and last slices.

2.7.4 Analysis of fixed images

Images were analysed by loading into FIJI and counting the number of bacteria in each aggregate. Internalised bacteria were recorded as those that were excited by the 561 nm laser for dsRed but were not excited by the 405 nm laser settings – representing that they had been internalised and could not be stained with the anti-*Listeria* antibody. The number of internalised bacteria and the size of internalised aggregates was recorded. Additionally, the size of each external aggregate, total number of aggregates and total number of host cells were recorded. The number of associated bacteria per cell was calculated by taking the total number of associated bacteria and dividing the total number of host cells. Probability of invasion was calculated by dividing the number of invading bacteria by the total number of imaged bacteria. Aggregate size probability was calculated by calculating the number of aggregates of a given size by the total number of objects (an object being defined as an aggregate of bacteria).

2.8 Infection Assay

2.8.1 Infection Assay in HeLa cells

HeLa cells were seeded from a cultured flask into an imaging dish to a density of 2.0 x 10^5 and incubated overnight. Bacterial inocula were defrosted on ice and then added to 3 ml of cell media with no FCS at 1.0 x 10^7 CFU/ml. The imaging dish was loaded onto a Zeiss 880 confocal microscope with an incubation unit set to 37°C and 5% CO2 (v/v). Images were taken using a 40x objective (1.4NA) oil immersion lens. For GFP excitation the 488 nm laser (3% strength) was used, and for dsRed the 561 nm (0.5% strength). A 9-tile scan of the HeLa cells before the addition of bacteria was taken using the Z-stack function taking 4 slices across 12.24 µm

between the first and last slice. The media was pipetted off the HeLa cells, they were washed with 2 ml PBS and then 1 ml of bacteria in media was added to give a multiplicity of infection (MOI) of 20 based on the CFU/ml of the inocula and the density of the HeLa cells.

A time series was taken every 15 seconds in an individual tile with brightfield, 488nm and 561nm lasers using the z-stack function taking 4 slices with 12.24 µM distance between the first and last slice. After 2 hours, the media was pipetted off, the cells were washed 3 times with PBS and 2 ml of DMEM containing 10 µg/ml of gentamicin was added to the dish. A time series 9-tile scan was taken imaging every 3 minutes with the same imaging settings described for the first 2 hours.

2.8.2 Infection Assay with HUVEC cells

HUVEC cells were seeded from a cultured flask into an imaging dish to a density of 2.0×10^5 and incubated at 37°C 5% CO_2 (v/v) overnight. Bacterial inocula were defrosted on ice then added to 3 ml of Human Large Vessel Endothelial Cell Basal Medium at a bacterial cell density of 2.5×10^6 CFU/ml. The imaging dish was transferred to a Zeiss 880 confocal microscope with an incubation unit set to 37°C and 5% CO_2 (v/v). Images were taken using a 40x objective (1.4NA) oil immersion lens. The cells were washed gently with cell media then 1 ml of bacteria in cell media (Lm-dsRed-P*actA*-GFP, Lm-*actA*-ΔC-dsRed-P*actA*-GFP) was added to the host cells at a MOI of 5. A time series was taken every 15 seconds in an individual tile with brightfield, 488nm and 561nm lasers using the z-stack function taking 4 slices with 12.24 µM distance between the first and last slice. After 2 hours, the media was pipetted off, the cells were washed 3 times with Human Large Vessel Endothelial Cell Basal Medium and 2 ml of Human Large Vessel Endothelial Cell Basal Medium containing 10 µg/ml of gentamicin was added to the dish. A time series 9-tile scan was taken imaging every 3 minutes with the same settings as described for the first 2 hours.

2.8.3 Infection Assay Data Analysis

The Z-stack images for the infection assays were analysed in ZEN Black. A maximum intensity projection was generated from the Z-stacks to produce a single plane image. This image was then manually analysed to look for individual events that lead to replicative invasions. Replicating bacteria were identified by tracking individual cells over time, once a replicative invasion had been identified it was tracked through the time points to identify individual invasion events. Infection assay success was analysed by calculating the number of successful replicative invasions and recording it as a proportion of the total number of host cells present in the image at the first time point.

Representative images of invasions were generated by using the crop function and exporting the image as .tif file using the export function in ZEN.

2.8.4 Gentamicin Protection Assay in HeLa cells

Cultured HeLa cells were seeded at a density of 2.0×10^5 in a 6 well plate and incubated overnight at 37°C 5% CO_2 (v/v). Subsequently the DMEM was aspirated off the cells and the cells were washed in PBS. PBS was aspirated off and serum-free DMEM containing 1.0×10^7 CFU/ml *L. monocytogenes* was added to the 6 well plates to give a MOI of 20 (this was changed as a variable in MOI experiments). The plates were incubated for 2 hours at 37°C 5% CO_2 (v/v). The serum-free DMEM was then aspirated from the wells and the wells were washed in 2 ml of PBS twice and then 2 ml of serum-free DMEM supplemented was added to all the wells except the wells being analysed for the first time point which were processed immediately. Remaining plates were then incubated until the required time point. Bacterial cells were retrieved and enumerated by aspirating the serum-free DMEM from the wells, washing the wells in 1 ml of PBS three times and then adding 1 ml of PBS with 0.5% (v/v) triton to lyse the host cells for 2 mins. This solution was then mixed with pipette in the well and transferred to a 1.5 ml Eppendorf. A serial dilution up to a

dilution factor of 10^{-5} was performed in PBS and 20 µl of all the dilutions was transferred in triplicate to a TSB agar plate. Plates were left to dry on the bench and then transferred to an incubator and incubated overnight at 37°C. Colonies were counted and multiplied by the dilution factor to retrieve the CFU/ml for each well.

2.8.5 Co-infection Assay with HeLa cells

HeLa cells were seeded from a cultured flask into an imaging dish to a density of 2.0 x 10^5 and incubated overnight. The strains used in the co-infection assay were Lm-GFP and Lm-*actA*-ΔC-dsRed (Table 2.1). Both strains used in the co-infection assay were defrosted on ice from inocula and then added to 3 ml of cell media with no FCS at 5.0 x 10^6 CFU/ml – making a total bacteria density of 1.0 x 10^7 CFU/ml. The imaging dish was transferred to a Zeiss 880 confocal microscope with an incubation unit set to 37°C and 5% CO_2 (v/v). Images were taken using a 40x objective (1.4NA) oil immersion lens. For GFP excitation the 488nm laser (1.5% strength) was used, and for dsRed the 561nm (0.5% strength). A 9-tile scan of the HeLa cells before the addition of bacteria was taken using the Z-stack function taking 4 slices across 12.24 µm between the first and last slice. The media was pipetted off the HeLa cells, they were washed with 2 ml PBS and then 1 ml of bacteria in media was added to give a multiplicity of infection (MOI) of 20 based on the CFU/ml of the inocula and the density of the HeLa cells.

A time series was taken every 15 seconds in an individual tile with brightfield, 488nm and 561nm lasers using the z-stack function taking 4 slices with 12.24 µM distance between the first and last slice. After 2 hours, the media was pipetted off, the cells were washed 3 times with PBS and 2 ml of DMEM containing 10 µg/ml of gentamicin was added to the dish. A time series 9-tile scan was taken imaging every 3 minutes with the same settings as described for the first 2 hours.

2.8.6 Competition Assay Data Analysis

The Z-stack images for the infection assays were analysed in ZEN Black. A maximum intensity projection was generated from the Z-stacks to produce a single plane image. This image was then manually analysed to look for individual events that lead to replicative invasions. Replicating bacteria were identified by tracking individual cells over time, once a replicative invasion had been identified it was tracked through the time points to identify individual invasion events. The proportion of successful replicative invasions was analysed separately for each strain by calculating the number of successful replicative invasions and recording it as a proportion of the total number of host cells present in the image at the first time point. These were directly compared between mutants

Representative images of invasions were generated by using the crop function and exporting the image as .tif file using the export function in ZEN.

2.9 MET Depletion

2.9.1 MET staining on HeLa cells

HeLa cells were cultured in an imaging dish to a density of 2.0×10^5 and incubated overnight. DMEM was removed from the imaging dish and the cells were washed twice with PBS. 1 ml of 4% paraformaldehyde (v/v) suspended in PBS was added and the dishes were incubated at room temperature for 20 mins. The PFA was removed and the cells were washed 3x in PBS. The cells were incubated with blocking buffer (1% (w/v) BSA, 22.52 mg/ml glycine, 0.1% (v/v) tween-20) for 30 mins and washed with PBS three times to remove residual buffer. 5 µg/ml of primary goat Anti-MET antibody (Abcam) suspended in blocking buffer was added to the dish and left for 1 min. The cells were washed 3x with PBS by adding the PBS and leaving it for 20 mins before removing and changing the PBS. After the washes the secondary antibody 10 µg/ml Alexafluor 488 anti-Goat (Abcam) was added and

incubated at room temperature for 30 mins. The cells were washed 3x with PBS for 20 mins per wash. DAPI Vectashield was added to the dish to preserve fluorescence and to stain cell nuclei with DAPI. The cells were imaged using a Zeiss 880 confocal microscope and a 40x objective (1.4NA) oil immersion lens. 488nm laser at 2% strength was used for excitation settings and background signal was removed by calibrating against a negative control with no staining.

2.9.2 MET depletion of HeLa cells

To deplete the cell surface of MET, 2 µg/ml of primary antibody was added to serum free DMEM and this was incubated on the cells for 1 hour at 37°C 5% CO_2 (v/v). Treating the cells with this antibody was previously shown to deplete the levels of Met on the cell surface, as Met is activated and internalised after exposure to the antibody (Li, Dick, Lu et al., 2019). The cells were then washed with serum-free DMEM and incubated for 2 hours in serum-free DMEM.

2.9.3 Infection assay on MET depleted HeLa cells

After MET depletion Lm-dsRed was added to the host cells at a MOI of 20 in serum free media and incubated for 2 hours at 37°C 5% CO_2 (v/v). Fixing of the cells and bacteria and imaging occurred as described in section 2.9.1, bacteria were also imaged in these settings using

2.9.4 Analysis of MET depleted infections

Analysis of depleted MET cells was done using FIJI to measure aggregate size and the average number of bacteria per cell. Aggregate size was analysed by using the Freehand tool to draw around the aggregates of bacteria identified by dsRed signal. They were analysed using the Measure function to calculate the average GFP signal across each identified object. Individual bacteria were also counted and divided by the total number of cells identified by DAPI stain.

2.10 Data analysis and presentation

2.10.1 Graphs and figures

Numerical data was tabulated into Graphpad Prism 9 software and graphs were generated using this software. Imaging data and representative images were annotated in Zen Black software and exported as .tif files. They were assembled into panels in Microsoft Powerpoint. Schematic figures were designed using BioRender.

2.10.2 Statistical analyses

Statistical analysis was performed using GraphPad Prism 9 software. Data was tested for normal distribution. Two-sample comparison was conducted using paired t-test for data that was normally distributed and non-parametric Mann Whitney test for data that was not normally distributed and. Multiple sample comparisons were analysed using ANOVA for normally distributed data and Kruskal-Wallis ANOVA for data that was not normally distributed.

3. Using live cell imaging to study *Listeria monocytogenes* infection

3.1 Introduction

The ability to follow host pathogen interactions via live cell confocal microscopy may provide new insights into understanding the kinetics of bacterial invasion, replication and spread, allowing real-time visualisation of *L. monocytogenes* interactions with host cells. These interactions should be clearly and accurately imaged and tracked over long periods of time to monitor infection outcomes. To achieve this, the experimental model must spatially separate individual interactions between host cells and bacteria in the field of view with enough of these events visible to provide an informative data set. Specifically, *L. monocytogenes* must be clearly visible and trackable both inside and outside of host cells, and bacteria that have established an intracellular invasion and begun replication must be identifiable.

3.2 Development of an experimental model for imaging *L. monocytogenes* infection

3.2.1 Establishing a host cell model for *L. monocytogenes* infection

HeLa cells are the most characterised cell line in terms of host response to *L. monocytogenes* infection. They were compared to another widely used cell line, Caco-2 (Francis and Thomas, 1996). Using these cell lines as an in-vitro model has advantages and disadvantages. Immortalised cell lines are not an accurate physiological representation of the environment *L. monocytogenes* encounters in the human body. However, they are able to be cultured in imaging dishes, survive long periods of time in imaging conditions and can be cultured quickly. There is a large body of widely-cited literature using both cell lines with *L. monocytogenes*.

HeLa cells and Caco-2 cells were infected with *L. monocytogenes* that constitutively expresses dsRed in addition to GFP tagged to the PrfA-regulated P*actA* promoter (Lm-dsRed-P*actA*-GFP), this strain allows tracking of an invidual bacterium's fate inside of host cells (Moran, Feltham, Bagnall et al., 2022). This bacterial strain was chosen as the constitutive red fluorescent protein allows the bacteria to be tracked by imaging at all times, and the chromosomally integrated P*actA*-GFP acts as a marker for the upregulation of PrfA-regulated virulence genes (P*actA* contains a PrfA box). Individual Caco-2 cells were not distinct from each other, were more heterogenous in shape than HeLa cells and formed structures that were difficult to image (Figure 3.1). For these reasons, HeLa cells were chosen as the host cell model in this study.

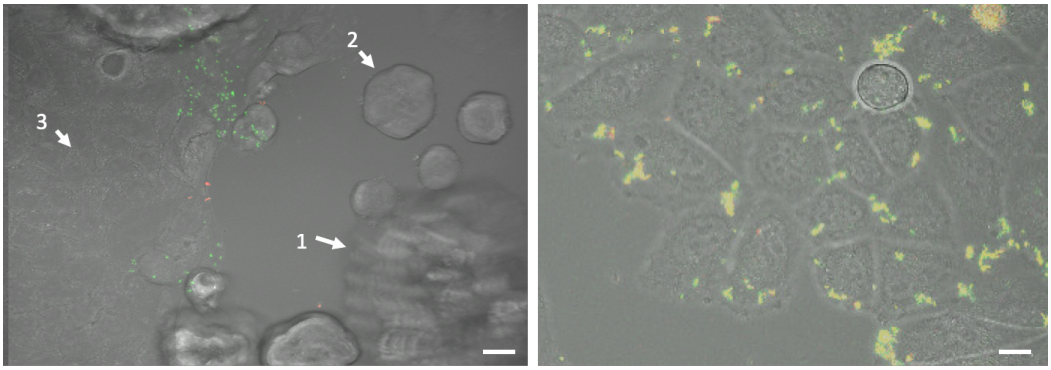

Figure 3. 1. Testing the suitability of Caco-2 cells and HeLa cells for imaging infection. Representative images of 3 biological replicates of Lm-dsRed-P*actA*-GFP infection of Caco-2 (left) and HeLa (right) cells. Lm-dsRed-P*actA*-GFP were infected with Lm-dsRed-P*actA*-GFP at MOI=20 and incubated for 2 hours, then gentamicin was added and the cells were imaged for a further 12 hours. Caco-2 cells points of interest are labelled: (1) formation of large difficult to image structures (2) heterogenous cell morphologies (3) individual cells were difficult to distinguish using brightfield. Scale bar 10 µm.

3.2.3 Optimising multiplicity of infection for imaging experiments

The multiplicity of infection (MOI) is a key variable in infection assays as it will affect the number of interactions between bacteria and host cells and affect the overall outcome of the infection. The aim of this study is to follow individual host-pathogen interactions over time and observe enough replicative outcomes, an interaction whereby *L. monocytogenes* successfully invades a host cell and replicates inside the host cell. This will allow a mechanistic understanding of the regulation of probabilistic infection outcomes. This requires spatially separated events for the purpose of understanding the relationship between an interaction and the infection outcome at the single cell level. Therefore, the imaging assay requires accurate optimisation, as if too high number of bacteria are present individual invasions cannot be reliably resolved or there may be additional cytotoxic effect from the presence of bacteria. If too few bacteria are present too few invasion events will be observed in the field of view of the microscope. A gentamicin protection assay (Section 2.8.4) was used to analyse the effect of MOI on HeLa cell invasion (Figure 3.2). At 3 hours after the addition of gentamicin there were 3.53×10^4 ($\pm 3.62 \times 10^3$) CFU/ml at MOI=20 which was at least 3-fold higher than all other MOIs. Similarly, at 8 hours MOI=20 had a CFU/ml of 1.34×10^5 ($\pm 3.1 \times 10^4$), at least 6.5-fold higher than all other conditions. Additionally, there was a deleterious effect of using a high MOI=100 as at sampled time points after the addition of gentamicin it showed the lowest CFU/ml of all conditions (Figure 3.2A). HeLa cells were then infected with Lm-dsRed-P*actA*-GFP at MOI=20 and imaged for 8 hours, and this showed that at MOI=20 multiple events where *L. monocytogenes* invades host cells and establishes a replicative invasion are visible over 9 imaged tiles, and these events are spatially distinct and interactions can be individually analysed (Figure 3.2B).

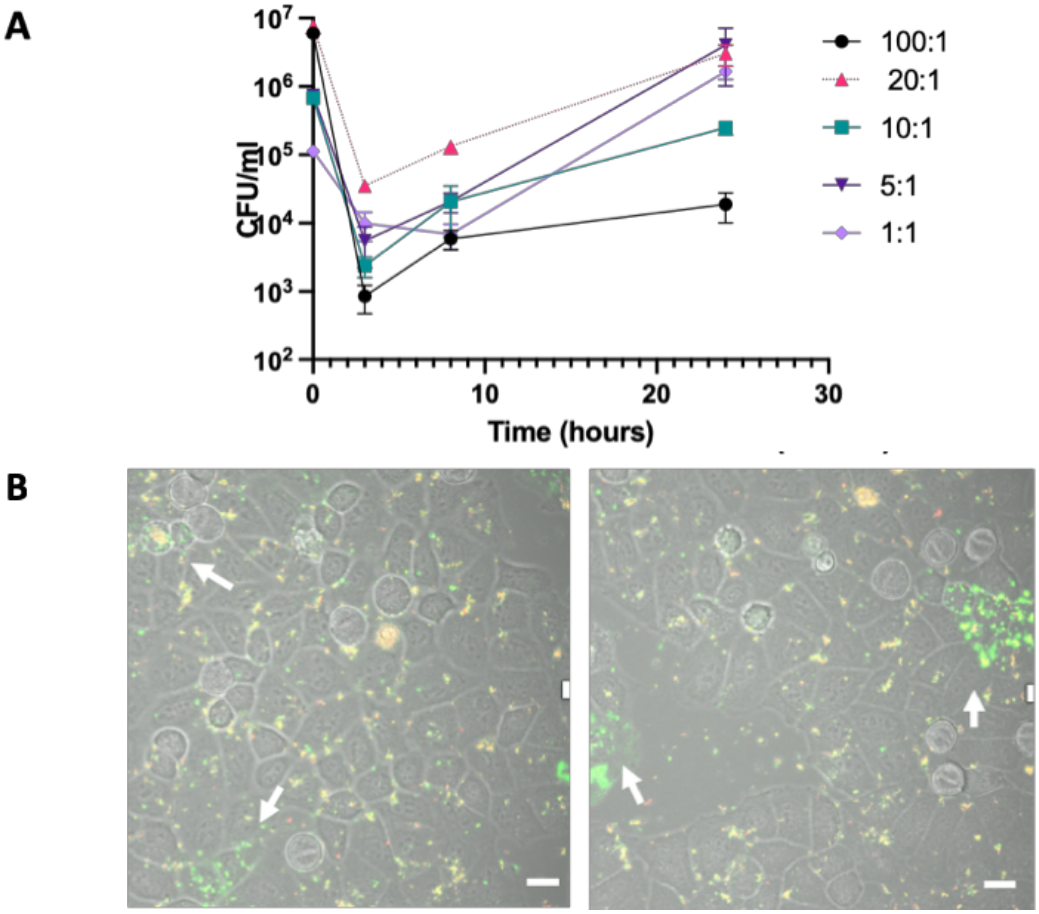

Figure 3. 2. Optimisation of MOI for use in imaging experiments. A) Gentamicin protection assay where HeLa cells were infected with different MOIs of wildtype *L. monocytogenes* for 2 hours. First data point is taken immediately before addition of gentamicin and X-axis shows time after addition of gentamicin. Data points show the average of 3 replicates with error bars representing the standard deviation. **B)** Representative images from 3 biological replicates of HeLa cells infected with Lm-dsRed-P*actA*-GFP at MOI=20 for 2 hours. Gentamicin was added after 2 hours and the cells were imaged for 8 hours. The images show the cells after 8 hours in 3 different locations. White arrows show individual replicative invasion events. Scale bar 20 µm.

3.2.4 Live cell imaging, the optimised infection assay

A successful model for imaging cell imaging was devised where HeLa cells seeded at 5.0 x 10^5 are infected with Lm-dsRed-P*actA*-GFP at MOI=20. The dsRed reporter allows bacteria to be tracked extracellularly to image their initial interactions with host cells. Gentamicin then is used to kill extracellular bacteria and bacteria that have successfully invaded host cells will go on to establish successful infections. These can be tracked via the expression of the P*actA*-GFP reporter which is upregulated in the host cytosol (Figure 3.3A). This optimised assay allows tracking of individual bacteria, host cells and interaction events. The conditions also spatially separate individual infections and allow continuous tracking over long periods of time (Figure 3.3B).

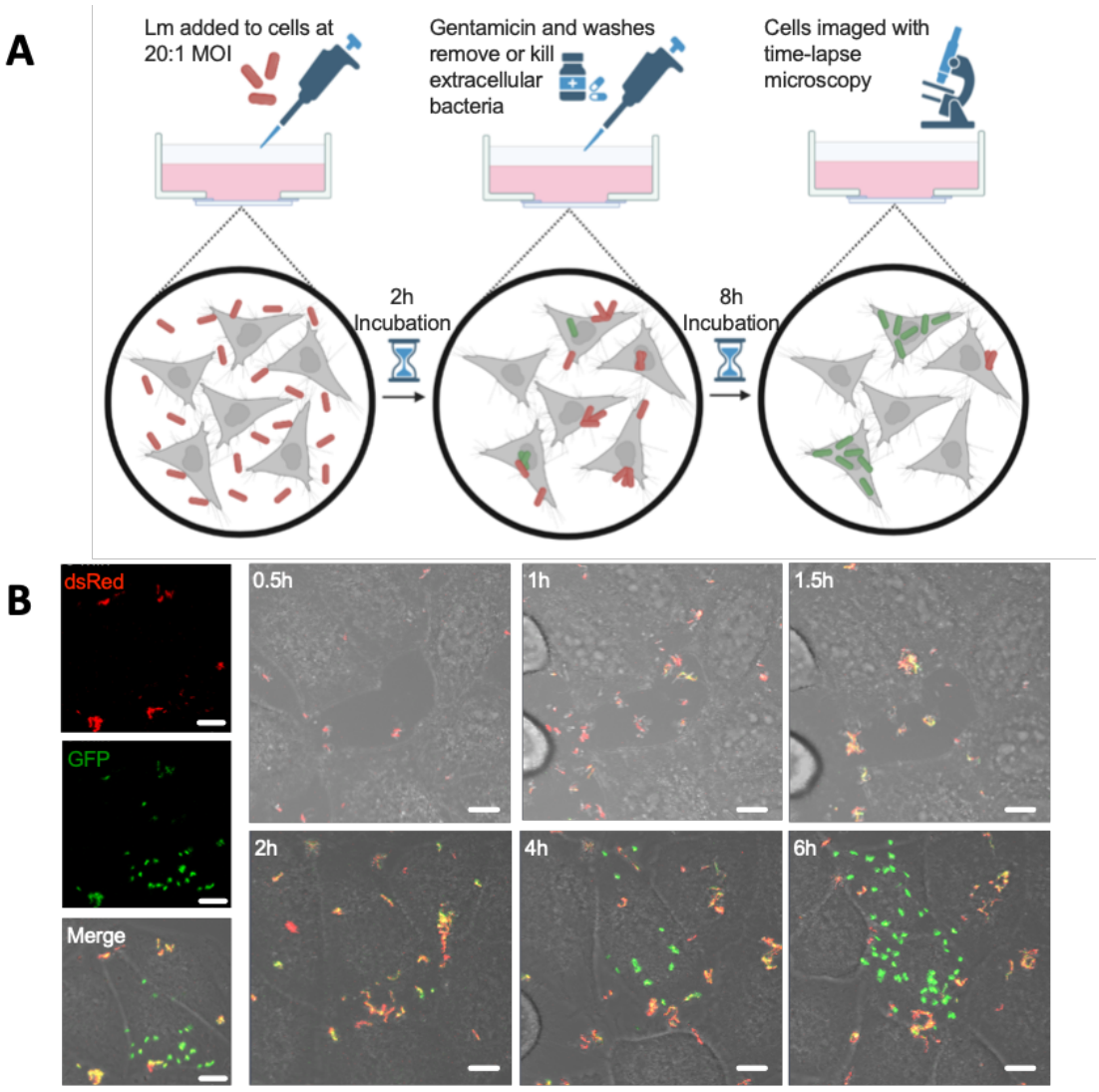

Figure 3. 3. Optimised infection model for studying *L. monocytogenes* infection in live cell imaging experiments. **A)** Schematic diagram of the infection assay. HeLa cells are infected with Lm-dsRed-P*actA*-GFP at MOI=20, incubated for 2 hours and then washed. Gentamicin is added to kill extracellular bacteria and remains in the media for the duration of the experiment. Intracellular bacteria express GFP from the P*actA*-GFP (promoter (green bacteria) and replicative invasions can be tracked over time. **B)** Representative confocal microscopy images of infection of HeLa cells at MOI=20 with the Lm-dsRed-P*actA*-GFP. The top panel shows the first 1.5 hours of infection before the addition of gentamicin and the bottom panel shows a replicative invasion event after gentamicin addition for up to 6 hours of the 8 hours imaged after infection. Images on the left show the individual fluorescent channels at 5 hours and the final image merged with the brightfield channel. Scale bar 10 µm.

3.3 Analysing infection strategies of *L. monocytogenes*

A triplicate of HeLa cell invasion assays were performed using the optimised conditions. The experiments identified 3 key observations that may be important for *L. monocytogenes* infection of host cells, which subsequently are investigated in detail in this work.

3.3.1 Replicative host cell invasion is a rare event

The number of invasion events was quantified by tracking replicative invasions over time. Replicative invasions were identified by *L. monocytogenes* P*actA*-GFP expression and intracellular replication. While all HeLa cells interacted with multiple bacteria over the course of the experiment, only 9.1% (±1.2%) of host cells were permissive to replicative invasions by *L. monocytogenes* (Figure 3.4A). This observation is even more striking when considering the bacterial population. The probability that an individual bacterium can successfully establish a replicative invasion in a host cell is extremely low, with only 0.4% (±0.05%) of the bacterial population able to do so (Figure 3.4B). This demonstrates that replicative invasions are a rare event.

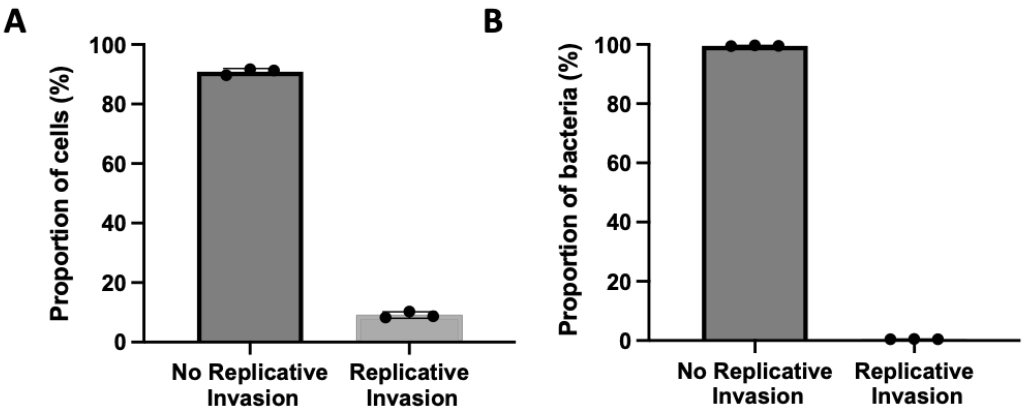

Figure 3. 4. The two infection outcomes of *L. monocytogenes* infection in HeLa cells. A) Proportion of HeLa cells that hosted replicative invasions by Lm-dsRed-P*actA*-GFP after 2 hours infection at MOI=20. Bar represents the mean, error bars represent standard deviation and circles represent values of 3 individual replicates. **B)** Proportion of Lm-dsRed-P*actA*-GFP that were able to establish successful replicate invasions in HeLa cells after 2 hours infection at MOI=20 over 3 biological replicates. Bar represents the mean, error bars represent standard deviation and circles represent values of individual replicates

3.3.2 *L. monocytogenes* uses aggregation to interact with host cell surface

During the first 2 hours of the infection experiments, bacteria tend to form distinct cluster or aggregates which were localised on the membranes of the host cells. Notably, the aggregation was associated with upregulation of P*actA*-GFP expression (Figure 3.5) (Supplementary Video 1 – Section 9.1). Interestingly, ActA secondary function in driving bacterial aggregation which aids biofilm formation and intestinal colonisation has been previously described (Travier and Lecuit, 2014). The upregulation of *actA* expression outside of the host has not been reported before. *actA* expression is tightly regulated and has an asymmetrical PrfA box due to 2 nucleotide mismatches – lowering its binding affinity for PrfA (Williams, Thayyullathil and Freitag, 2000). Expression of *actA* outside of the host within 90

mins of exposure may therefore indicate PrfA regulation, whereas ActA upregulation is not thought to occur until the bacteria is in the cytosol and exposed to host glutathione (Freitag, Port and Miner, 2009).

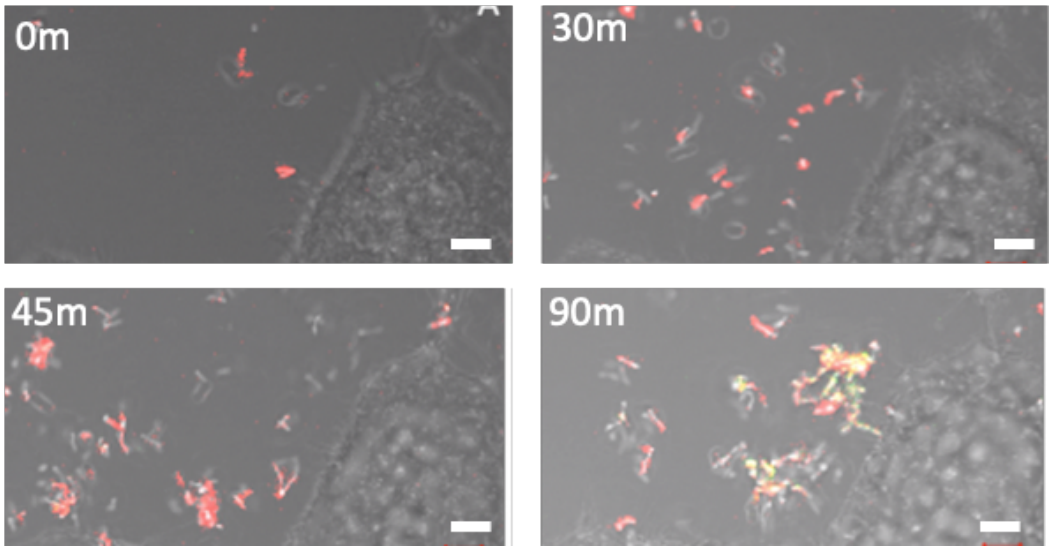

Figure 3. 5. Formation of *L. monocytogenes* aggregates. Representative confocal microscopy images of 3 biological replicates of HeLa cells infected with Lm-dsRed-*PactA*-GFP MOI=20 for 2 hours. Images show the formation of bacterial aggregates and upregulation of *actA* expression as shown by increased GFP expression. Scale bar 5 µm.

Formation of aggregates on the membrane of host cells, and the concurrent upregulation of *actA* (and subsequently the upregulation of other PrfA-regulated virulence genes) may represent a novel strategy utilised by *L. monocytogenes*. It was observed that more than one bacterium from a single aggregate can enter a host cell simultaneously, which presumably increases the probability of intracellular invasion (Figure 3.6) (see also Supplementary Video 2 – Section 9.1). This provides further context for *actA* expression and ActA-mediated aggregation observed outside of the intracellular environment.

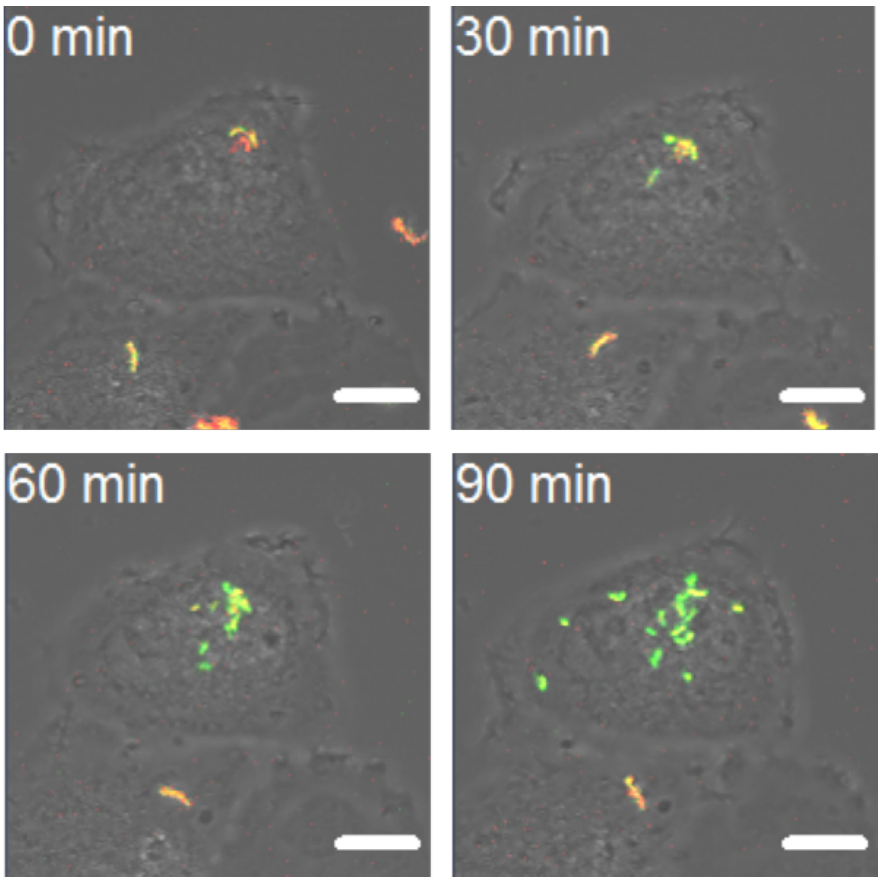

Figure 3. 6. Multiple bacteria may successfully invade the host cell from a single aggregate. Representative confocal microscopy images of 3 biological replicates of HeLa cells infected with Lm-dsRed-*PactA*-GFP MOI=20 for 2 hours. Images show an aggregate of 4 bacteria invading a HeLa cell and establishing a successful replicative invasion. Scale bar 10 µm

3.3.3 *L. monocytogenes* invasion is dependent on the host cell cycle

A third observation noted during the preliminary analyses of the invasion assays was that many *L. monocytogenes* replicative infection events were followed by host cell division. *L. monocytogenes* successfully establishes a replicative infection in a HeLa cell – which then divides resulting in infected daughter cell (Figure 3.7A). 32.9% (±7.3%) of host cells harbouring a replicative invasion underwent cell division during the time course of the experiment. When the population of dividing cells

were analysed by measuring the time from the first intracellular replication of *L. monocytogenes* to the time of host cell mitosis they showed a striking distribution. 48.8% of host cells were found to divide within 2 hours of *L. monocytogenes* intracellular replication and 77.7% within 4 hours (Figure 3.7B). A HeLa cells cycle lasts 19.9 hours, M phase lasts 0.8 hours, the G1 phase lasts 9.2 hours, the S phase lasts 5.5 hours and the G2 phase lasts 4.4 hours (Ankers, Awais, Jones et al., 2016). This therefore suggests that *L. monocytogenes* preferentially established replicative invasions in host cells that are in the G2 phase of the cell cycle.

Interestingly, this type of behaviour has been reported in epithelial (Caco-2) and placental (Jeg-3) cells, whereby *L. monocytogenes* preferentially infects cells that were in the G2/M phase and secretes virulence factors to interfere with the host cell cycle (Costa, Pinheiro, Reis et al., 2020). This has relevance outside of immortalised cell lines as although primary cells have a finite or limited proliferative lifespan they also undergo the cell cycle and may also have transient susceptibilities to infection by *L. monocytogenes* (Campisi and d'Adda di Fagagna, 2007).

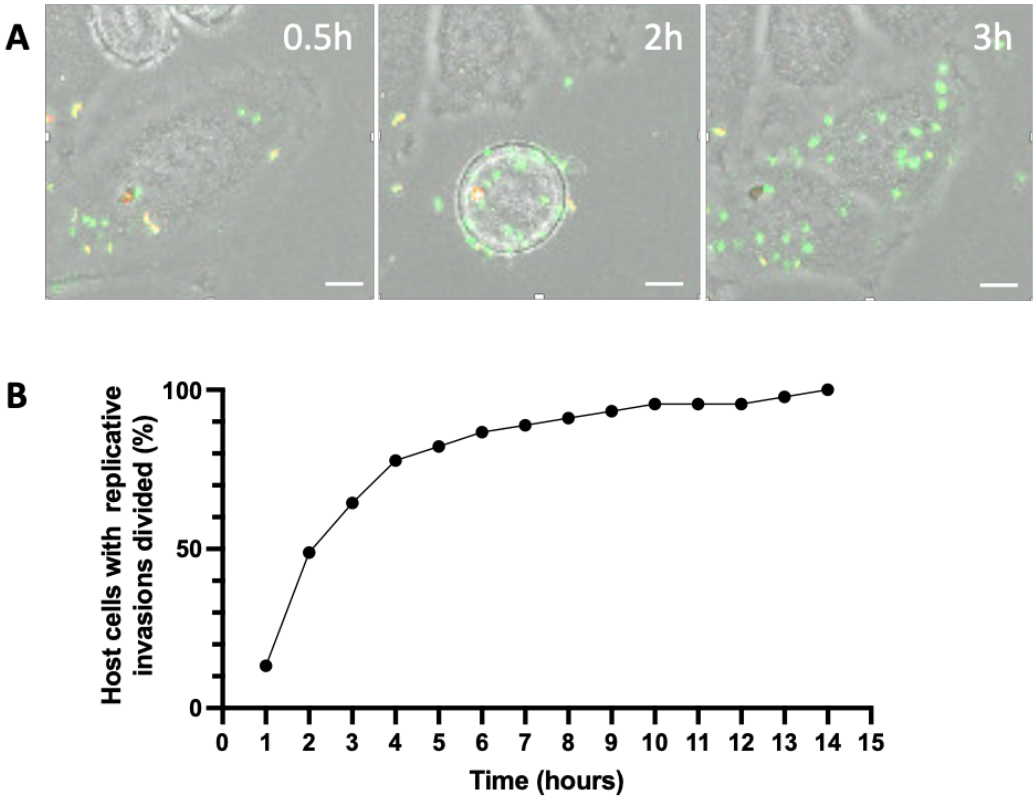

Figure 3. 7. Host cells harbouring replicative invasions undergo cell division within a short time frame. A) Representative images from 3 biological replicates of HeLa cells infected with Lm-dsRed-P*actA*-GFP at MOI=20 for 2 hours. Shows an example of a replicative invasion followed by host cell division. Scale bar 10 µm **B)** Distribution of the total time taken for a HeLa cell harbouring a *L. monocytogenes* replicative invasion to undergo division. Shows the cumulative percentage across time of the analysed population of HeLa cells (harbours replicative invasion and undergoes mitosis). A total of 1563 cells were analysed, 62 of these harboured replicative invasions.

To investigate this further and determine if this phenomenon was linked to aggregate formation and subsequent invasion, a HeLa cell line transfected with E2F1-Venus was used (Ankers, Awais, Jones et al., 2016). E2F1-Venus is expressed in G1phase and can be used to track the cell cycle status of individual host cells (Figure 3.8A). When these cells were infected with *L. monocytogenes* aggregates bound preferentially to cells late in the cell cycle around the G2/M phase (Figure 3.8B) (Liu, Lui, Mok et al., 1997; Whitfield, Sherlock, Saldanha et al., 2002).

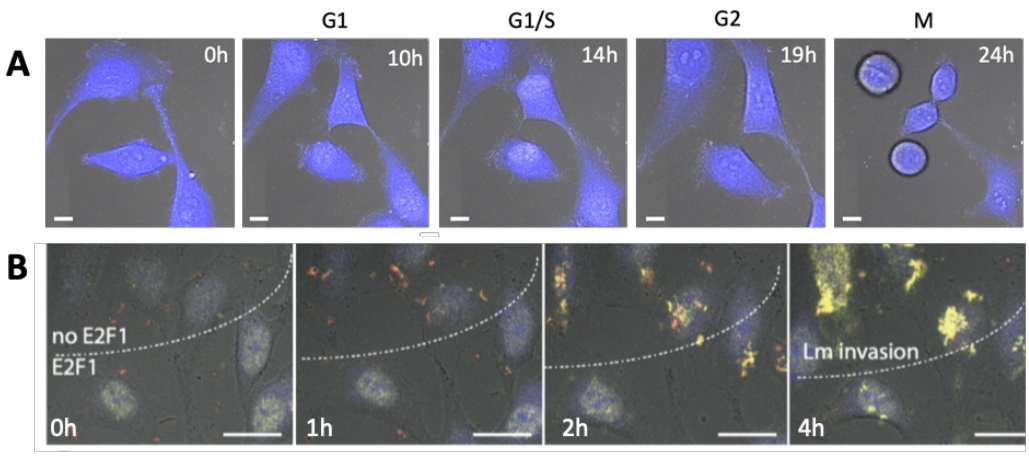

Figure 3. 8. Aggregates form preferentially on cells in the G2/M phase. A) Representative images showing the differential expression of E2F1-Venus (yellow) in the transfected HeLa cells stained with CellTracker (blue) through the different phases of the cell cycle over 24 hours. Scale bar 10 µm. **B)** HeLa cells transfected with E2F1-Venus (yellow) were infected with Lm-dsRed-P*actA*-GFP at MOI=20 for 4 hours. The dotted lines separate groups of cells that are in G1/S phase (bottom) and G2 phase (top) categorised by E2F1 expression. Scale bar 20 µm.

3.4 Discussion

The live cell imaging experiments have shown that intracellular replication event is rare event and few host cells are permissive for invasion and even fewer bacteria can establish replicative invasions. This low rate of invasion for *L. monocytogenes* is reflected by experimental conditions in other studies where high MOIs are required to infect non phagocytic cell lines such as MOI =140 in MDCK cells (Pentecost, Otto, Theriot et al., 2006) and MOI = 200 in Henle-407 cells (Grundling, Gonzalez and Higgins, 2003).

These experiments also demonstrate that the subset of susceptible host cells were often in the G2/M phase and close to cell division. 32.9% (±7.3%) of host cells underwent division while harbouring a *L. monocytogenes* replicative invasion and of this population 48.8% divided within 2 hours and 77.7% within 4 hours (Figure 3.8).

Subpopulations of susceptible host cells has previously been shown in vascular endothelial cells (Rengarajan and Theriot, 2020) and this was shown to be temporally transient, with susceptibility lasting 30-60 mins.

Additionally, *L. monocytogenes* induces host DNA damage and extends the cell cycle for its own benefit, delaying the S phase and increasing the length of the G2/M phase and this benefits *L. monocytogenes* through an increase in resource availability (Leitao, Costa, Brito et al., 2014). This suggests the possibility that some of the population of non-dividing cells harbouring replicative invasions (66.1%) represent cases where *L. monocytogenes* has successfully subverted the host cell in this manner of cycle gating effect and extension of the G2/M phase. This is supported by the data that showed that bacteria preferentially interact with cells that are in the G2/M phase. In agreement with the data in this study, this preferential binding effect to cells in GM/2 has been shown in JEG-3 cells and Caco-2 cells, which also showed an extension of the G2/M phase and mitotic delay induced by InlC and ActA. (Costa, Pinheiro, Reis et al., 2020).

The manipulation of the host cell cycle is also seen in other intracellular pathogens such as *Shigella* which also blocks cells in the G2/M phase (Iwai, Kim, Yoshikawa et al., 2007) and *Neisseria gonorrhoeae* which inhibit host cell proliferation by G1 arrest (Jones, Jonsson and Aro, 2007).

This study demonstrated that the probability a single bacterium will invade a susceptible host cell and form a replicative invasion is low. For the first time we quantified this effect and characterised a novel invasion strategy *L. monocytogenes* uses, forming aggregates to increase the probability of individual bacteria to invade host cells.

The model system developed in this study allows for live cell imaging of *L. monocytogenes* infection of human cells. However, the model has several limitations and confounding factors. For example, gentamicin being present in the cell media kills bacteria that exit the host cell into the media, *in vivo* these bacteria are viable and could go on to infect other human cells (Ortega, Koslover and

Theriot, 2019). The use of an immortal cell line is not physiologically representative of the conditions under which *L. monocytogenes* infection of human cells occurs. HeLa cells are a cervical cell line which is not a tissue commonly associated with listeriosis (Mylonakis, Paliou, Hohmann et al., 2002).

In summary, aggregation may be a novel strategy to promote more robust host cell entry and intracellular replication. Aggregation coincided with upregulation of *actA* gene expression prior to entry suggesting that virulence gene regulation plays a key role in aggregate formation and possibly function. Additionally, the data suggests that entry into host cells is dependent on the phase of the host cell cycle.

In the remaining part of the thesis these observations are analysed in detail to understand the mechanisms and function of aggregation and cell cycle associated host cell susceptibility during *L. monocytogenes* intracellular infection.

4. Regulation of aggregate formation in *L. monocytogenes*

4.1 Development of spent media assay for analysing aggregation and virulence gene expression

The initial imaging experiments show that in the early stages of the infection assay *L. monocytogenes* upregulates virulence genes and forms aggregates that associate with the host cell surface. Consequently, multiple bacteria may invade a host cell during a single invasion event. Aggregation occurs within the first 2 hours of exposure to host cells; therefore, it is possible that bacteria are responding to an external or excreted host cell factor. To test this hypothesis *L. monocytogenes* were exposed to spent media retrieved from HeLa cell culture (as described in Section 2.6.1). Interestingly, this caused a similar response to the one observed in the infection assay of HeLa cells. There was an increase of virulence gene expression observed by GFP fluorescence from the PrfA-regulated P*actA* promoter (Lm-dsRed-P*actA*-GFP). This was followed by the formation of aggregates within 2 hours. When the bacteria were exposed to fresh media, no upregulation of virulence genes was seen in the images and no aggregates were formed (Figure 4.1). There were also changes in the adherence of *L. monocytogenes,* in the fresh media the bacteria quickly settled and adhered to the bottom of the imaging dish, whereas in the spent media they moved through the spent media (Supplementary Video 3 – Section 9.1). A major advantage of aggregation being induced by spent media was that it allows investigations without the presence of host cells.

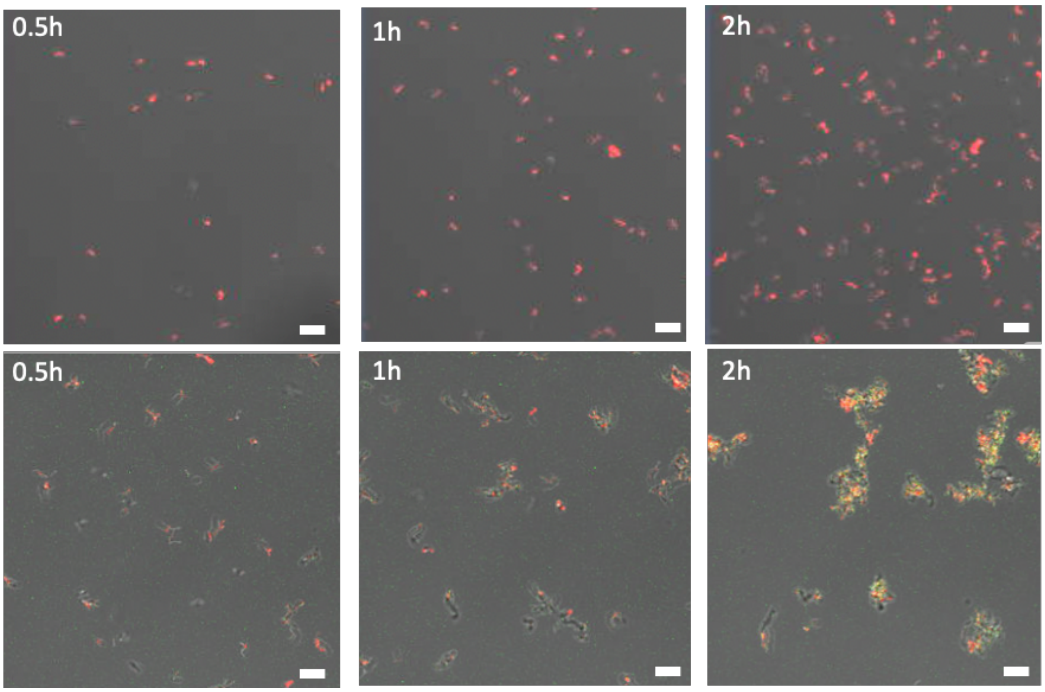

Figure 4. 1. *L. monocytogenes* exposed to spent host cell media. 1.0 x 10^7 Lm-dsRed-P*actA*-GFP was incubated for 2 hours at 37°C in fresh media (top) and spent media (bottom) (retrieved as described in Section 2.6.1). Representative images of 3 biological replicate experiment show upregulation of PrfA-regulated virulence genes via *PactA*-GFP (green) expression and the formation of aggregates occurs when exposed to spent media, but not fresh media. Scale bar 5 µm.

To validate the observation of aggregate formation in spent but not fresh media, the size of the aggregates were quantified using image analysis software FIJI. Aggregates were measured as individual objects, defined as a distinct area of bacteria that form a single object spatially distinct to other nearby objects (Figure 4.2A). This analysis showed an increasing trend in size over 2 hours. After 0.5 hours the mean size of objects is 7.7 µm^2 (±4.6) µm^2. After 1.5 hours the mean increased to 11.3 µm^2 (±8.3) µm^2. After 2 hours the mean was 14.2 µm^2 (±15.4) µm^2 (Figure 4.2B). At both timepoints the object sizes were significantly larger than at 0.5 hours, demonstrating the aggregation is a temporal process within the 2-hour time course.

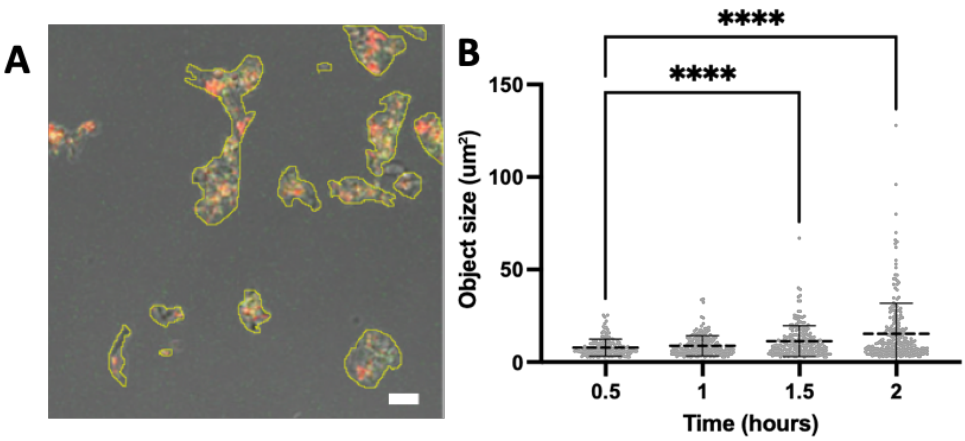

Figure 4. 2. Size of aggregate formation in response to spent media. 1.0 x 10^7 Lm-dsRed-*PactA*-GFP was incubated for 2 hours at 37°C in spent media (retrieved as described in Section 2.6.1). **A)** Representative image demonstrating how individual objects were segmented, distinct aggregates were labelled as a single object (yellow outlines). Scale bar 5 µm. **B)** Increase in object size when Lm-dsRed-P*actA*-GFP was incubated in spent media and imaged then measured every 0.5 hours for 2 hours. Dots represent individual objects, error bars show standard deviation with horizontal dotted line corresponding to sample average based on 3 biological replicates. At least 100 objects were analysed at each time point. Statistical analysis was performed using a Kruskal-Wallis test (**** = $p < 0.0001$)

4.2 Aggregation in response to a host cell factor in spent media

One explanation for aggregation induced by spent media is that it is a response to a secreted host factor detected by *L. monocytogenes*. Spent media will contain many different host factors, from small molecules to large proteins (Hathout, 2007). To assess whether the potential host factor that induces aggregation is a protein - the spent media was boiled at 100°C for 1 minute before performing the aggregation assay. Boiling the spent media denatures any proteins present (Boob, Wang and Gruebele, 2019). The aggregation assay was then performed by exposing Lm-dsRed-P*actA*-GFP to the boiled spent media and a control spent media that was not heat-treated. Boiling impaired the formation of aggregates with a statistically significant

decrease in aggregate size (Figure 4.3A). In the control sample the mean aggregate size was 40.9 (±65.7) μm^2, but in the boiled sample the mean object size was significantly reduced to 12.8 (±8.6) μm^2 (Figure 4.3B). This suggests that the host factor *L. monocytogenes* is responding to is heat sensitive and possibly proteinaceous.

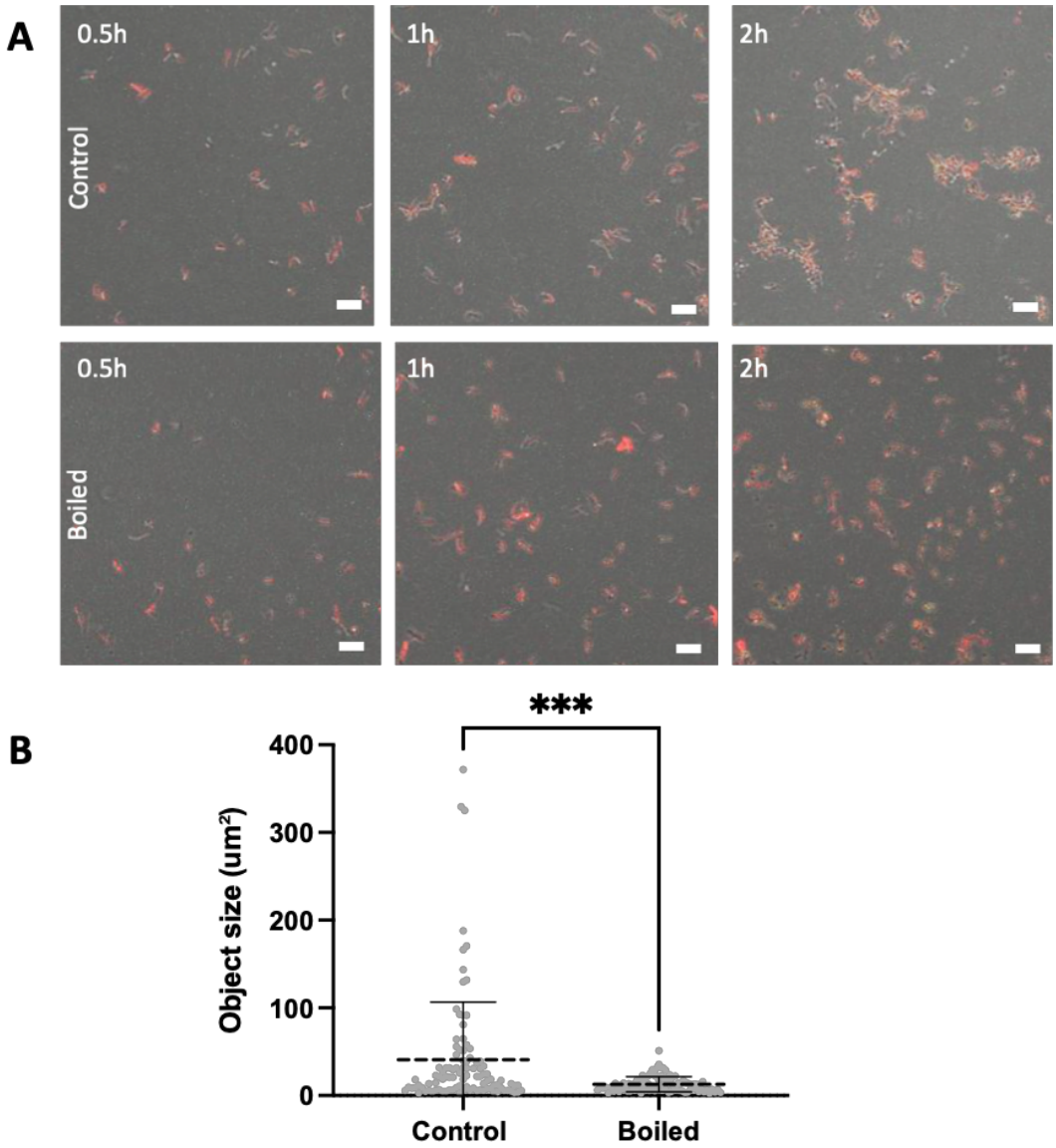

Figure 4. 3. Analysis of aggregation assay in boiled spent media. A) Representative images showing 1.0 x 10^7 CFU of Lm-dsRed-P*actA*-GFP incubated for 2 hours at 37°C in untreated spent media (top) and spent media heat treated at 100°C for 1 min prior to the assay (bottom) (retrieved as described in Section 2.6.3). Scale bar 5 µm. **B)** Size of individual objects in the untreated spent media (Control) and the boiled spent media (Boiled) after 2 hours incubation. Each dot represents an individual object and line represents the mean of 3 biological replicates. At least 100 objects were analysed for each condition. Statistical analysis was performed using a Mann-Whitney test (*** = $p < 0.001$).

To investigate the specific properties of the host factor causing aggregation - a 10 kDa protein filter was used to separate out components of the spent media by size (section 2.6.3). Separating the sample in this way gives two distinct components: the filtrate (containing components of the spent media <10 kDa) and the concentrate (contains components >10 kDa). Only the concentrate sample induced the aggregation phenotype (Figure 4.4A). When these images were quantified to analyse aggregate size at 2 hours, the filtrate sample had a mean object size of 17.9 (±13.2) μm^2, whereas the concentrate sample had a size 114.8 (±116.1) μm^2 (Figure 4.4B). Therefore, these data suggest that the host factor that causes the aggregation response is larger in size than 10 kDa and from the previous analyses denatured by heat which means the host factor is likely a host secreted protein. Additionally, despite the lack of aggregation *actA* gene expression was observed in the filtrate. This suggests that virulence gene expression may also be linked to a separate, low molecular weight host factor. An explanation may be the presence of glutathione in the spent cell media which would activate PrfA and cause virulence gene upregulation (Reniere, Whiteley, Hamilton et al., 2015). However, the amount of protein in each sample was not included in a control in this experiment, a future set of experiments could perform a more detailed analysis by including this as control by checking protein concentrations through western blots or a Bradford assay. Further analyses on the specifics of the host factor were considered for this study, however it falls outside of the scope of the originally posed research aims. Instead, this study aims to investigate how *L. monocytogenes* responds to the host factor and the biological role that aggregation plays in invasion of host cells.

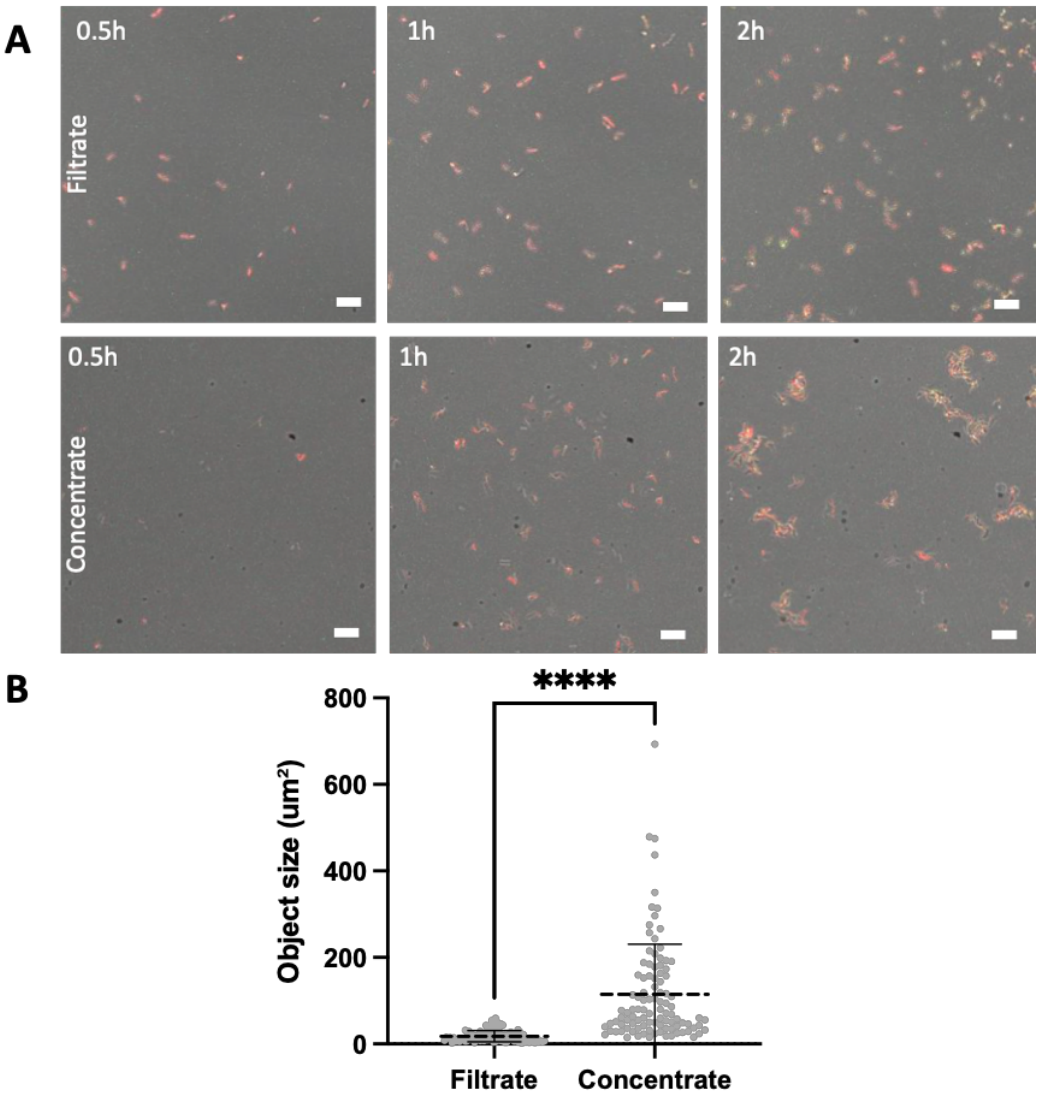

Figure 4. 4. Analysis of aggregation in spent media samples separated with a 10 kDa filter. A) Representative images showing 1.0 x 10^7 CFU of Lm-dsRed-P*actA*-GFP incubated for 2 hours at 37°C in filtrate sample (top) or the concentrate sample (bottom) (retrieved as described in Section 2.6.4). Scale bar 5 µm. **B)** Size of individual objects in the filtrate sample (left) and the concentrate sample (right) after 2 hours incubation. Each dot represents an individual object, error bars show standard deviation, and the dotted line represents the mean of 3 biological replicates. At least 100 objects were analysed for each condition. Statistical analysis was performed using a Mann-Whitney test (**** = $p < 0.0001$).

4.3 Aggregation is ActA-dependent and regulated by PrfA but not SigB

Analysing the genes involved in aggregation is key to understanding how *L. monocytogenes* is responding to the presence of host cells. The two most important regulators of gene expression in the context of infection are SigB and PrfA. Both regulons have genes that are involved in aggregation. SigB is related to environmental stresses and biofilm formation (van der Veen and Abee, 2010). PrfA regulates *actA* which has been shown to have a secondary aggregation function to aid lumen persistence and faecal shedding (Travier and Lecuit, 2014). SigB also directly regulates *prfA* through the P2 promoter (de las Heras, Cain, Bielecka et al., 2011). One way to analyse the effect is to expose knockout mutants of both these genes to spent media. This would identify which regulon is involved in regulation of aggregation.

A fluorescently tagged mutant of *L. monocytogenes* with a Δ*sigB* mutation (Lm-Δ*sigB*-dsRed-*PactA*-GFP) was exposed to spent media in the aggregation assay for 2 hours at 37°C and directly compared against the fluorescently labelled wildtype Lm-dsRed-P*actA*-GFP strain used in previous experiments. The Δ*sigB* mutant formed aggregates after 2 hours and the increase in virulence gene expression was observable (Figure 4.5A). Quantification of the size of the aggregates at 2 hours showed no significant difference between the wildtype strain and the Δ*sigB* mutant. The wildtype had an average object size of 132.7 (±130.8) μm^2, which was not significantly different that from the Δ*sigB* mutant (90.8 (±130.1) μm^2) (Figure 4.5B). Additionally, there appeared to be no difference in virulence gene expression between the wildtype and the Δ*sigB* mutant. Therefore, it is unlikely that SigB is regulating the aggregation response to spent media.

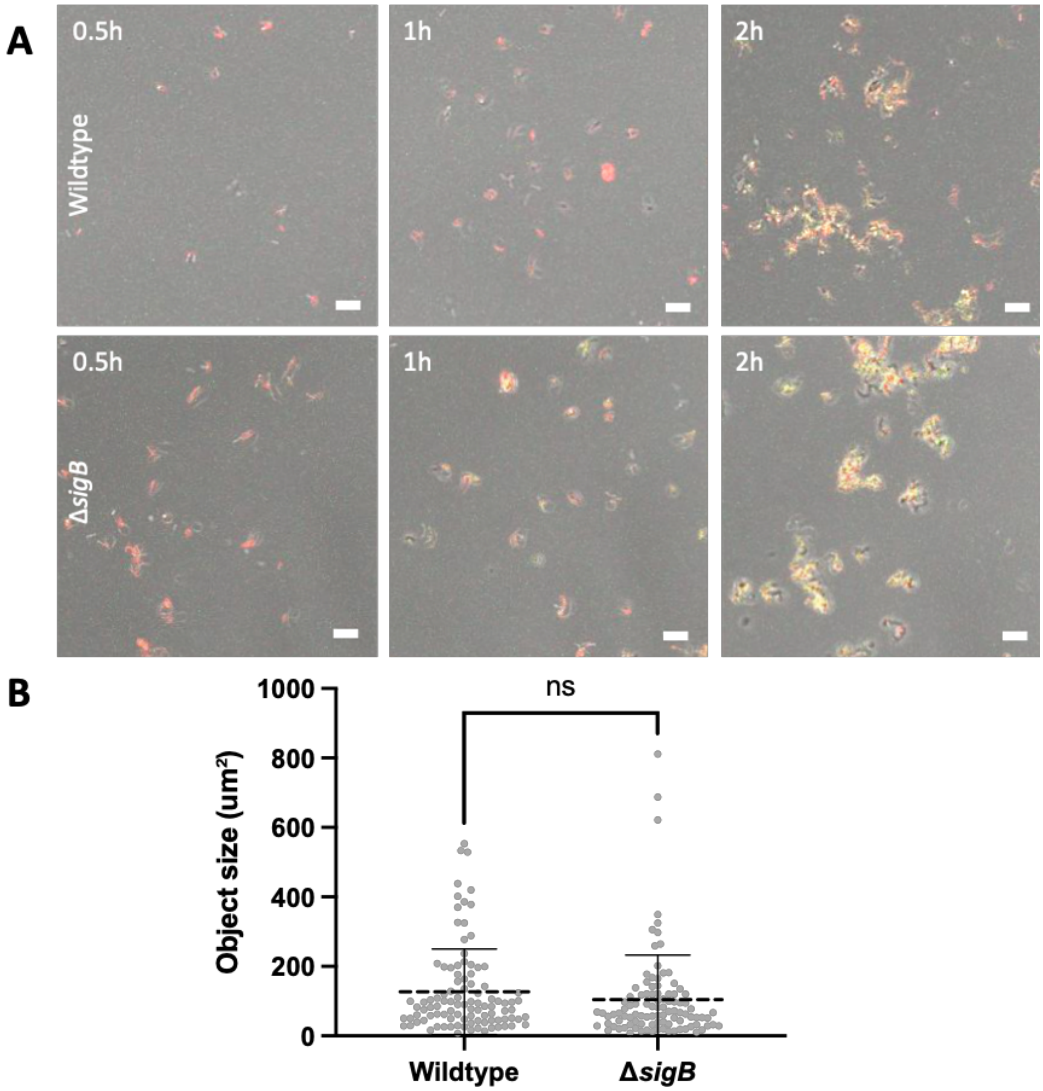

Figure 4. 5. Analysis of aggregate formation in Δ*sigB* mutant. A) Representative images showing 1.0 x 10^7 CFU of Lm-dsRed-P*actA*-GFP (top) or Lm-Δ*sigB*-dsRed-*PactA*-GFP (bottom) incubated for 2 hours at 37°C in spent media (retrieved as described in Section 2.6.1). Scale bar 5 µm. **B)** Size of individual objects formed by Lm-dsRed-*PactA*-GFP (left) and Lm-Δ*sigB*-dsRed-*PactA*-GFP (right) after 2 hours incubation. Each dot represents an individual object and line represents analysis of representative images from 3 biological replicates. At least 100 objects were analysed for each. Statistical analysis was performed using a Mann-Whitney test (ns = p >0.05).

To test whether the aggregation is PrfA-regulated and ActA-mediated - both a Δ*prfA* mutant and Δ*actA* mutant were tested in the aggregation assay in spent media and compared to wildtype *L. monocytogenes* using brightfield microscopy. Both Δ*prfA* and Δ*actA* showed impaired formation of aggregates after 2 hours incubation at 37°C in spent media (Figure 4.6A). When the size of the aggregates was analysed, both Δ*prfA* and Δ*actA* had a significantly reduced mean object size compared to the wildtype, but were not significantly different from each other. Wildtype *L. monocytogenes* had a mean object size of 139.6 (±139.6) μm^2. The Δ*prfA* mutant had a mean object size of 40.5 (±42.2) μm^2, while the Δ*actA* mutant had a mean object size of 36.37 (±30.8) μm^2 (Figure 4.6B). Therefore, this data strongly suggests that the aggregation is PrfA-regulated and ActA-dependant.

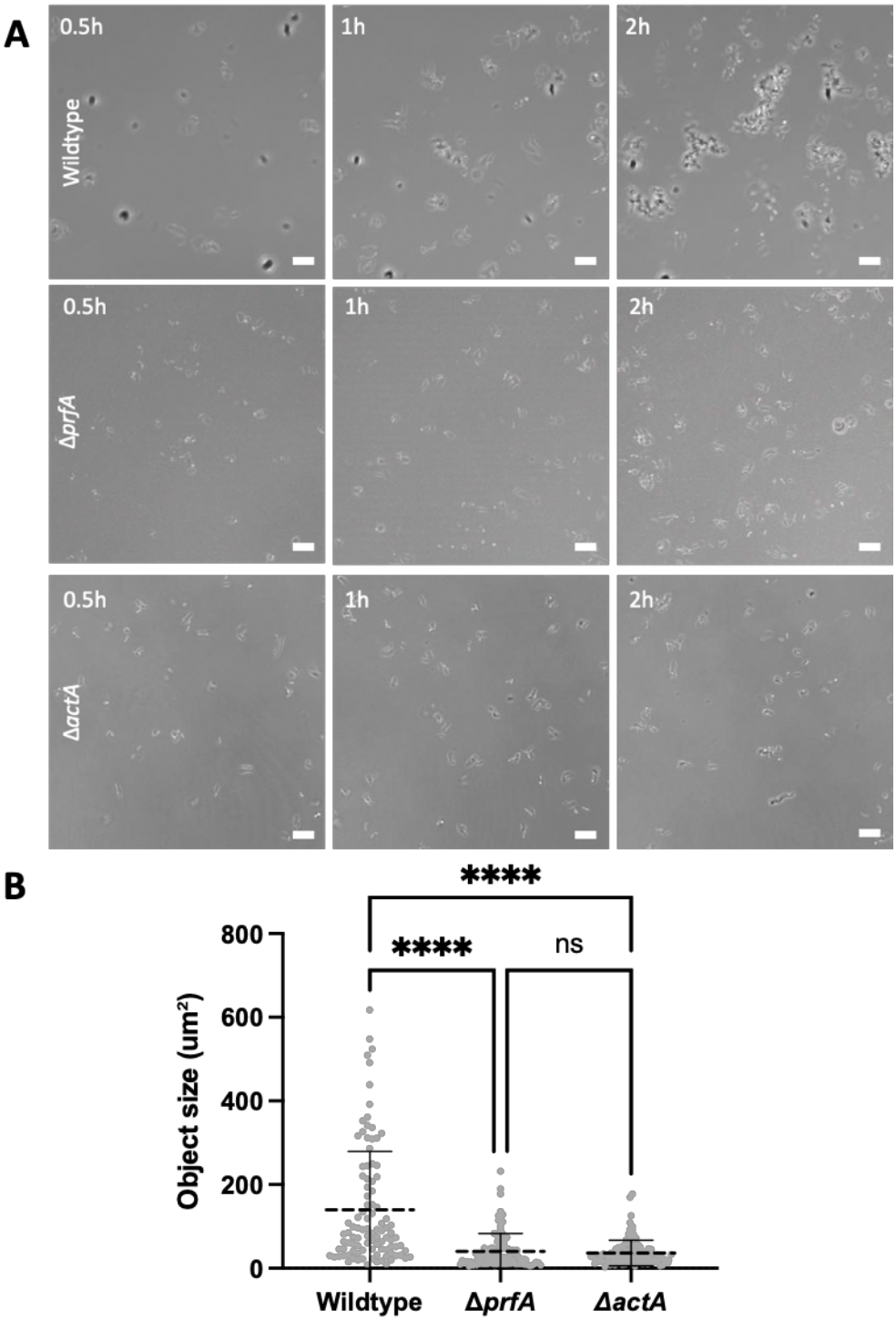

Figure 4. 6. Analysis of aggregate formation in Δ*prfA* and Δ*actA* strains. A) Representative images showing 1.0 x 10^7 CFU of wildtype *L. monocytogenes* (top), a Δ*prfA* mutant (middle) and an Δ*actA* mutant (bottom) incubated for 2 hours at 37°C in spent media (retrieved as described in Section 2.6.1). Scale bar 5 µm. **B)** Size of individual objects formed by wildtype *L. monocytogenes* (left) Δ*prfA* mutant (middle) and Δ*actA* mutant (right) after 2 hours incubation. Each dot represents an

individual object and the dotted line represent the mean from analysis of representative images from 3 biological replicates. At least 100 objects were analysed for each condition. Statistical analysis was performed using Krusal-Wallis test (**** = $p < 0.0001$ ns = $p>0.05$)

4.4 Discussion

The key observation in these experiments is the upregulation of virulence genes and formation of aggregates that associated with the cell surface. By developing an aggregation assay using spent cell media this study showed that that aggregation is a response to a secreted, proteinaceous host factor that is >10 kDa. Aggregation was shown to be PrfA-regulated and ActA-mediated. Although identifying the host factor fell outside the scope of this study, the effect it had on the bacterial phenotype, gene expression and the consequences this had on the replicative invasion rate of *L. monocytogenes* on was extensively examined.

ActA-mediated aggregation has previously been described, it has been shown to be important for intestinal colonisation, carriage, and faecal shedding (Travier, Guadagnini, Gouin et al., 2013). Aggregation as an invasion strategy has been described in *Bartonella henselae* (Dehio, Meyer, Berger et al., 1997) and *Pseudomonas aeruginosa* (Lepanto, Bryant, Rossello et al., 2011). However, the role of *L. monocytogenes* aggregation in intracellular invasion has not been previously described despite the fact these aggregates are found in tissue during *in vivo* studies (Travier, Guadagnini, Gouin et al., 2013).

Aggregation factors outside of ActA-mediated aggregation are not well described in *L. monocytogenes*. A family of cold shock proteins (CspABCD) have been linked to aggregation and biofilm formation, but these have also been linked to post-transcriptional regulation of *actA* (Eshwar, Guldimann, Oevermann et al., 2017). This lack of described aggregation factors coupled with the presented evidence that

an *actA* mutant showed a loss of aggregatory phenotype suggests ActA is the main mechanism for the induced aggregation.

In addition to aggregation, *actA* expression outside of the host may also have consequences for *L. monocytogenes* ability to invade host cells. This study showed evidence of *actA* expression outside of the host through imaging of the P*actA*-GFP reporter, and *actA*. ActA is implicated in the invasion of epithelial cells. The N-terminal region of ActA is similar to the domain of the *Plasmodium falciparum* circumsporozoite protein involved in heparate sulphate recognition and hepatocyte binding and presence of heparan sulphate at the surface of CHO epithelial cells is required for the entry *of L. monocytogenes* in an ActA-dependent manner (Alvarez-Dominguez, Vazquez-Boland, Carrasco-Marin et al., 1997). Additionally, deletion of the *actA* gene in a hypervirulent PrfA* background strain (constitutively active PrfA due to a conformation change caused by an amino acid substitution) led to a large reduction in *L. monocytogenes* invasiveness in epithelial cells, and ActA was shown to induce cytoskeletal re-arrangement the host cell membrane to facilitate entry through pseudopods (Suarez, Gonzalez-Zorn, Vega et al., 2001). It is therefore possible that upregulation of *actA* outside of the host is important for cell entry and aggregation of several bacteria on the surface of a cell facilitates this invasion strategy.

There are a few limitations to consider in the experiments in this chapter. Although spent media allowed for induction of aggregation without the presence of cells, the mechanism remains unknown. Using the spent media method without knowing the factor that induces aggregation is a crude induction of the phenotype with no clear indication of mechanisms or activation pathways. Additionally, the use of DMEM, a media generally only used in cell culture may have unforeseen effects on the phenotype of the bacteria. However, as aggregation is described *in vivo* and was observed in the initial infection assays, its biological role requires further investigation, which follows in the remaining chapters of this thesis.

To summarise, by utilising live cell imaging and knockout mutants of *L. monocytogenes* the results demonstrate that aggregation occurs in response a secreted and heat-labile host cell factor >10 kDa. The upregulation of virulence genes is not dependent on this host cell factor and was seen in the filtrate (<10 kDa) and may be due to a small molecular weight factor, possibly glutathione which activates PrfA. The results also show that aggregation is PrfA-regulated and ActA mediated. The previous chapter suggested that these aggregates interact with host cells in a way to potentially increase the bacterial invasion success rate, the next chapter will further explore the role that aggregation plays in host-pathogen interactions and aim to mechanistically understand the regulation of probabilistic infection outcomes.

5. Function of *L. monocytogenes* aggregates in infection of human cells

5.1 Introduction

Aggregation on the surface of host cells is a response by *L. monocytogenes* to the presence of a host factor. Additionally, the occurrence of multiple invasion events, where bacteria in an aggregate can enter a host cell simultaneously suggests this aggregation may also play a role in the invasion process. Aggregation has been shown to play an important role in the colonisation of the intestinal lumen and the persistence of *L. monocytogenes* over long time periods (Travier and Lecuit, 2014), however its role in cell invasion has not been elucidated. To investigate this a non-aggregating *actA*-ΔC mutant was utilised to study the effect that ActA-mediated aggregation has on infection of human cells.

5.2 Construction of a non-aggregating mutant strain

The *actA* protein has 3 regions: The N-region (AA21-231) is responsible for recruiting actin for actin-tail formation (Figure 1.4). The P-Region (AA231-393) is binding to Enabled/vasodilator-stimulated phosphoprotein (Ena/VASP) family proteins, which in turn bind to actin filaments and facilitate intracellular motility. The C-region (AA-393-585) plays no role in actin tail formation or intracellular motility and is responsible for ActA-mediated aggregation via direct ActA-ActA interactions. The *actA*-Δ*C* fragment is a deletion of the C-region with a 486bp C-terminal deletion from nucleotides 693-1179 (Travier and Lecuit, 2014). This was constructed using the methods described in Section 2.3 and Section 2.4. The DNA strand was synthesised externally with appropriate restriction sites on the 5' and 3' ends and inserted into pAUL-A by restriction cloning. This was then cloned into *E. coli* DH5α to produce a high number of plasmids. After cloning the plasmid into *L.*

monocytogenes this mutation successfully introduced onto the *L. monocytogenes* chromosome by inducing homologous recombination of the mutant onto *L. monocytogenes* genome (Section 2.4) (Chakraborty, Leimeister-Wachter, Domann et al., 1992). A schematic detailing of the region can be seen in Figure 5.1. The successful generation of the mutation on the chromosome was confirmed by PCR with primers V-actAC-F and V-actAC-R (Table 2.3) that flank the deleted region of the *actA* gene. The successful induction of the mutation was verified by a primer pair flanking the deleted region and comparing the size of this band to wildtype *L. monocytogenes*. It was also verified by confirming the loss of erythromycin resistance.

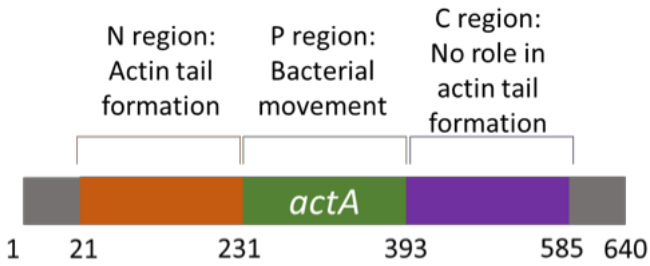

Figure 5. 1. Schematic of a non-aggregating C-terminal deletion of *actA* gene. A) Schematic representing the ActA protein and highlighting the role each domain of its translated protein. The *actA-ΔC* mutant has a deletion from AA 393-585 to remove the C-region responsible for aggregation phenotype. Primers used for validation are shown in black on the schematic of the mutant gene.

5.3 Phenotypic analysis of *actA-ΔC*

When the probability of the *actA-ΔC* mutant to form aggregates was compared to the wildtype after exposure to host cells for 2 hours, the *actA-ΔC* mutant was impaired with most bacteria clustered as 3 or less bacteria, and the majority of bacteria being single cells or in pairs (Figure 5.2A). In contrast, the wildtype consistently formed aggregates of variable size, the probability of aggregates up to

25 bacteria size are shown in Figure 5.2A, but rare occurrences of aggregates up to 60 bacteria in size were observed (Figure 5.2A). Imaging an infection assay of HeLa cells with Lm-*actaA-Δ*C-GFP strain demonstrated it is unable to form aggregates over the 2-hour infection period, and the small groups of 2-3 bacteria observed in Figure 5.2A were either bacteria replicating outside of the host cell or random distribution of cells leading to two bacteria occupying the same area. However, the *actA-ΔC* mutant is still able to form replicative invasions (Figure 5.2B).

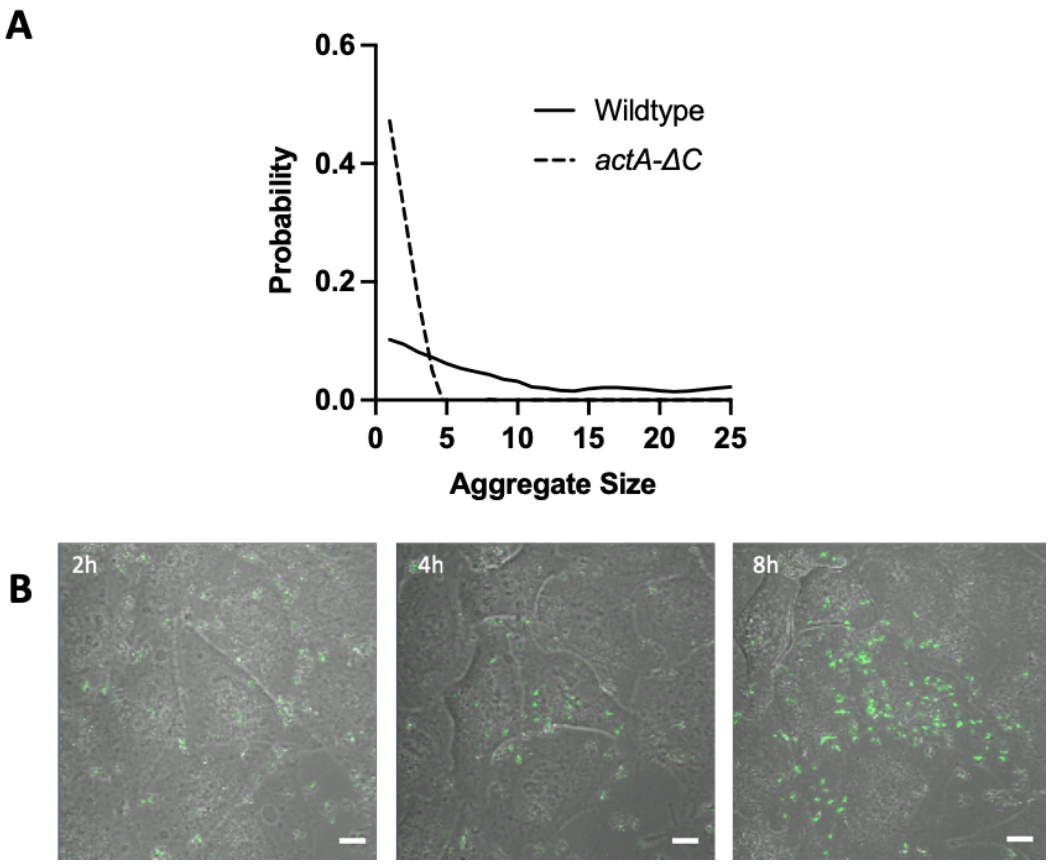

Figure 5. 2. Lm-*actA-ΔC* does not form aggregates but still forms replicative invasions. **A)** Probability distribution of aggregate size for wildtype *L. monocytogenes* and the non-aggregating Lm-*actA-ΔC* mutant. Data is pooled from 4 biological replicates of HeLa cell infected at MOI=20. Wildtype bacteria analysed = 1517, *actA-Δ*C bacteria analysed = 659. **B)** Representative confocal microscopy images of Lm-*actA-ΔC*-GFP (green) exposed to HeLa cells for 2 hours at MOI = 20. After 2 hours gentamicin was added and the cells were imaged for a further 8 hours showing a replicative invasion. Scale bar 10 µm. Replicative invasions of the wildtype bacteria can be seen in Figure 3.3.

5.4 Internalisation assay to measure probability of intracellular invasion of *L. monocytogenes*

Invasion of host cells is a multistep process involving attachment to host cells, intracellular invasion, vacuole escape, cytoplasmic replication and spread. To understand the role of aggregation in this process, the ability of *L. monocytogenes*

aggregates to form intracellular invasions was analysed against the non-aggregating mutant. The invasion ability of the *actA-ΔC* mutant was assessed using an internalisation assay with Lm-dsRed and Lm-*actA-Δ*C-dsRed counterstained with an anti-*Listeria* antibody and secondary antibody conjugated with the fluorphore Brilliant Violet to differentiate intracellular and extracellular bacteria (Section 2.7). The mutant has impaired invasion into host cells compared to the wildtype (Figure 5.3A). The representative images show that the mutant associates with the host cell surface mostly as single cells, whereas aggregates are seen in wildtype *L. monocytogenes*. Multiple invasion events were also seen in the wildtype, where multiple bacteria had invaded a single host cell (Figure from individual aggregates (Figure 5.3B).

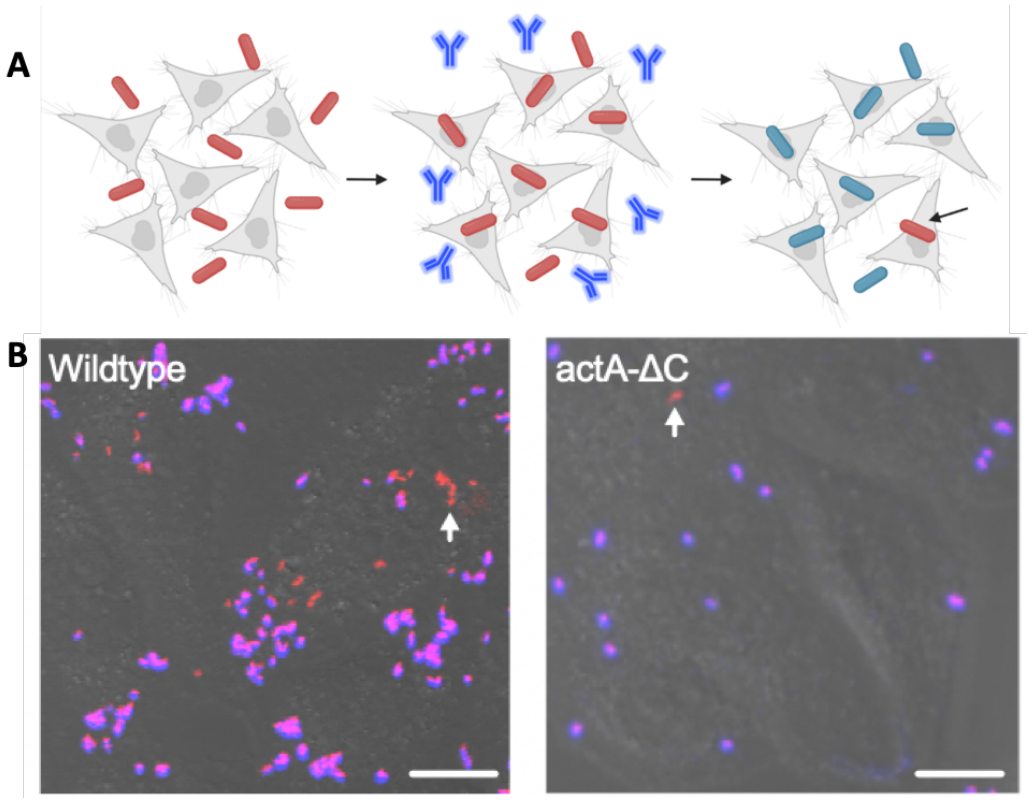

Figure 5. 3. Internalization assay for assessing successful internalization of *L. monocytogenes* into HeLa cells. A) Schematic representation of internalisation assay. HeLa cells infected with Lm-dsRed or Lm-*actA*-*Δ*C-dsRed (red bacteria) at a MOI of 20:1 for 2 hours. The cells were stained with a conjugated fluorescent antibody (blue) counterstain targeting extracellular bacteria. Unstained bacteria are therefore intracellular and can still be identified by dsRed (arrowhead). **B)** Representative images of the internalization assay for Lm-dsRed and non-aggregating Lm-*actA*-*ΔC*-dsRed. Constitutively expressing dsRed and the antibody stain can be used to distinguish between extracellular bacteria (blue/purple) and intracellular bacteria (red, white arrow). White arrow in the wildtype panel also shows evidence of a multiple invasion event Scale bar 5 µm.

A quantitative analysis of the internalisation assay was used to assess the role that aggregation plays on internalisation. This showed that aggregation facilitates a significantly greater number of bacteria to adhere to the host cells after 2 hours incubation. Wildtype *L. monocytogenes* had an average of 20.7 (±1.7) bacteria

associated with a host cell, and the *actA-ΔC* mutant had an average of 3.8 (±0.5) bacteria per host cell, an approximately 5.5-fold decrease in the number of host cell-associated bacteria (Figure 5.4A). Further to this, the probability for a single associated bacterium to establish an intracellular invasion in proportion of the entire population of host cell-associated bacteria was analysed. The probability for a bacterium to establish an intracellular invasion in the wildtype population was 0.02 (±0.006) and in the *acta-ΔC* mutant population this probability was significantly reduced by 3.5-fold to 0.007 (±0.002) (Figure 5.4B).

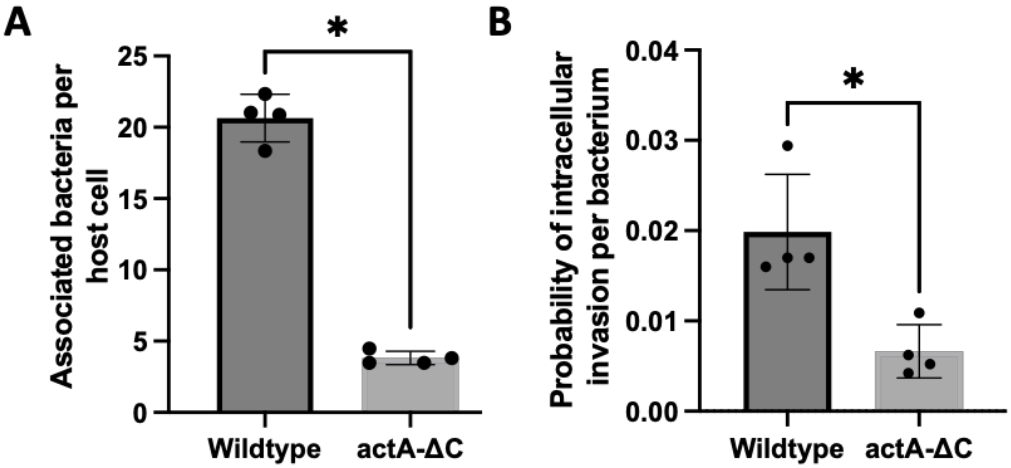

Figure 5. 4. Quantitative analysis of the intracellular invasion rate of wildtype and the *actA*-ΔC mutant. A) The average number of associated bacteria per host cell for Lm-dsRed (left) and for Lm-*actA*-ΔC-dsRed (right). Circles represent individual replicates (n=4), bars shown the mean and error bars represent standard deviation for data in the invasion assay shown in Figure 5.3. Statistical significance (* = $p < 0.05$) was calculated using a non-parametric one-sided Mann-Whitney test. At least 100 host cells were analysed for each replicate. **B)** The probability of a single cell-associated bacterium invading a host cell for Lm-dsRed (left) and for Lm-*actA*-ΔC-dsRed (right). Circles represent individual replicates (n=4), bars show the mean and error bars represent standard deviation for data in the invasion assay shown in Figure 5.3. Statistical significance (* = $p < 0.05$) was calculated using a non-parametric one-sided Mann-Whitney test. At least 100 host cells were analysed for each replicate.

Further analysis was performed on the proportion of intracellular bacteria in these populations. Internalised bacteria were categorised as either “Single” (not aggregated to other bacteria) or as “Aggregated” (internalised bacteria are associated as a part of a larger aggregate of other bacteria). This showed that in the wildtype 69.4% (±0.3%) of intracellular invasions were aggregate-associated and 30.3% (±0.3%) were single cell invasions. In *actA-ΔC* mutant 100% of internalisations were single-celled across all replicates and no aggregate-associated infections were observed (Figure 5.5).

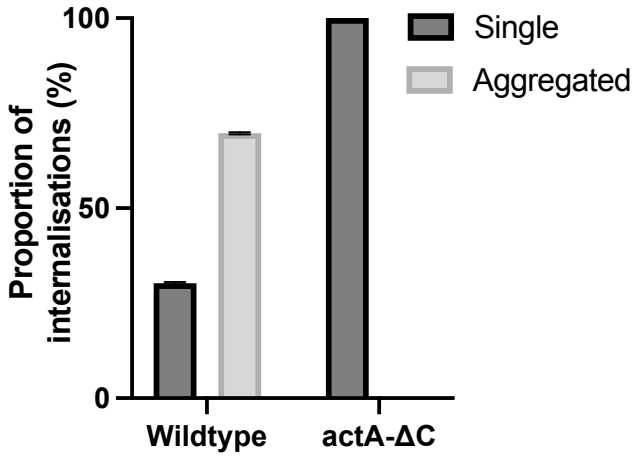

Figure 5. 5. **Aggregate-associated internalisation is common in wildtype *L. monocytogenes* but not in *actA*-ΔC mutant.** The proportion of internalisations in Lm-dsRed (left) and Lm-*actA-ΔC*-dsRed (right) that are either “Aggregated” (aggregate associated internalisations where the internalised bacteria is associated with other bacteria in an aggregate) or “Single” (the internalised bacteria is isolated and not associated with other bacteria). Bars represent the average across 4 replicates and error bars represent standard deviation for data in the invasion assay shown in Figure 5.3. At least 100 cells were analysed for each replicate.

5.5 Live cell imaging of HeLa cell infections with non-aggregating mutants

ActA-mediated aggregation of *L. monocytogenes* increases both the ability to associate with the host cell and the probability that an individual bacterium will successfully invade a host cell. Therefore, aggregation may represent an invasion strategy that allows *L. monocytogenes* to increase the invasion rate of individual bacteria and enhance the ability to invade susceptible host cells. The HeLa cell model previously developed for studying individual invasion events in Section 3 was used to track and quantify individual invasion events and replicative invasions in wildtype (Lm-dsRed-P*actA*-GFP), *actA-ΔC* mutant *(*Lm-*actA*-ΔC-dsRed-P*actA*-GFP) and a full *ΔactA* deletion mutant (Lm-actA-P*actA*-GFP). Quantification of the effect aggregation has on infection success rate showed that wild-type *L. monocytogenes* was able to establish a successful replicating invasion in 8.8% (±1.2%) of host cells. In contrast, only 2.3% (±1.2%) of cells were successfully infected with non-aggregating Lm-*actA-ΔC,* approximately 4 times less than the wildtype. This was further reduced to 0.9% (±0.06%) in a mutant with a full knockout of the *ΔactA* gene (Figure 5.6).

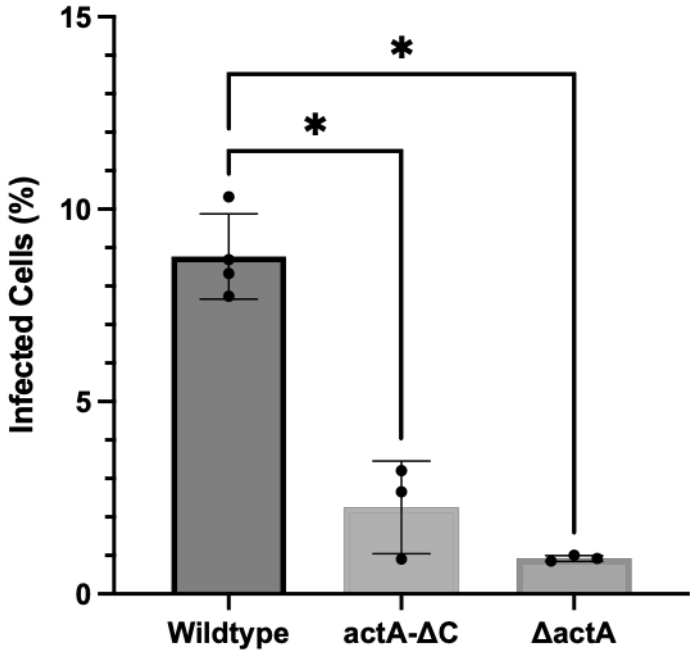

Figure 5. 6. Aggregation impaired mutants have a decreased invasion success rate in HeLa cells. Percentage of HeLa cells harboring replicative invasion events. HeLa cells infected with wildtype Lm-dsRed-P*actA*-GFP (left), Lm-*actA*-ΔC-dsRed-P*actA*-GFP (middle) and *Δ*actA- *PactA*-GFP (right) strains at MOI=20. Shown is the proportion of host cells harboring a replicative invasion event at 2 h after gentamicin treatment. Circles represent individual replicates (n=4) and error bars represent standard deviation. Statistical significance (* = $p < 0.05$) was calculated using a Kruskal-Wallis test. At least 200 host cells were analysed for each replicate.

5.6 Non-aggregating mutant exhibits reduced replicative invasions in a co-infection assay

A co-infection assay is used to simultaneously infect the host with different strains of *L. monocytogenes*, and experimentally analyse the mutation-associated fitness of a mutant against the wildtype strain. It has successfully been used in *L. monocytogenes* (Pentecost, Kumaran, Ghosh et al., 2010). A co-infection assay (Section 2.8.5) was used to analyse the role that aggregation has in the invasion and subsequent establishment of a replicative invasion in HeLa cells. A mixed, but equal population of differentially fluorescently labelled Lm-GFP (MOI = 10) and Lm-actA-

ΔC-dsRed (MOI = 10) were used to infect host cells for a total MOI of 20. The images show that wildtype *L. monocytogenes* forms aggregates on the surface of host cells while associated *actA-Δ*C mutants are single cells, but both were able to form replicative invasions (Figure 5.7A). Additionally, there is a lack of co-operativity between the strains, there were instances where single actA-*Δ*C mutants became associated with wildtype aggregates, yet no evidence that this results in replication of the mutant strain in the host cells associated with these aggregates (Figure 5.7B). The proportion of replicative invasions in wildtype Lm-GFP was 4.8% (+-0.5%). In the mutant this success rate was over 10-fold lower, 0.4% (±0.1%) of the host cells harboured infections from Lm-*actA-ΔC*-dsRed (Figure 5.7B).

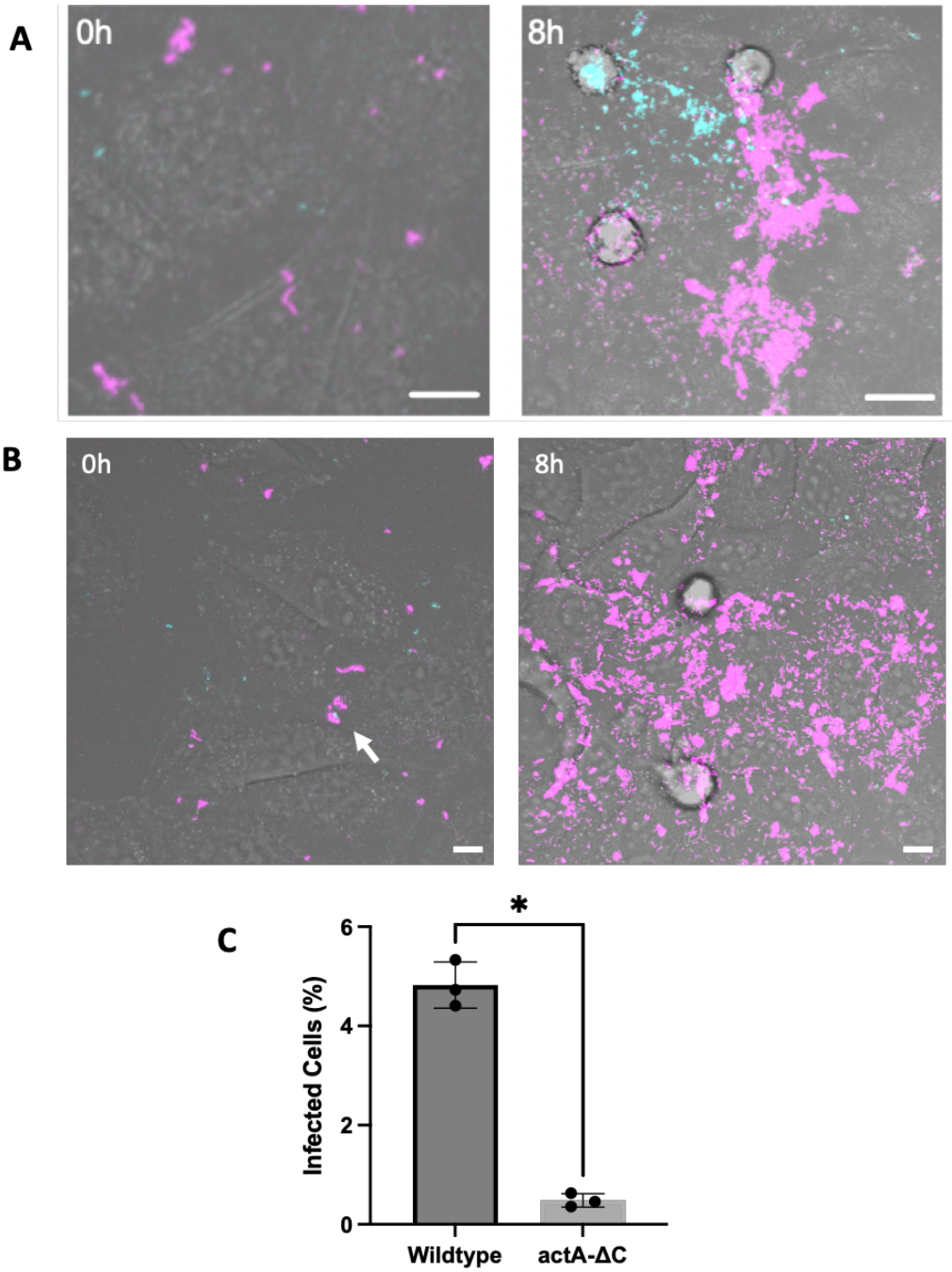

Figure 5. 7. Live cell imaging and analysis of co-infection assay. A) Representative microscopy images of a co-infection experiment at indicated times. HeLa cells co-infected with wildtype Lm-GFP (depicted in magenta) and Lm-*actA-ΔC*-dsRed (depicted in cyan) strains, MOI=10 of each strain was used for a total MOI=20. Scale bar 10 µm **B)** Representative images showing that *Lm-actA-ΔC*-dsRed became associated with Lm-GFP aggregates but was not involved in the replicative invasion. Scale bar 10 µm **C)** Percentage of HeLa cells harboring replicative invasion events. HeLa cells infected with wildtype Lm-GFP (left) and Lm-*actA-ΔC*-dsRed (right) strains at

MOI=10 each (total MOI=20). Shown is the fraction of host cells harboring a replicative invasion event at 2 hours after gentamicin treatment. Individual replicates are shown in circles with mean of 3 biological replicate experiments as solid bars and standard deviation represented by error bars. Statistical significance (* = p-value < 0.05) assessed using non-parametric one-sided Mann-Whitney test.

5.7 The role of aggregation during invasion of the primary HUVEC cells

HeLa cells have been widely used as host cells to study infection by *L. monocytogenes in vitro* (Batan, Braselmann, Minson et al., 2018; Francis and Thomas, 1996; Quereda, Morel, Lopez-Montero et al., 2022). Primary cells can be used to verify observations in a more physiological context and validate observations in primary tissue. HUVEC cells, which are primary endothelial cells from the umbilical cord, have been previously used in studies of *L. monocytogenes* infection (Parida, Domann, Rohde et al., 1998). Using the live cell infection assay developed in section 3.1, the invasion of HUVEC cells was analysed to determine whether aggregation plays a role in establishing robust invasion and subsequent infection in these primary cells. Due to increased sensitivity to the cytotoxicity of *L. monocytogenes* to high MOI (Figure 5.8A) a lower MOI of 5 was used to infect the host cells, however even at this lower infectious dose aggregates were formed (Figure 5.8B), which resulted in replicative invasions (Figure 5.8C). The images show that successful invasions and imaging using the HUVEC cells and *L. monocytogenes* and track individual infection events in a similar way to the live cell experiments in HeLa cells. In agreement with experimental data from the HeLa cells, we found that approximately 2.1% (±0.3%) HUVEC cells were infected with the wildtype Lm-dsRed-P*actA*-GFP strain, and 3-times less 0.7% (±0.6%) were infected with non-aggregating Lm-*actA-ΔC*-dsRed-P*actA*-GFP (Figure 5.8D). Overall the data is in agreement with observations in the HeLa cell model – wildtype aggregating *L. monocytogenes* has a higher rate of replicative invasions than the non-aggregating *actA*-Δ*C* mutant.

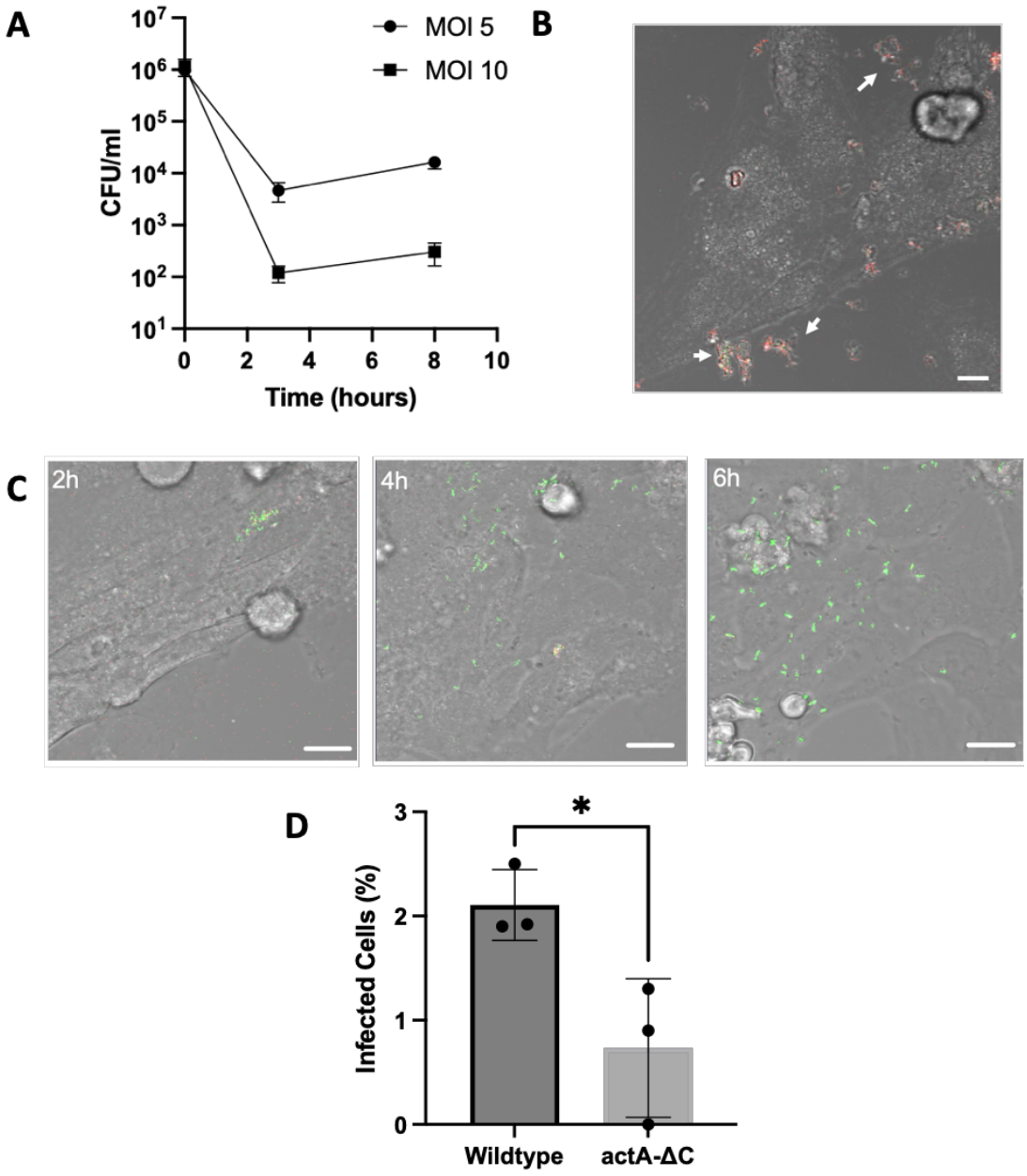

Figure 5. 8. Aggregation impaired mutant has decreased invasion in HUVEC cells.
A) Gentamicin protection assay where different MOIs of wildtype *L. monocytogenes* were used to infect HUVEC cells for 2 hours, gentamicin added and bacterial counts taken at 3 hour and 8 hours. The experiment was performed as 3 biological replicates and data points represent the average with error bars showing standard deviation
B) Representative image from the first 2 hours of the infection assay showing aggregate formation on the surface of HUVEC cells. Lm-dsRed-*PactA*-GFP were used to infect HUVEC cells at MOI=5 for 2 hours. Arrows show aggregates of bacteria. Scale bar 10 µm

C) Time lapse showing the establishment of a successful replicative invasion in primary HUVEC cells over 8 hours after addition of gentamicin. Lm-dsRed-*PactA-GFP* was used to infect HUVEC cells at MOI=5 for 2 hours. After 2 hours gentamicin was added and the cells were imaged for a further 8 hours **C)** Percentage of primary HUVEC cells harboring replicative invasion events. HUVEC cells infected with wildtype Lm-dsRed-*PactA*-GFP (left) and Lm-*actA-ΔC*-dsRed-*PactA*-GFP (right) strains at MOI=5. Individual replicates are shown in circles with mean of 3 biological replicate experiments as solid bars and standard deviation represented by error bars. Statistical significance (* = $p < 0.05$) assessed using one-sided Mann-Whitney test.

5.8 MET-InlB interactions and aggregation

In HeLa cells E-cadherin, the receptor for InlA-mediated invasion, is not expressed (Vessey, Wilding, Folarin et al., 1995) therefore the internalisation pathway occurs mostly through the InlB-Met clathrin-mediated uptake pathway (Braun, Ohayon and Cossart, 1998). Interestingly, previous data suggest that expression of the Met receptor exclusively is regulated by the host cell cycle, with a peak of expression at the G2/M phase (Liu, Lui, Mok et al., 1997; Whitfield, Sherlock, Saldanha et al., 2002). This may suggest that Met expression is the factor underlying cell-cycle dependency of the host cell entry of *L. monocytogenes* as described in Section 3. A gentamicin protection assay was used to validate the degree which InlB-mediated invasion is required in HeLa cell invasion. HeLa cells were infected with wildtype *L. monocytogenes* and an *ΔinlB* deletion mutant and after 2 hours gentamicin was added to kill extracellular bacteria. 3 hours after the addition of gentamicin the total number of CFU per well in the wildtype was 8.52×10^4 ($\pm 3.71 \times 10^4$) CFU/mL. In the *ΔinlB* mutant there was a 9-fold decrease in viable intracellular bacteria to 9.29×10^3 ($\pm 5.74 \times 10^3$) CFU/ml (Figure 5.9). The difference in CFU between the wildtype and the mutant was maintained for 24h.This confirmed that the invasion process of HeLa cells is InlB and thus MET dependent.

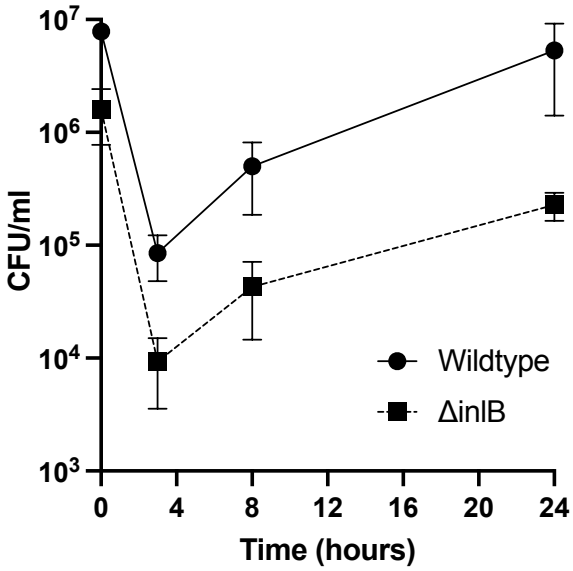

Figure 5. 9. InlB is required for efficient invasion of HeLa cells. HeLa cells were infected with either wildtype *L. monocytogenes* (circles) or *ΔinlB* deletion mutant (squares) for 2 hours at MOI=20. After 2 hours the first time point sample was taken and then gentamicin was added to kill intracellular bacteria. Data points were taken at 3 hours, 8 hours and 24 hours after the addition of gentamicin. The experiment was performed as 3 biological replicates and data points represent the average with error bars showing standard deviation.

To investigate the interactions of aggregates and Met receptors an anti-Met antibody with a fluorescently tagged secondary antibody was used to stain Met on the HeLa cells infected with fluorescently labelled strains of wildtype *L. monocytogenes* and *actA-ΔC* mutant at a MOI=20. Strikingly, wildtype aggregates were associated with areas where Met signal was the strongest. In contrast, there seemed to be no correlation between single *actA-ΔC* mutants and levels of Met in the non-aggregating mutant (Figure 5.10).

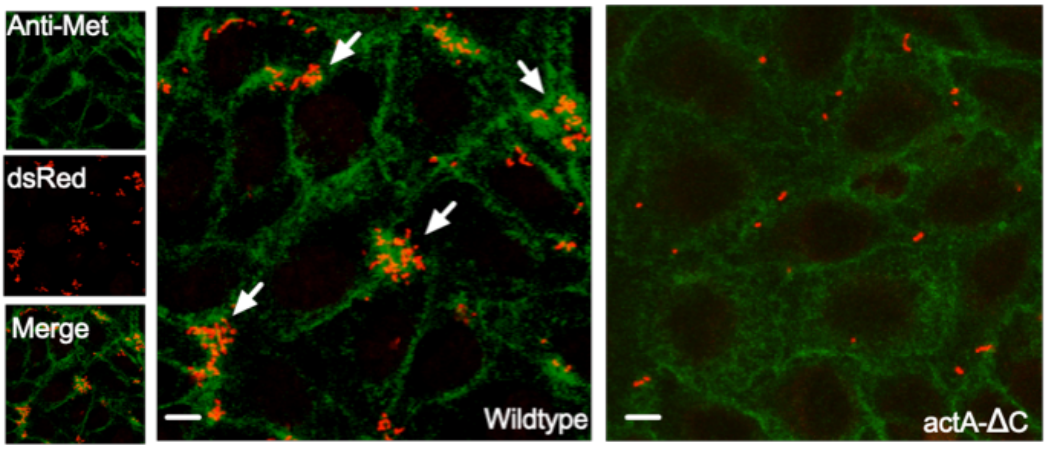

Figure 5. 10. Aggregates form on areas of high MET receptors. A) Representative images from 3 biological replicates of experiments where HeLa cells stained with Anti-Met antibody (green) were infected with both wildtype Lm-dsRed (left) and Lm-*actA-ΔC*-dsRed (right) constitutively expressing dsRed (red) for 2 hours at MOI=20. Arrows point to areas where aggregates are associated with high levels of Met. Images on the left show individually imaged fluorophores as well as the merged final image (bottom). Scale bar 5 µm.

To further investigate this interaction, a pulse and chase method was used to deplete the HeLa cells of available Met receptors, as previously described (Li, Dick, Lu et al., 2019). A pulse and chase method is performed by adding a high concentration of specific antibody for the receptor to the cells, incubating for 1 hour and then washing and incubating the cells in media for 2 hours (Section 2.9.2). This has been shown to deplete the cell surface of Met (Li, Dick, Lu et al., 2019) . By reducing or depleting the available Met on the cell surface there would be a reduction in the ability of wildtype *L. monocytogenes* to form successful aggregates on HeLa cells. After treating HeLa cells with anti-Met for 1 hour there was an almost total depletion in the level of Met on the cell surface (Figure 5.11A). Infection of Met-depleted cells with Lm-dsRed resulted in a reduction in the number and size of aggregates formed after a 2 hour infection period compared to control cells in which Met had not been depleted (Figure 5.11B).

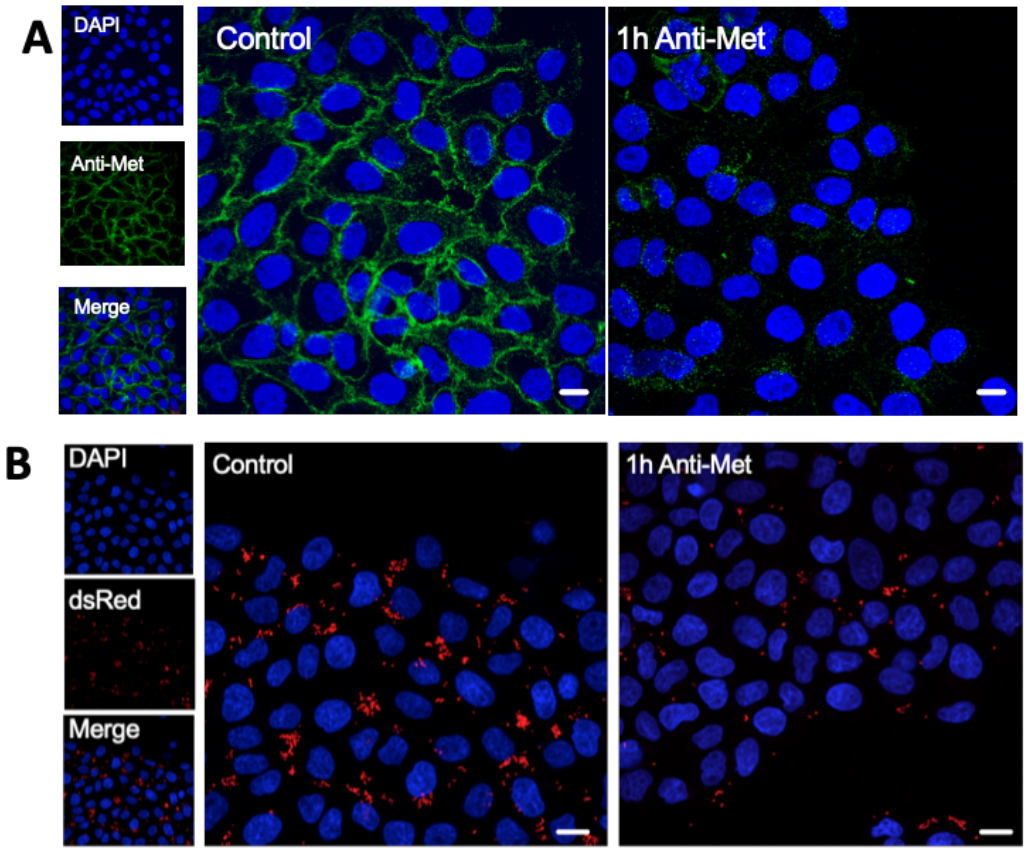

Figure 5. 11. MET depletion impairs aggregate association with host cells. A) Representative images showing the depletion of Met on the cell surface. HeLa cells were treated with anti-Met antibody for 1 hour (right), incubated for 2 hours and then stained with anti-met (green) and DAPI (blue). An untreated control is shown for comparison (left). The small images on the left show individually imaged channels with the corresponding merged image. Scale bar 10 µm. **B)** Representative images of HeLa cells stained with DAPI (blue) treated with Anti-Met antibody for 1 hour (right) and an untreated control (left). The HeLa cells were infected with both wildtype *L. monocytogenes* constitutively expressing dsRed (red) for 2 hours at MOI=20. The images on the left show individual channels with the corresponding merged image. Scale bar 10 µm

Quantitative analysis of these images showed that there was a reduction in the average bacteria per cell in the Met-treated cells, from 8.17 (±0.27) bacteria per cell on the untreated control cells to 3.25 (±1.07) bacteria per cell in the Met-treated cells (Figure 5.12A). The average size of aggregates is also reduced, from 8.2 (±11.7) μm^2 in size in the control sample to 4.7 (±5.5) μm^2 in the Anti-Met treated cells (Figure 5.12B)

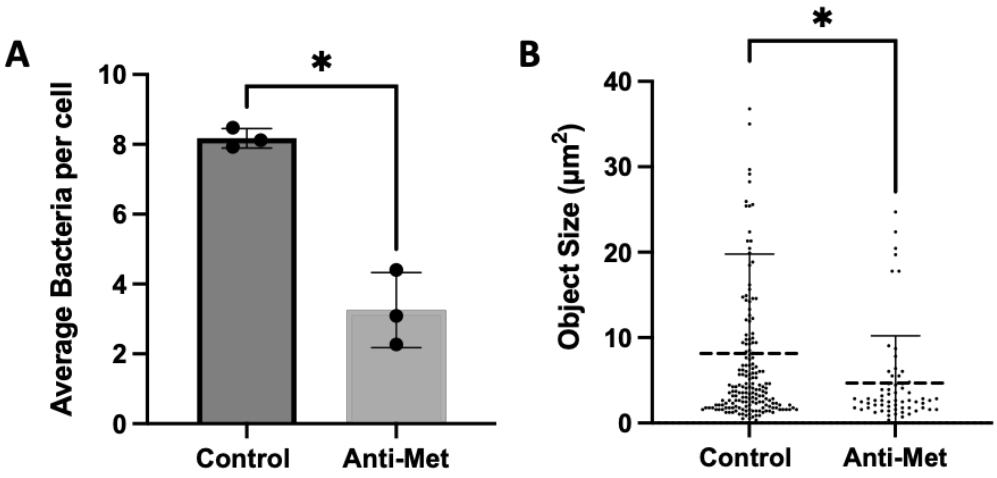

Figure 5. 12. MET depletion reduces number of associated bacteria and aggregate size. A) Graph showing the average number of bacteria per host in untreated (left) and anti-Met treated cell (right) cells after infecting with MOI=20 wildtype Lm-dsRed across 4 replicates. Averages for individual replicates are shown by circles and the bar represents the overall average. The error bars represent standard deviation and statistical significance is calculated using a non-parametric one-tailed Mann-Whitney test. **B)** The average size of bacterial objects with data pooled from across 4 individual replicates in the control cells (left) and the anti-Met treated cells (right). Individual circles represent individual object. Dashed line shows the mean value and error bars show the standard deviation. Statistical significance is calculated using a Mann-Whitney test (* = $p < 0.05$)

5.9 Discussion

Through a range of experiments utilising a non-aggregating *L. monocytogenes* mutant in live cell imaging this study demonstrated a novel and undescribed interaction in *L. monocytogenes* whereby aggregates of bacteria enter the host cell simultaneously. Because the non-aggregating mutant was impaired in its ability to form replicative invasions in HeLa cells (4-fold reduction) and primary HUVEC cells (3-fold reduction), had a lower probability of intracellular invasion in HeLa cells (3.5-fold reduction) and was outcompeted by the wildtype in a co-infection assay, this study has provided strong evidence that aggregation and multiple invasion events is a novel invasion strategy used by *L. monocytogenes*, possibly to increase its low invasion success rate.

The experiments also show a potential mechanistic explanation for the link to the cell cycle. Staining host cells for Met, the receptor for InlB and the main route of entry for *L. monocytogenes* in HeLa cells (Cruz, Pereira-Castro, Almeida et al., 2018; Vessey, Wilding, Folarin et al., 1995) showed an association of Met and *L. monocytogenes* aggregates. When the cells were depleted of Met there was a reduction in the number of bacteria associating with the host cells and the size of the aggregates. A link between Met and the cell cycle has previously been established where expression of Met was shown to be higher during the G2/M phase (Liu, Lui, Mok et al., 1997; Whitfield, Sherlock, Saldanha et al., 2002). Indeed, if cells in the G2/M phase are most susceptible to because of an increased Met expression and interactions with *L. monocytogenes* – then this may explain the low probability of individual *L. monocytogenes* to form replicative invasions, the heterogeneity of host cell susceptibility across the population and the observation that host cells harbouring *L. monocytogenes* undergo mitosis within a short time frame.

This has relevance outside of immortalised cell lines as although primary cells have a finite or limited proliferative lifespan they also undergo the cell cycle and may

also have transient susceptibilities to infection by *L. monocytogenes* (Campisi and d'Adda di Fagagna, 2007).

In summary, through a combination of live cell and fixed imaging this study demonstrated that ActA-mediated aggregation is a novel invasion strategy utilised by *L. monocytogenes* that increases the probability that individual bacterial cells establish a replicative invasion. Aggregation increases the intracellular invasion rate and the capacity for *L. monocytogenes* to form replicative invasions compared the non-aggregating mutant which exhibited a reduced probability for these. Importantly, association with host cells is dependent on the presence of Met receptors which implies that aggregation occurs on the surface of cells.

6. Understanding the role of virulence factors during *L. monocytogenes* aggregation

6.1 Spent media upregulates virulence gene expression

A key observation in chapter 4 was the activation of PrfA that occurred during the formation of aggregates, as shown by a fluorescent reporter of *actA* transcription (Figure 4.1). This effect was seen in the infection assays and the spent media assay. To further investigate the changes in P*actA* reporter expression, quantification at a single cell level was taken by measuring the total level of GFP (Lm-dsRed-*PactA*-GFP) in individual bacteria by live cell confocal microscopy after incubation in spent or fresh media for 2 hours. GFP expression was analysed at the single cell level using image analysis software FIJI. Individual bacteria were segmented manually and the average mean intensity of GFP fluorescence was measured per object (Figure 6.1A). At 2 hours after incubation, bacteria in fresh media had a mean intensity of 6.3 (±4.3), bacteria incubated in spent media had a mean intensity of 18.6 (±20.54) a 3-fold increase in mean intensity (Figure 6.1B).

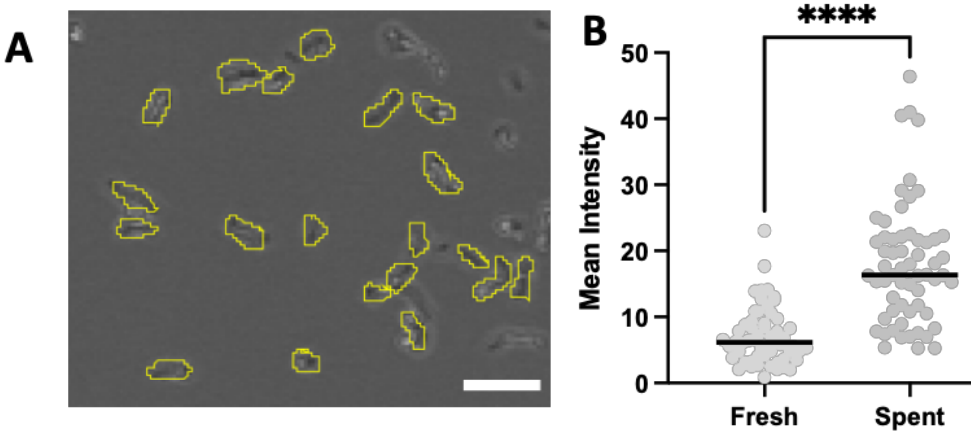

Figure 6. 1. Analysis of *PactA*-GFP expression in fresh and spent media at the single-cell level. 1.0 x 10^7 CFU of Lm-dsRed-P*actA*-GFP were incubated in fresh or spent media (retrieved as described in Section 2.6.1) for 2 hours and imaged with live cell confocal microscopy. **A)** Representative image showing segmentation of individual bacteria in FIJI for measuring mean intensity of GFP across the area (yellow lines). **B)** Mean intensity of GFP across 60 objects for each fresh (left) and spent (right) media. Each dot represents an individual object, error bars show standard deviation and the dotted line represents the mean of 3 biological replicates. Statistical analysis was performed using a Mann-Whitney test (**** = $p < 0.0001$)

Further to this, virulence gene expression in spent media in the wildtype and the *actA*-ΔC mutant was analysed to determine if the process of aggregation induces changes in gene expression. Both wildtype and mutant bacteria were exposed to spent media for 2 hours as per the aggregation assay. The mean expression of GFP by bacteria in aggregates was compared against planktonic non-aggregating mutant. This was performed in FIJI using the freehand draw tool to define regions of interest to be analysed. This data was collected and analysed with the help of MSc project student Kristina Stambolyiska, who assisted with experiments under the author's supervision and analysed the data. In the wildtype, the mean intensity of GFP fluorescence was 20.8 (±17.3) and in the non-aggregating *actA*-ΔC mutant it

was reduced to 10.9 (±14.3) (Figure 6.2). This suggests the process of aggregation has an effect on virulence gene expression.

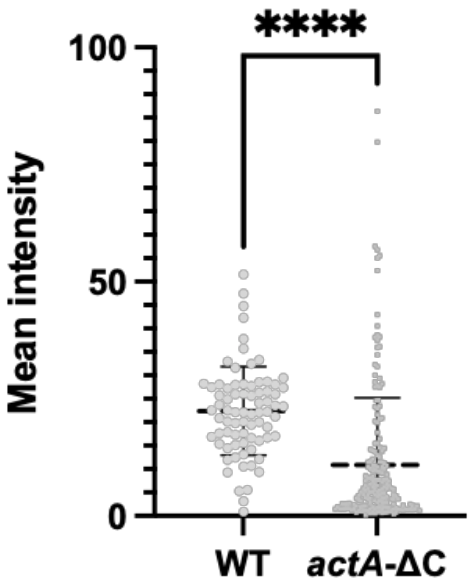

Figure 6. 2. Analysis of *PactA*-GFP expression in spent media for wildtype L. monocytogenes and *actA*-ΔC mutant the single-cell level. Mean intensity of GFP across at least 75 objects for wildtype (left) and *actA*-ΔC (right). Each dot represents an individual object, error bars show standard deviation and the dotted line represents the mean of 3 biological replicates. Statistical analysis was performed using a Mann-Whitney test (**** = $p < 0.0001$)

6.2 Transcriptomic analysis of wildtype and *actA*-ΔC *L. monocytogenes* in spent and fresh media

There is a clear transcriptional response to the host factor in spent media. This leads to aggregation which was shown in the previous chapter to increase the probability of bacteria to form replicative invasions in host cells. Additionally, the process of aggregation by *L. monocytogenes* may induce further transcriptional changes, as suggested by the P*actA* reporter analysis. This suggests there may be a positive feedback loop during aggregation on PrfA-regulated gene expression. In

addition, the regulation of genes during aggregation must be further understood. To investigate this the gene expression changes during the formation of aggregates after exposure to spent media in the wildtype and *actA*-ΔC mutant was analysed. RNA-Seq was performed on *L. monocytogenes* incubated in either spent or fresh media for 2 hours at 37°C for both wildtype *L. monocytogenes* and the *actA*-ΔC mutant. This analysis will investigate into the effect of the host factor in spent media on gene expression and additionally whether aggregated bacteria have differential gene expression to planktonic bacteria in key genes such as those in the PrfA regulon.

This RNA-seq data represents a preliminary study of 2 replicates for each condition with the intention to add 2 more replicates in the immediate future. Principal component analysis (PCA) of the different conditions showed robust separation. In the analysis 71% of the variance was captured by the 1st principal component (PC1) and 21% of the variance was captured by PC2 (Figure 6.3). All 4 conditions showed robust separation and media type (spent or fresh) caused a larger effect on gene expression than genotype (wildtype and *actA*-ΔC). Statistical analysis of differentially expressed genes was performed on the replicates to obtain p values and padj values, which in part involved using information about all dataset (section 2.6.10). Bioinformatic analysis of RNA-seq data was performed by Dr Leo Zeef from the Genomic Technologies Core Facility at the University of Manchester.

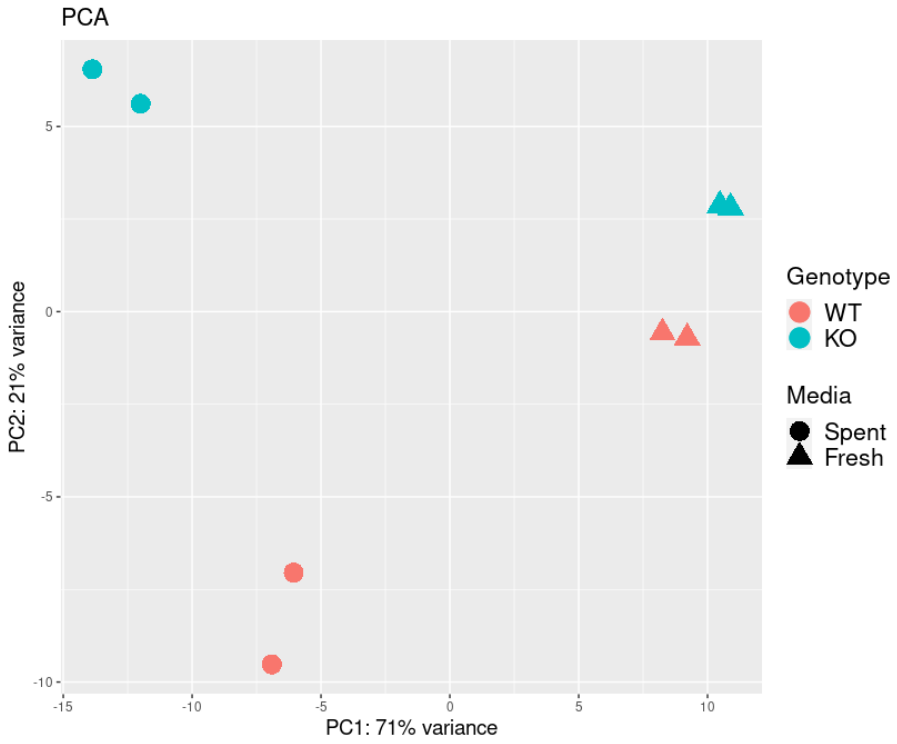

Figure 6. 3. Principal component analysis of gene expression for wildtype and *actA*-ΔC L. monocytogenes in spent and fresh media. 2 replicates were performed for each of the 4 conditions for a total of 8 samples. Individual data points represent an individual replicate. Wildtype *L. monocytogenes* are represented in pink and *actA*-ΔC mutants are represented in blue. Bacteria incubated in fresh media are represented by triangles and spent media (obtained as described in Section 2.6.1) are shown by circles. Variance explained by PC1 and PC2 are shown on the x-axis and y-axis respectively.

Differential gene expression analysis was performed in DESeq2_1.36.0 (Love, Huber and Anders, 2014), across combination of different conditions to understand regulation of genes associated with spend media and aggregation. Venn diagrams of overlapping gene sets corresponding to the performed pairwise comparisons are shown in Figure 6.4. All genes had a padj < 0.05 which represents statistical significance, as the padj retrieved by DESeq2 performs a Bonferoni correction to adjust the p-value to filter out false-positive errors (section 2.6.10).

After exposure to spent media 405 genes were upregulated and 377 genes downregulated in the wildtype in spent media (compared to the fresh media control). 130 of those genes were upregulated and 103 were downregulated in the wildtype exposed to spent media, but not in other conditions – these are the genes exclusively regulated by spent media in aggregates (Figure 6.4, shown in blue). In the *actA*-ΔC mutant after exposure to spent media 435 genes were upregulated and 168 genes were downregulated (compared to the fresh media control). Of these, 130 genes were upregulated and 154 genes were downregulated by the *actA*-ΔC mutant in spent media but not in other conditions (Figure 6.4, shown in purple). 489 regulated gene sets were shared between the wildtype and *actA*-ΔC mutant in response to spent media, 236 genes were upregulated and 253 were downregulated, demonstrating that spent media induces a generic response across both strains (Figure 6.4, shown in the blue-purple overlap). Importantly, the genes belonging to the PrfA regulon were upregulated in both strains due to spent media treatment and are included in this set of shared genes. These data suggest that spent media induces a significant transcriptional change in bacteria, and the process of aggregation also alters the expression a subset of these genes. However, the PrfA regulon is upregulated by spent media but not by aggregation. A more detailed analysis of differentially regulated genes across the conditions is presented below.

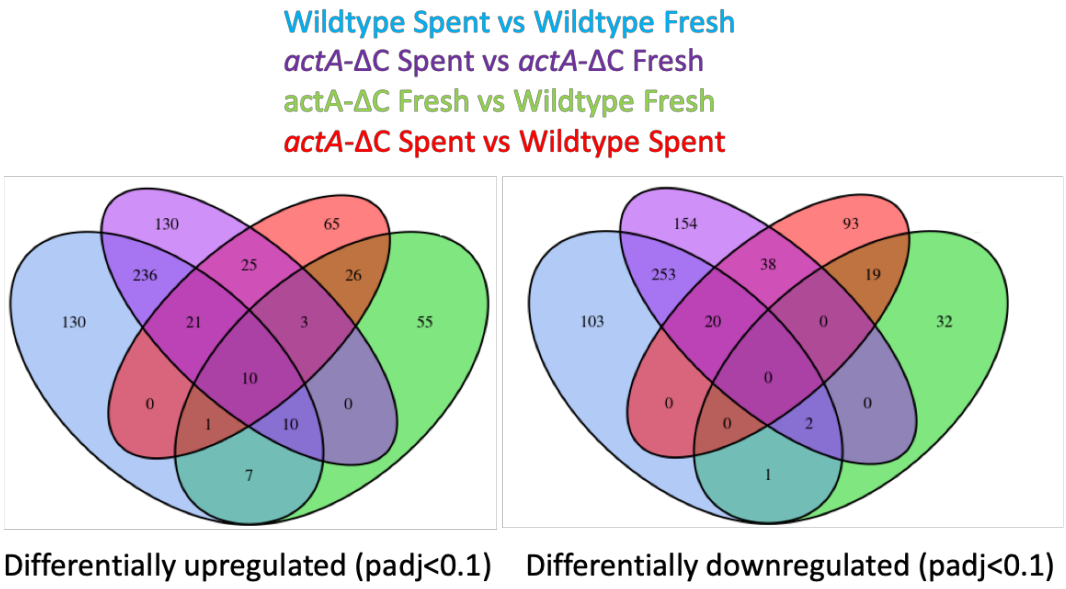

Figure 6. 4. Venn diagram showing overlapping gene sets between the analysed conditions. Left Venn diagram shows genes differentially upregulated and right show genes differentially downregulated. Blue circle represents genes differentially expressed in wildtype bacteria in spent media compared to fresh media, purple represents genes differentially expressed in *actA*-ΔC in spent media compared to fresh media. Green represents genes differentially expressed in *actA*-ΔC in fresh media compared to the wildtype and red represents genes differentially expressed in *actA*-ΔC in spent media compared to the wildtype. Numbers represent the number of genes and overlaps show the number of shared gene sets between analysed conditions.

6.3 Differentially expressed genes in spent media

From these lists of differentially analysed genes, analysis of the specific genes that were differentially regulated in spent media compared to fresh media in the wildtype was performed. A threshold of padj < 0.05 and Log2 fold change <-1 or >1 were set, the number of genes that fall within these parameters are shown on a volcano plot (Figure 6.5A). The Log2 fold changes and names of characterised genes are shown on a heat map sorted by gene function (Figure 6.5B).

There were 7 differentially upregulated genes that were directly involved in iron scavenging and iron uptake. The gene *srtB* had a mean log2 fold change of 2.6 and encodes Sortase B (SrtB), a second class sortase in *L. monocytogenes* which is involved in the attachment of a subset of proteins to the cell wall by recognising an NXZTN sorting motif (Bierne, Garandeau, Pucciarelli et al., 2004).

isdC and *isdE* showed log2 fold increases of 2.5 and 2.0 respectively. These genes encode for proteins in a high-affinity heme uptake system protein required for scavenging and Fe^{2+}/Fe^{3+} binding (Grigg, Vermeiren, Heinrichs et al., 2007). These proteins are linked to SrtB which acts on their recognisable motifs (NxyTN) (Newton, Klebba, Raynaud et al., 2005).

efeB showed a mean Log2 fold increase of 2.4. It encodes for deferrochelatase, which is involved in the recovery of exogenous heme iron. It extracts iron from heme while preserving the protoporphyrin ring intact (Lechowicz and Krawczyk-Balska, 2015).

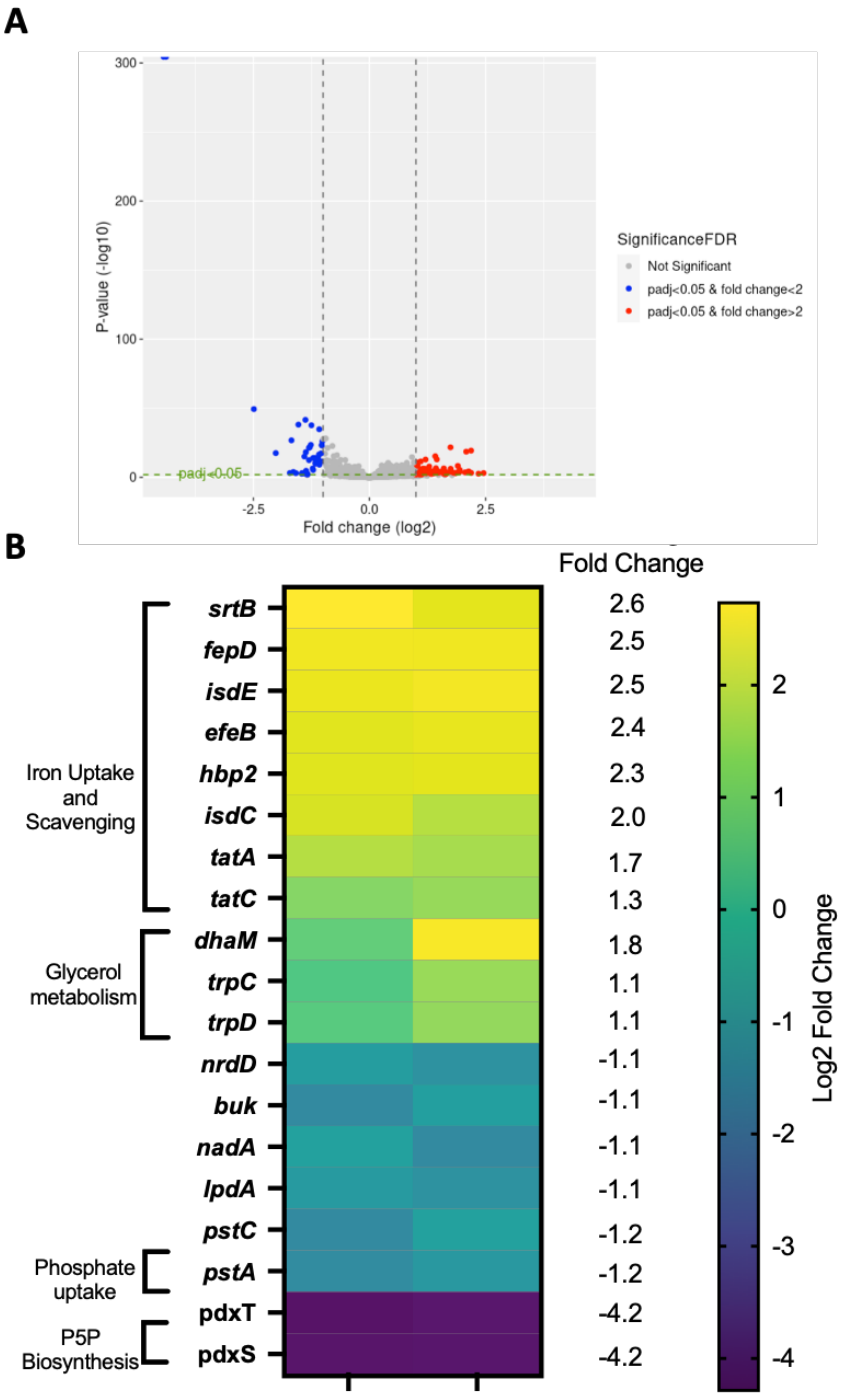

Figure 6. 5. Genes showing significant transcriptomic changes after wildtype *L. monocytogenes* exposure to spent media. A) Volcano plot showing differentially regulated genes in spent media compared to fresh in 2 biological replicates. Circles represent individual genes. Dotted lines represent the thresholds set for filtering differentially expressed genes, a padj < 0.05 and a Log2 fold change <-1 or >1. Red circles represent differentially upregulated genes and blue circles represent differentially downregulated genes. **B)** A heat map showing Log2 fold-change values

for all characterised genes that had a Log2 fold change >1 or <-1. Log2 fold change shows the change in transcript levels in spent media compared to the fresh media baseline. The values for 2 replicates for each gene listed on the left are shown. Genes are sorted from the highest mean fold change (top) to the lowest (bottom) and the values are shown on the right. The key shows the Log2 fold change values each colour represents. All Log2 fold changes are significant with padj < 0.05.

hbp2 showed a mean Log2 fold increase of 2.3 and encodes for Hemoglobin binding protein 2. This is a hemophore that scavenges heme from the environment. It is expressed under iron-deficient conditions from the *svpA-srtB* operon, which also encodes SrtB. It is predicted to be covalently attached to the cell wall by the SrtB sortase because it contains the appropriate recognition motif (Malmirchegini, Sjodt, Shnitkind et al., 2014).

tatA and *tatC* are genes in Twin-arginine translocation pathway and showed Log2 fold increases in of 1.7 and 1.3 respectively. Homologous genes in *S. aureus*, show evidence of the involvement of the Tat pathway in transporting an iron dependent peroxidase (FepB, homologous to the protein *efeB* codes) and in successful in vivo infections (Machado, Lourenco, Carvalho et al., 2013).

3 genes involved in glycerol metabolism were also upregulated. *dhaM,* showed a mean Log2 fold increase of 1.8. It encodes PEP-dependent dihydroxyacetone kinase 1 phosphoryl donor subunit DhaM, which is a part of the transformation of glycerol into dihydroxyacetone (Monniot, Zebre, Ake et al., 2012). *trpD* and *trpC* showed 1.1 mean Log2 fold increases and encode for anthranilate phosphoribosyltransferase and indole-3-glycerol phosphate synthase respectively**.** These proteins are involved in the biosynthesis of L-tryptophan from glycerol metabolism (Joseph, Mertins, Stoll et al., 2008).

Significantly downregulated genes included two genes involved in pyridoxal 5'-phosphate (P5P) biosynthesis, *pdxT* and *pdxS* showed a mean Log2 fold decrease of -4.2. P5P is an essential cofactor for numerous metabolic enzymes (Belitsky, 2004). *pstA* and *pstC* encode two transmembrane proteins involved in the phosphate

transport system (Choi, Sureka, Woodward et al., 2015; Moreno-Letelier, Olmedo, Eguiarte et al., 2011) and showed a mean Log2 fold change of -1.2. The other downregulated genes were *buk*, *nadA*, *nrdD* and *lpdA* which had mean Log2 fold changes of -1.1. *buk* encodes butyrate kinase which in *L. monocytogenes* allows utilisation of multiple substrates for energy (Sirobhushanam, Galva, Saunders et al., 2017). *nadA* is involved in the biosynthesis of quinoline and subsequently Nicotinamide adenine dinucleotide (NAD) (Rousset, Fontecave and Ollagnier de Choudens, 2008). *nrdD* encodes class III anaerobic ribonucleotide reductase used in anaerobic conditions, however this protein has impaired function in EGD-e due to a 6 amino acid deletion (Ofer, Kreft, Logan et al., 2011). *lpdA* forms part of the *bkd* operon of branched-chain alpha-keto acid dehydrogenases (Stasiewicz, Wiedmann and Bergholz, 2011).

Next, the core PrfA regulon was analysed to determine the effect that spent media has on PrfA-regulated virulence gene expression in wildtype *L. monocytogenes* (Figure 6.6). As expected, many of the genes in the core PrfA regulon were upregulated. The Log2 fold change of *plcB* and *actA* were the highest, both showing mean Log2 fold change of 2.5 across the replicates. *orfX (2.1)*, *hly (1.9)*, *hpt (1.7)*, *plcA* (1.7) *inlC (1.5)*, *mpl (1.5)* and *prfA* (1.3) itself all showed statistically significant (padj < 0.05) Log2 fold increase. Interestingly, of all the genes *inlA* and *inlB* showed the lowest increase with 1.2 and 1.1 mean Log2 fold change respectively. These genes are also regulated by SigB which was previously shown to have no role in aggregation. SigB did not show significant upregulation by spent media (Log2 fold change -0.08, padj = 0.496, data not shown).

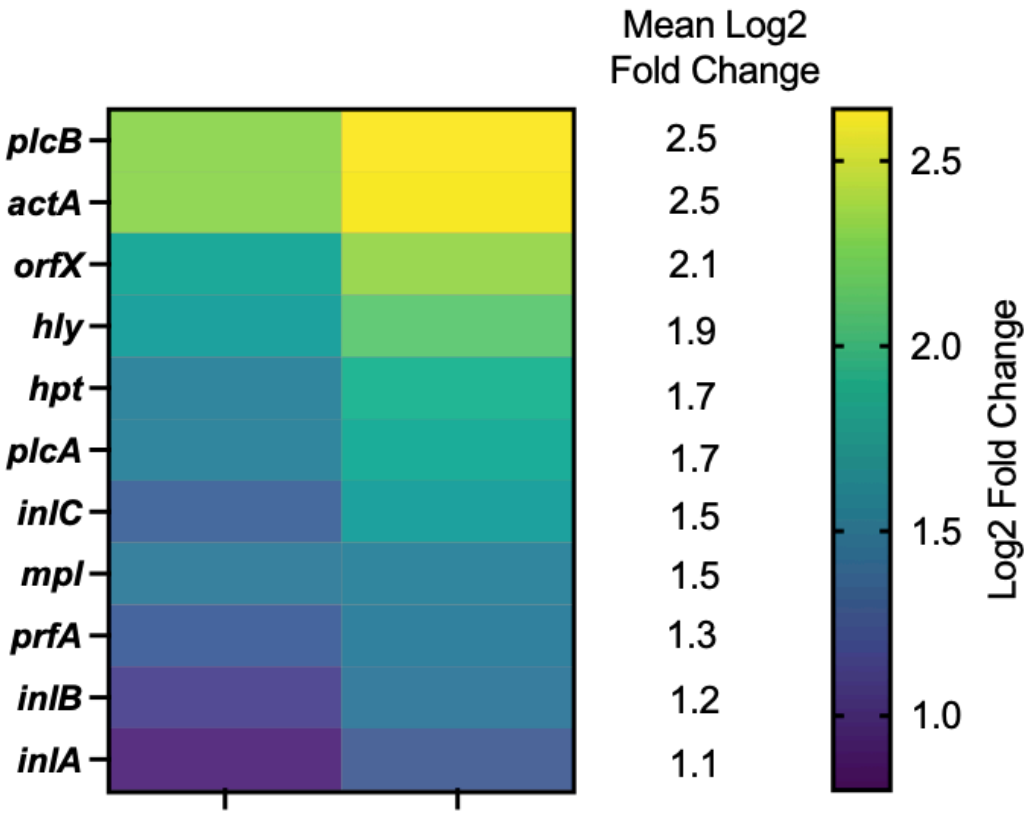

Figure 6. 6.Transcriptomic changes to the core PrfA regulon after wildtype *L. monocytogenes* exposure to spent media. Heat map showing log2 fold-change in spent vs fresh media for the core genes of the PrfA-regulon for two replicates. Genes are sorted from the highest Log2 fold change (top) to the lowest (bottom) and the key shows the Log2 fold change values each colour represents. Mean Log2 fold change of the replicates is reported in the list on the right. All log2 fold changes are significant with padj < 0.05.

6.4 Differentially expressed genes in *actA-ΔC* mutant in spent media

The process of aggregation itself may change the transcription profile of *L. monocytogenes*. These transcriptional changes may be important in the formation of aggregates and the biological role of aggregates in invasion. To investigate this, differentially expressed genes between wildtype *L. monocytogenes* and the non-aggregating *actA-ΔC* mutant exposed to spent media for 2 hours at 37°C were analysed. A threshold of padj < 0.05 and Log2 fold change <-1 or >1 were set and

these are shown on a volcano plot (Figure 6.7A). The Log2 fold changes and names of previously characterised genes are shown on a heat map sorted by gene function (Figure 6.7B).

Several genes involved in cationic peptide resistance were upregulated in the non-aggregating mutant. *mprF* showed a mean Log2 fold change of 2.9. *mprF* encodes for multiple peptide resistance factor and is involved in cationic antimicrobial peptide resistance by reducing the charge of the bacterial cell wall (Thedieck, Hain, Mohamed et al., 2006). All 4 genes of the *dlt* operon – *dltA*, *dltB*, *dltC* and *dltD* showed mean Log2 fold changes of 1.7, 1.6, 1.5 and 1.3 respectively. These genes catalyse the incorporation of d-alanine residues onto the bacterial cell wall and confer resistance to cationic antimicrobial peptides and play a role in adhesion and virulence (Abachin, Poyart, Pellegrini et al., 2002). These genes are regulated by VirR, a regulator that forms part of a two-component sensing system (VirR/VirS) that is important to *L. monocytogenes* virulence (Mandin, Fsihi, Dussurget et al., 2005).

Significantly downregulated genes in the *actA-ΔC* mutant included *trpD* and *trpC* which had a mean Log2 fold change of -1.1 These are involved in the biosynthesis of L-tryptophan from glycerol metabolism (Joseph, Mertins, Stoll et al., 2008). *nadB* had a Log2 fold change of -1.1 and is involved in biosynthesis of quinoline and subsequently Nicotinamide adenine dinucleotide (NAD) (Rousset, Fontecave and Ollagnier de Choudens, 2008).

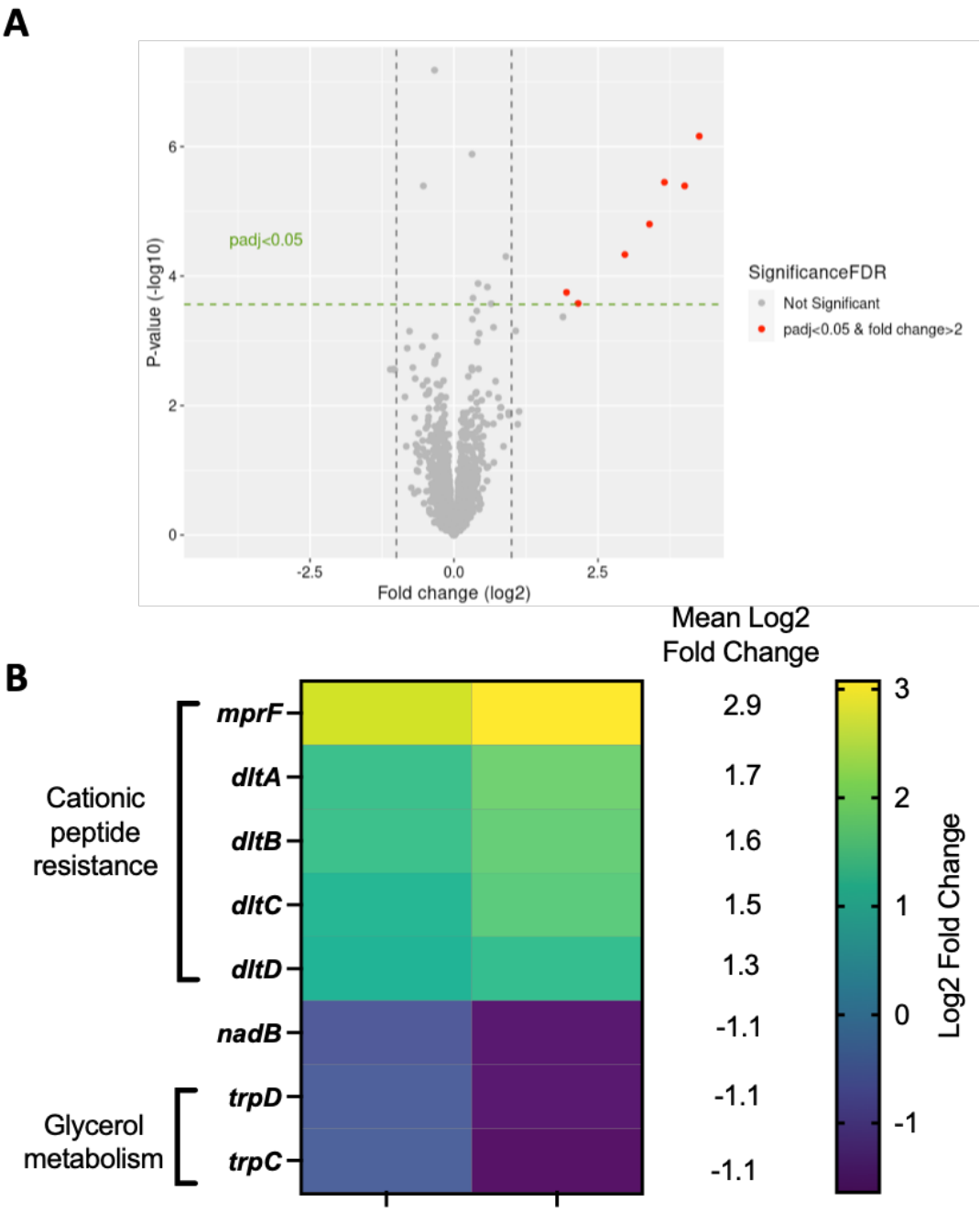

Figure 6. 7 Genes showing significant transcriptional changes in spent media treated *actA-ΔC* compared to wildtype. A) Volcano plot showing differentially regulated genes in spent media compared to fresh in 2 biological replicates. Circles represent individual genes. Dotted lines represent the thresholds set for filtering differentially expressed genes, a padj < 0.05 and a Log2 fold change <-1 or >1. Red circles represent differentially upregulated genes and blue circles represent differentially downregulated genes. **B)** A heat map showing Log2 fold-change values

for all characterised genes that had a fold change >1 or <-1. Log2 fold change shows the change in transcript levels non-aggregating *actA-ΔC* mutant compared to the wildtype baseline. The values for two replicates for each gene listed on the left are shown. Genes are sorted from the highest mean fold change (top) to the lowest (bottom) and grouped by function and mean Log2 fold change is reported on the right. The key shows the Log2 fold change values each colour represents. All Log2 fold changes are significant with padj < 0.05.

Next, the PrfA-regulon was analysed. In the data set all the genes in the PrfA regulon had a padj < 0.05 but did not show significant transcriptional change the non-aggregating mutant compared to the wildtype, all mean Log2 fold changes were between 1 and -1 (Figure 6.8).

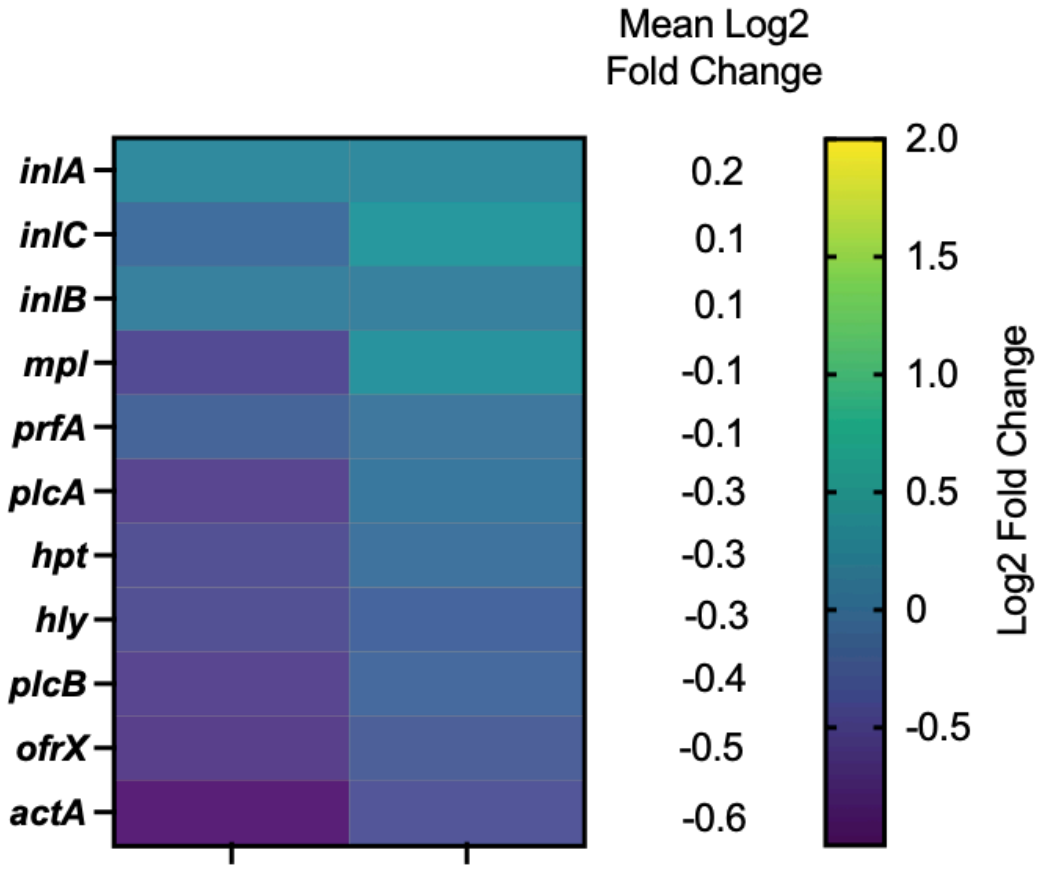

Figure 6. 8. Transcriptomic changes to the core PrfA regulon when comparing wildtype *L. monocytogenes* and the non-aggregating *actA-ΔC* mutant exposure to spent media. Heat map showing Log2 fold-change values for the core genes of the PrfA-regulon. Log2 fold change shows the change in transcript levels in the non-aggregating *actA-ΔC* mutant compared to the wildtype. The values for two replicates for each gene listed on the left are shown Mean Log2 fold change is reported in the list on the right. Genes are sorted from the highest mean fold change (top) to the lowest (bottom) and the key shows the Log2 fold change values each colour represents.

6.5 Discussion

6.5.1 Differential gene expression in *L. monocytogenes* during aggregation

The imaging experiments showed that ActA mediated aggregation is a key interaction between host cells and bacteria that affects infection outcomes. To further investigate the patterns of gene expression that underlie this interaction a transcriptomic analysis of aggregating wildtype and non-aggregating *actA-Δ*C bacteria exposed to spent media. The RNA-Seq experiment revealed intriguing differential gene expression patterns that may indicate some of the mechanisms that are involved in the response to the host cell factor and subsequent aggregation phenotype.

6.5.2 Exposure to host factor in spent media induces a virulence-related transcriptional change

Analysis of gene expression in wildtype *L. monocytogenes* in response to the host factor in spent media revealed an upregulation in iron scavenging and uptake genes. Iron is an element that is required by almost all living organisms and is required for many biological processes such as oxygen transport, DNA biosynthesis and energy production (Andrews, Robinson and Rodriguez-Quinones, 2003). Despite being widespread in the environment iron has a low availability for living organisms due to its low solubility (Lechowicz and Krawczyk-Balska, 2015). Iron sequestration is a strategy employed by hosts protect themselves from bacterial infection by causing the concentration of iron to be too low to support bacterial growth, this is known as nutritional immunity (Latunde-Dada, 2009). The host binds iron with transferrin in the serum and lactoferrin in the mucus membranes (Hammer and Skaar, 2011). Iron is also bound to haem in proteins such as haemoglobin used to oxygen transport. Iron acquisition in pathogens is a key

survival mechanism and *L. monocytogenes* has transport systems that are specifically designed for scavenging iron from host proteins (Lechowicz and Krawczyk-Balska, 2015). This study showed upregulation of genes (*srtB*, *hbpB*) that are directly involved in iron scavenging from haem (Xiao, Jiang, Moore et al., 2011), showing that the bacteria is upregulating genes specifically for surviving in a host environment. Several pathogenic bacteria have receptors for detecting transferrin and lactoferrin (Braun, 2005). It would be interesting to test whether these iron-containing proteins are the >10 kDa host factor that induces aggregation.

Regardless of its identity the host cell factor acts as a signal to *L. monocytogenes* and the RNA-seq data suggests that it is preparing to scavenge iron from intracellular components such as transferrin, lactoferrin and haem-containing proteins to aid in intracellular proliferation. Whether the lack of iron directly affects pathogenicity of *L. monocytogenes*, virulence gene expression or induces aggregation requires further investigation.

The host factor also causes *L. monocytogenes* to change alter its metabolic profile. Genes for glycerol metabolism are upregulated while genes for P5P synthesis and phosphate uptake are downregulated. Glycerol is one of the non-PTS sugars that *L. monocytogenes* utilises in the host cell and is linked to PrfA activity (Joseph, Mertins, Stoll et al., 2008). This suggests that the presence of the host factor primes the bacteria to switch to intracellular gene expression. It is unclear why phosphate uptake and P5P synthesis would be downregulated but these may represent part of the metabolic shift for *L. monocytogenes*.

An alternative explanation for the differential expression in iron uptake genes and genes related to metabolism is due to the nutrient changes in spent media. The spent media has been incubated on live, metabolising human cells for up to 18 hours. This could mean any number of metabolites are increased or depleted in the media, or that available iron is increased/decreased. The bacteria would alter its metabolic state in response to this and this could result in a differential gene expression pattern in spent media compared to fresh media.

The RNAseq experiment also validated the observations of the imaging experiments that there is an increase in virulence gene expression and confirmed that this is across the whole PrfA regulon. *inlA* and *inlB* were the least upregulated, these genes are also SigB regulated (Toledo-Arana, Dussurget, Nikitas et al., 2009) and no increase was seen in *sigB* expression.

6.5.3 The process of aggregation induces a transcriptional change

When comparing the gene expression of the wildtype against the non-aggregating *actA*-ΔC mutant, the most striking observation was the higher transcription levels of genes involved in cationic antimicrobial peptide resistance in the non-aggregating bacteria. This raises an interesting question of whether aggregation itself may protect against cationic peptides, and whether aggregated bacteria do not require upregulation of these genes as much as planktonic cells do. In a study in *P. aeruginosa* genes involved in aggregate formation, aggregation genes were shown to increase resistance to a cationic antimicrobial peptide (Santos-Lopez, Fritz, Lombardo et al., 2021). Further work would be required to understand the specific role these genes play in aggregation in aggregate formation and virulence. Overall, the presence of the host factor in spent media induced transcriptional changes in *L. monocytogenes* that are related to survival in the host and virulence. Aggregation may afford some protection against cationic peptides, another potential adaption for *L. monocytogenes* survival in the host.

Overall, this RNA-seq analysis provides an insightful analysis of the gene expression patterns associated with aggregation. However, only two replicates were analysed for each condition. For these results to be fully validated more biological replicates of condition must be obtained and combined with the analysis here.

To summarise, spent media causes a transcriptional change in a set of genes, but only a subset of these genes are associated with aggregation. Specific analysis of differentially regulated genes showed that PrfA upregulation is the effect of the host factor in the spent media, and not by the process of aggregation. In spent media *L. monocytogenes* also upregulates genes involved in iron scavenging/iron uptake and glycerol metabolism while downregulating genes involved in phosphate uptake and P5P biosynthesis. The genes regulated by the process of aggregation include genes involved in cationic antimicrobial peptide resistance and glycerol metabolism.

7. Discussion and Future Work

7.1 Discussion

L. monocytogenes is a ubiquitous human pathogen that can cause serious disease in immunocompromised people and remains a global challenge for the food industry, particularly in ready to eat food pipeline (European Food Safety, European Centre for Disease and Control, 2021). *L. monocytogenes* intracellular life cycle is well studied and well characterised (Freitag, Port and Miner, 2009), as are the functions of many of its virulence genes (Tiensuu, Guerreiro, Oliveira et al., 2019). A key aim of this study was to use live cell microscopy to uncover novel host-pathogen interactions of *L. monocytogenes* at the single cell level and to characterise these key interactions to contribute to the understanding of how *L. monocytogenes* interacts with human cells.

By developing and using a live cell imaging model several undescribed mechanisms were observed in the experiments shown in the results chapters (Figure 7.1). The imaging model showed that invasion is a rare event and that bacteria aggregate on the surface of host cells to increase the success rate of invasion by multiple invasions events. This is also associated with host susceptibility via the cell cycle and through InlB-Met interactions, with cells being in the G2/M phase showing a higher association with bacterial aggregates. Through the development of a spent media assay this aggregation was shown to be induced by a host cell factor which induces a transcriptional change including upregulation of the core PrfA regulon (Figure 7.1).

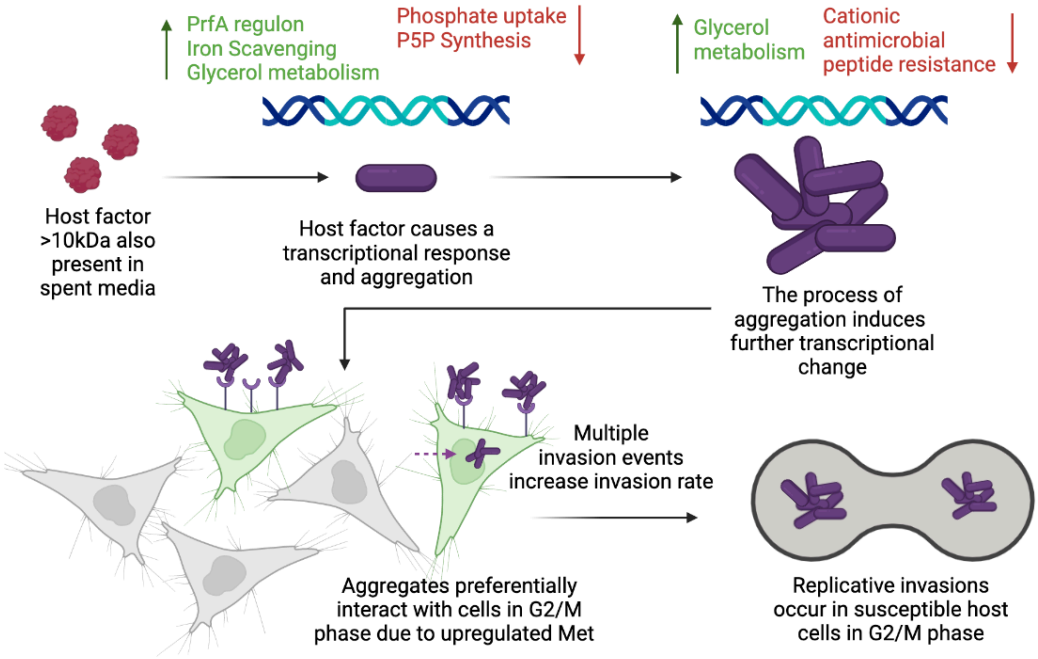

Figure 7. 1. Schematic model of the findings in this study. A proteinaceous >10 kDa host factor, present in spent media, induces a change in gene expression in *L. monocytogenes* including upregulation the PrfA regulon and ActA-mediated aggregation. Aggregation induces a further change in gene expression but does not alter expression of the PrfA regulon. Aggregates associate preferentially with host cells in G2/M phase due to increased expression of Met and aggregates invade the host cells through multiple invasion events that increase both the bacterial invasion rate and the number of replicative invasions.

This study set out three aims. Firstly, to use live-cell microscopy approaches to develop an in vitro infection model for monitoring single-cell host pathogen interactions of *L. monocytogenes*. A HeLa cell and HUVEC cell model was established for live cell imaging of infection and these experiments revealed novel interactions that showed heterogeneity between interactions of single bacterial cells and single host cells and novel processes such as multiple invasion events.

The second aim was to characterise key interactions between *L. monocytogenes* and host cells and mechanistically understand regulation of probabilistic infection outcomes. This study employed a range of techniques including an aggregation assay to determine the genes involved in aggregation, fixed imaging experiments to show host receptor interactions and invasion rates of *L. monocytogenes* and live cell imaging to show the kinetics of host-pathogen interactions and monitor infection outcomes. The data shows that aggregation is a strategy employed by *L. monocytogenes* to increase its low invasion success rate in a subset of susceptible host cells that are in a specific phase of the cell cycle.

The final aim was to use molecular microbiology and next-generation sequencing to characterise the role of PrfA regulon in controlling outcomes of single-cell host pathogen interactions of *L. monocytogenes.* The preliminary RNA-seq analysis showed that the PrfA regulon is upregulated outside of the host cell and in response to a host factor and showed some intriguing changes in gene expression that provide further evidence that aggregation is involved in *L. monocytogenes* virulence and survival inside of the host.

In conclusion, this study has demonstrated the value of imaging interactions between human cells and pathogens and how this can uncover novel interactions that lead to a greater understanding of the biology of infection.

7.3 Future Work

Several findings in this study require further investigation. The host factor that induces the aggregation phenotype remains uncharacterised. By fractionating spent media and utilising a proteomics approach the identity of the host factor could be elucidated, providing a further understanding of the mechanisms that induce the upregulation of virulence genes and subsequent aggregation.

Further validation of the InlB-Met interaction and its role in aggregation would strengthen the hypothesis that this interaction plays a role in aggregation. For example, HeLa cell lines that are deficient in Met expression are commercially available. Translating the findings of the biological role of aggregation into more physiologically accurate tissue models such as organoids would be advantageous.

The RNA-Seq data requires further replicates to statistically validate the findings. They could also be further validated by qRT-PCR of several genes that showed a significant differential expression.

8. Bibliography

Abachin, E., et al. (2002). 'Formation of D-alanyl-lipoteichoic acid is required for adhesion and virulence of Listeria monocytogenes' *Mol Microbiol*, 43 (1), pp. 1-14. doi: 10.1046/j.1365-2958.2002.02723.x.

Adamson, A., et al. (2016). 'Signal transduction controls heterogeneous NF-kappaB dynamics and target gene expression through cytokine-specific refractory states' *Nat Commun*, 7 p. 12057. doi: 10.1038/ncomms12057.

Alberti-Segui, C., Goeden, K. R. & Higgins, D. E. (2007). 'Differential function of Listeria monocytogenes listeriolysin O and phospholipases C in vacuolar dissolution following cell-to-cell spread' *Cell Microbiol*, 9 (1), pp. 179-95. doi: 10.1111/j.1462-5822.2006.00780.x.

Alvarez, D. E. & Agaisse, H. (2016). 'The Metalloprotease Mpl Supports Listeria monocytogenes Dissemination through Resolution of Membrane Protrusions into Vacuoles' *Infect Immun*, 84 (6), pp. 1806-1814. doi: 10.1128/IAI.00130-16.

Alvarez-Dominguez, C., et al. (1997). 'Host cell heparan sulfate proteoglycans mediate attachment and entry of Listeria monocytogenes, and the listerial surface protein ActA is involved in heparan sulfate receptor recognition' *Infect Immun*, 65 (1), pp. 78-88. doi: 10.1128/iai.65.1.78-88.1997.

Andersen, J. B., et al. (2006). 'Construction of a multiple fluorescence labelling system for use in co-invasion studies of Listeria monocytogenes' *BMC Microbiol*, 6 p. 86. doi: 10.1186/1471-2180-6-86.

Andrews, S. C., Robinson, A. K. & Rodriguez-Quinones, F. (2003). 'Bacterial iron homeostasis' *FEMS Microbiol Rev*, 27 (2-3), pp. 215-37. doi: 10.1016/S0168-6445(03)00055-X.

Ankers, J. M., et al. (2016). 'Dynamic NF-kappaB and E2F interactions control the priority and timing of inflammatory signalling and cell proliferation' *Elife*, 5. doi: 10.7554/eLife.10473.

Archambaud, C., et al. (2012). 'Impact of lactobacilli on orally acquired listeriosis' *Proc Natl Acad Sci U S A*, 109 (41), pp. 16684-9. doi: 10.1073/pnas.1212809109.

Archambaud, C., et al. (2013). 'The intestinal microbiota interferes with the microRNA response upon oral Listeria infection' *mBio*, 4 (6), pp. e00707-13. doi: 10.1128/mBio.00707-13.

Arizcun, C., Vasseur, C. & Labadie, J. C. (1998). 'Effect of several decontamination procedures on Listeria monocytogenes growing in biofilms' *J Food Prot*, 61 (6), pp. 731-4. doi: 10.4315/0362-028x-61.6.731.

Badar, F., Bhuiyan, R. & Nabeel, S. (2022). 'A Case of Listeria monocytogenes Infective Endocarditis' *Case Rep Infect Dis*, 2022 p. 5958017. doi: 10.1155/2022/5958017.

Bagnall, J., et al. (2020). 'Gene-Specific Linear Trends Constrain Transcriptional Variability of the Toll-like Receptor Signaling' *Cell Syst*, 11 (3), pp. 300-314 e8. doi: 10.1016/j.cels.2020.08.007.

Bain, J., Gow, N. A. & Erwig, L. P. (2015). 'Novel insights into host-fungal pathogen interactions derived from live-cell imaging' *Semin Immunopathol*, 37 (2), pp. 131-9. doi: 10.1007/s00281-014-0463-3.

Bakardjiev, A. I., Theriot, J. A. & Portnoy, D. A. (2006). 'Listeria monocytogenes traffics from maternal organs to the placenta and back' *PLoS Pathog*, 2 (6), p. e66. doi: 10.1371/journal.ppat.0020066.

Balestrino, D., et al. (2010). 'Single-cell techniques using chromosomally tagged fluorescent bacteria to study Listeria monocytogenes infection processes' *Appl Environ Microbiol*, 76 (11), pp. 3625-36. doi: 10.1128/AEM.02612-09.

Banovic, F., Schroten, H. & Schwerk, C. (2020). 'Potential Roles and Functions of Listerial Virulence Factors during Brain Entry' *Toxins (Basel)*, 12 (5). doi: 10.3390/toxins12050297.

Batan, D., et al. (2018). 'A Multicolor Split-Fluorescent Protein Approach to Visualize Listeria Protein Secretion in Infection' *Biophys J*, 115 (2), pp. 251-262. doi: 10.1016/j.bpj.2018.03.016.

Bavdek, A., et al. (2012). 'pH dependence of listeriolysin O aggregation and pore-forming ability' *FEBS J*, 279 (1), pp. 126-41. doi: 10.1111/j.1742-4658.2011.08405.x.

Bayles, D. O., Annous, B. A. & Wilkinson, B. J. (1996). 'Cold stress proteins induced in Listeria monocytogenes in response to temperature downshock and growth at low temperatures' *Appl Environ Microbiol*, 62 (3), pp. 1116-9. doi: 10.1128/aem.62.3.1116-1119.1996.

Becattini, S. & Pamer, E. G. (2017). 'Multifaceted Defense against Listeria monocytogenes in the Gastro-Intestinal Lumen' *Pathogens*, 7 (1). doi: 10.3390/pathogens7010001.

Begley, M., Gahan, C. G. & Hill, C. (2005). 'The interaction between bacteria and bile' *FEMS Microbiol Rev*, 29 (4), pp. 625-51. doi: 10.1016/j.femsre.2004.09.003.

Belitsky, B. R. (2004). 'Physical and enzymological interaction of Bacillus subtilis proteins required for de novo pyridoxal 5'-phosphate biosynthesis' *J Bacteriol*, 186 (4), pp. 1191-6. doi: 10.1128/JB.186.4.1191-1196.2004.

Bennett, H. J., et al. (2007). 'Characterization of relA and codY mutants of Listeria monocytogenes: identification of the CodY regulon and its role in virulence' *Mol Microbiol*, 63 (5), pp. 1453-67. doi: 10.1111/j.1365-2958.2007.05597.x.

Bhardwaj, V., et al. (1998). 'Chronic Listeria infection in SCID mice: requirements for the carrier state and the dual role of T cells in transferring protection or suppression' *J Immunol*, 160 (1), pp. 376-84. Available at: https://www.ncbi.nlm.nih.gov/pubmed/9551994.

Bierne, H., et al. (2004). 'Sortase B, a new class of sortase in Listeria monocytogenes' *J Bacteriol*, 186 (7), pp. 1972-82. doi: 10.1128/JB.186.7.1972-1982.2004.

Birmingham, C. L., et al. (2008). 'Listeriolysin O allows Listeria monocytogenes replication in macrophage vacuoles' *Nature*, 451 (7176), pp. 350-4. doi: 10.1038/nature06479.

Bleriot, C., et al. (2015). 'Liver-resident macrophage necroptosis orchestrates type 1 microbicidal inflammation and type-2-mediated tissue repair during

bacterial infection' *Immunity*, 42 (1), pp. 145-58. doi: 10.1016/j.immuni.2014.12.020.
Bohme, K., et al. (2012). 'Concerted actions of a thermo-labile regulator and a unique intergenic RNA thermosensor control Yersinia virulence' *PLoS Pathog*, 8 (2), p. e1002518. doi: 10.1371/journal.ppat.1002518.
Bolger, A. M., Lohse, M. & Usadel, B. (2014). 'Trimmomatic: a flexible trimmer for Illumina sequence data' *Bioinformatics*, 30 (15), pp. 2114-20. doi: 10.1093/bioinformatics/btu170.
Boneca, I. G., et al. (2007). 'A critical role for peptidoglycan N-deacetylation in Listeria evasion from the host innate immune system' *Proc Natl Acad Sci U S A*, 104 (3), pp. 997-1002. doi: 10.1073/pnas.0609672104.
Boob, M., Wang, Y. & Gruebele, M. (2019). 'Proteins: "Boil 'Em, Mash 'Em, Stick 'Em in a Stew"' *J Phys Chem B*, 123 (40), pp. 8341-8350. doi: 10.1021/acs.jpcb.9b05467.
Boratyn, G. M., et al. (2013). 'BLAST: a more efficient report with usability improvements' *Nucleic Acids Res*, 41 (Web Server issue), pp. W29-33. doi: 10.1093/nar/gkt282.
Bottaro, D. P., et al. (1991). 'Identification of the hepatocyte growth factor receptor as the c-met proto-oncogene product' *Science*, 251 (4995), pp. 802-4. doi: 10.1126/science.1846706.
Bou Ghanem, E. N., et al. (2012). 'InlA promotes dissemination of Listeria monocytogenes to the mesenteric lymph nodes during food borne infection of mice' *PLoS Pathog*, 8 (11), p. e1003015. doi: 10.1371/journal.ppat.1003015.
Braun, L., Ohayon, H. & Cossart, P. (1998). 'The InlB protein of Listeria monocytogenes is sufficient to promote entry into mammalian cells' *Mol Microbiol*, 27 (5), pp. 1077-87. doi: 10.1046/j.1365-2958.1998.00750.x.
Braun, V. (2005). 'Bacterial iron transport related to virulence' *Contrib Microbiol*, 12 pp. 210-233. doi: 10.1159/000081697.
Brennan, R. G. & Matthews, B. W. (1989). 'Structural basis of DNA-protein recognition' *Trends Biochem Sci*, 14 (7), pp. 286-90. doi: 10.1016/0968-0004(89)90066-2.
Brzoza, K. L., Rockel, A. B. & Hiltbold, E. M. (2004). 'Cytoplasmic entry of Listeria monocytogenes enhances dendritic cell maturation and T cell differentiation and function' *J Immunol*, 173 (4), pp. 2641-51. doi: 10.4049/jimmunol.173.4.2641.
Burgess, C. M., et al. (2016). 'The response of foodborne pathogens to osmotic and desiccation stresses in the food chain' *Int J Food Microbiol*, 221 pp. 37-53. doi: 10.1016/j.ijfoodmicro.2015.12.014.
Busch, D. H., et al. (1998). 'Coordinate regulation of complex T cell populations responding to bacterial infection' *Immunity*, 8 (3), pp. 353-62. doi: 10.1016/s1074-7613(00)80540-3.
Camejo, A., et al. (2011). 'The arsenal of virulence factors deployed by Listeria monocytogenes to promote its cell infection cycle' *Virulence*, 2 (5), pp. 379-94. doi: 10.4161/viru.2.5.17703.

Campisi, J. & d'Adda di Fagagna, F. (2007). 'Cellular senescence: when bad things happen to good cells' *Nat Rev Mol Cell Biol*, 8 (9), pp. 729-40. doi: 10.1038/nrm2233.

Chakraborty, T., et al. (1992). 'Coordinate regulation of virulence genes in Listeria monocytogenes requires the product of the prfA gene' *J Bacteriol*, 174 (2), pp. 568-74. doi: 10.1128/jb.174.2.568-574.1992.

Chan, Y. C., et al. (2008). 'Contributions of two-component regulatory systems, alternative sigma factors, and negative regulators to Listeria monocytogenes cold adaptation and cold growth' *J Food Prot*, 71 (2), pp. 420-5. doi: 10.4315/0362-028x-71.2.420.

Chan, Y. C. & Wiedmann, M. (2009). 'Physiology and genetics of Listeria monocytogenes survival and growth at cold temperatures' *Crit Rev Food Sci Nutr*, 49 (3), pp. 237-53. doi: 10.1080/10408390701856272.

Charlier, C., Disson, O. & Lecuit, M. (2020). 'Maternal-neonatal listeriosis' *Virulence*, 11 (1), pp. 391-397. doi: 10.1080/21505594.2020.1759287.

Charlier, C., et al. (2014). 'Listeria monocytogenes-associated biliary tract infections: a study of 12 consecutive cases and review' *Medicine (Baltimore)*, 93 (18), p. e105. doi: 10.1097/MD.0000000000000105.

Charlier, C., et al. (2012). 'Listeria monocytogenes-associated joint and bone infections: a study of 43 consecutive cases' *Clin Infect Dis*, 54 (2), pp. 240-8. doi: 10.1093/cid/cir803.

Charlier, C., et al. (2017). 'Clinical features and prognostic factors of listeriosis: the MONALISA national prospective cohort study' *Lancet Infect Dis*, 17 (5), pp. 510-519. doi: 10.1016/S1473-3099(16)30521-7.

Chen, C., et al. (2018). 'The Listeriolysin O PEST-like Sequence Co-opts AP-2-Mediated Endocytosis to Prevent Plasma Membrane Damage during Listeria Infection' *Cell Host Microbe*, 23 (6), pp. 786-795 e5. doi: 10.1016/j.chom.2018.05.006.

Cheng, M. I., et al. (2018). 'Actin-based motility allows Listeria monocytogenes to avoid autophagy in the macrophage cytosol' *Cell Microbiol*, 20 (9), p. e12854. doi: 10.1111/cmi.12854.

Chiba, S., et al. (2011). 'Listerial invasion protein internalin B promotes entry into ileal Peyer's patches in vivo' *Microbiol Immunol*, 55 (2), pp. 123-9. doi: 10.1111/j.1348-0421.2010.00292.x.

Chico-Calero, I., et al. (2002). 'Hpt, a bacterial homolog of the microsomal glucose-6-phosphate translocase, mediates rapid intracellular proliferation in Listeria' *Proc Natl Acad Sci U S A*, 99 (1), pp. 431-6. doi: 10.1073/pnas.012363899.

Choi, P. H., et al. (2015). 'Molecular basis for the recognition of cyclic-di-AMP by PstA, a PII-like signal transduction protein' *Microbiologyopen*, 4 (3), pp. 361-74. doi: 10.1002/mbo3.243.

Conner, S. D. & Schmid, S. L. (2003). 'Regulated portals of entry into the cell' *Nature*, 422 (6927), pp. 37-44. doi: 10.1038/nature01451.

Costa, A. C., et al. (2020). 'Listeria monocytogenes Interferes with Host Cell Mitosis through Its Virulence Factors InlC and ActA' *Toxins (Basel)*, 12 (6). doi: 10.3390/toxins12060411.

Cotter, P. D., et al. (2008). 'Listeriolysin S, a novel peptide haemolysin associated with a subset of lineage I Listeria monocytogenes' *PLoS Pathog*, 4 (9), p. e1000144. doi: 10.1371/journal.ppat.1000144.

Cotter, P. D., et al. (1999). 'Identification and disruption of lisRK, a genetic locus encoding a two-component signal transduction system involved in stress tolerance and virulence in Listeria monocytogenes' *J Bacteriol*, 181 (21), pp. 6840-3. doi: 10.1128/JB.181.21.6840-6843.1999.

Cremers, C. M., et al. (2014). 'Bile salts act as effective protein-unfolding agents and instigators of disulfide stress in vivo' *Proc Natl Acad Sci U S A*, 111 (16), pp. E1610-9. doi: 10.1073/pnas.1401941111.

Cruz, R., et al. (2018). 'Epithelial Keratins Modulate cMet Expression and Signaling and Promote InlB-Mediated Listeria monocytogenes Infection of HeLa Cells' *Front Cell Infect Microbiol*, 8 p. 146. doi: 10.3389/fcimb.2018.00146.

D'Orazio, S. E. F. (2019). 'Innate and Adaptive Immune Responses during Listeria monocytogenes Infection' *Microbiol Spectr*, 7 (3). doi: 10.1128/microbiolspec.GPP3-0065-2019.

de las Heras, A., et al. (2011). 'Regulation of Listeria virulence: PrfA master and commander' *Curr Opin Microbiol*, 14 (2), pp. 118-27. doi: 10.1016/j.mib.2011.01.005.

Dehio, C., et al. (1997). 'Interaction of Bartonella henselae with endothelial cells results in bacterial aggregation on the cell surface and the subsequent engulfment and internalisation of the bacterial aggregate by a unique structure, the invasome' *J Cell Sci*, 110 (Pt 18) pp. 2141-54. doi: 10.1242/jcs.110.18.2141.

Disson, O., et al. (2008). 'Conjugated action of two species-specific invasion proteins for fetoplacental listeriosis' *Nature*, 455 (7216), pp. 1114-8. doi: 10.1038/nature07303.

Doganay, M. (2003). 'Listeriosis: clinical presentation' *FEMS Immunol Med Microbiol*, 35 (3), pp. 173-5. doi: 10.1016/S0928-8244(02)00467-4.

Dowd, G. C., et al. (2020). 'Listeria monocytogenes exploits host exocytosis to promote cell-to-cell spread' *Proc Natl Acad Sci U S A*, 117 (7), pp. 3789-3796. doi: 10.1073/pnas.1916676117.

Drecktrah, D., et al. (2008). 'Dynamic behavior of Salmonella-induced membrane tubules in epithelial cells' *Traffic*, 9 (12), pp. 2117-29. doi: 10.1111/j.1600-0854.2008.00830.x.

Drevets, D. A. (1999). 'Dissemination of Listeria monocytogenes by infected phagocytes' *Infect Immun*, 67 (7), pp. 3512-7. doi: 10.1128/IAI.67.7.3512-3517.1999.

Drolia, R., et al. (2018). 'Listeria Adhesion Protein Induces Intestinal Epithelial Barrier Dysfunction for Bacterial Translocation' *Cell Host Microbe*, 23 (4), pp. 470-484 e7. doi: 10.1016/j.chom.2018.03.004.

Dutta, V., Elhanafi, D. & Kathariou, S. (2013). 'Conservation and distribution of the benzalkonium chloride resistance cassette bcrABC in Listeria monocytogenes' *Appl Environ Microbiol*, 79 (19), pp. 6067-74. doi: 10.1128/AEM.01751-13.

Edelson, B. T., et al. (2011). 'CD8alpha(+) dendritic cells are an obligate cellular entry point for productive infection by Listeria monocytogenes' *Immunity*, 35 (2), pp. 236-48. doi: 10.1016/j.immuni.2011.06.012.

Eiting, M., et al. (2005). 'The mutation G145S in PrfA, a key virulence regulator of Listeria monocytogenes, increases DNA-binding affinity by stabilizing the HTH motif' *Mol Microbiol*, 56 (2), pp. 433-46. doi: 10.1111/j.1365-2958.2005.04561.x.

Eshwar, A. K., et al. (2017). 'Cold-Shock Domain Family Proteins (Csps) Are Involved in Regulation of Virulence, Cellular Aggregation, and Flagella-Based Motility in Listeria monocytogenes' *Front Cell Infect Microbiol*, 7 p. 453. doi: 10.3389/fcimb.2017.00453.

European Food Safety, A., European Centre for Disease, P. & Control (2021). 'The European Union One Health 2019 Zoonoses Report' *EFSA J*, 19 (2), p. e06406. doi: 10.2903/j.efsa.2021.6406.

Faralla, C., et al. (2016). 'InlP, a New Virulence Factor with Strong Placental Tropism' *Infect Immun*, 84 (12), pp. 3584-3596. doi: 10.1128/IAI.00625-16.

Francis, M. S. & Thomas, C. J. (1996). 'Effect of multiplicity of infection on Listeria monocytogenes pathogenicity for HeLa and Caco-2 cell lines' *J Med Microbiol*, 45 (5), pp. 323-30. doi: 10.1099/00222615-45-5-323.

Freitag, N. E., Port, G. C. & Miner, M. D. (2009). 'Listeria monocytogenes - from saprophyte to intracellular pathogen' *Nat Rev Microbiol*, 7 (9), pp. 623-8. doi: 10.1038/nrmicro2171.

Gaballa, A., et al. (2019). 'Cross Talk between SigB and PrfA in Listeria monocytogenes Facilitates Transitions between Extra- and Intracellular Environments' *Microbiol Mol Biol Rev*, 83 (4). doi: 10.1128/MMBR.00034-19.

Gahan, C. G. & Hill, C. (2014). 'Listeria monocytogenes: survival and adaptation in the gastrointestinal tract' *Front Cell Infect Microbiol*, 4 p. 9. doi: 10.3389/fcimb.2014.00009.

Garcia-Del Portillo, F. (2008). 'Heterogeneity in tissue culture infection models: a source of novel host-pathogen interactions?' *Microbes Infect*, 10 (9), pp. 1063-6. doi: 10.1016/j.micinf.2008.07.004.

Gekara, N. O., et al. (2010). 'Listeria monocytogenes induces T cell receptor unresponsiveness through pore-forming toxin listeriolysin O' *J Infect Dis*, 202 (11), pp. 1698-707. doi: 10.1086/657145.

Gessain, G., et al. (2015). 'PI3-kinase activation is critical for host barrier permissiveness to Listeria monocytogenes' *J Exp Med*, 212 (2), pp. 165-83. doi: 10.1084/jem.20141406.

Ghosh, P., et al. (2018). 'Invasion of the Brain by Listeria monocytogenes Is Mediated by InlF and Host Cell Vimentin' *mBio*, 9 (1). doi: 10.1128/mBio.00160-18.

Gouin, E., et al. (2010). 'The Listeria monocytogenes InlC protein interferes with innate immune responses by targeting the I{kappa}B kinase subunit IKK{alpha}' *Proc Natl Acad Sci U S A*, 107 (40), pp. 17333-8. doi: 10.1073/pnas.1007765107.

Goulet, V., et al. (2012). 'Incidence of listeriosis and related mortality among groups at risk of acquiring listeriosis' *Clin Infect Dis*, 54 (5), pp. 652-60. doi: 10.1093/cid/cir902.

Goulet, V., et al. (2013). 'What is the incubation period for listeriosis?' *BMC Infect Dis*, 13 p. 11. doi: 10.1186/1471-2334-13-11.

Gray, M. L. & Killinger, A. H. (1966). 'Listeria monocytogenes and listeric infections' *Bacteriol Rev*, 30 (2), pp. 309-82. doi: 10.1128/br.30.2.309-382.1966.

Greiffenberg, L., et al. (1998). 'Interaction of Listeria monocytogenes with human brain microvascular endothelial cells: InlB-dependent invasion, long-term intracellular growth, and spread from macrophages to endothelial cells' *Infect Immun*, 66 (11), pp. 5260-7. doi: 10.1128/IAI.66.11.5260-5267.1998.

Grif, K., et al. (2003). 'Incidence of fecal carriage of Listeria monocytogenes in three healthy volunteers: a one-year prospective stool survey' *Eur J Clin Microbiol Infect Dis*, 22 (1), pp. 16-20. doi: 10.1007/s10096-002-0835-9.

Grigg, J. C., et al. (2007). 'Heme coordination by Staphylococcus aureus IsdE' *J Biol Chem*, 282 (39), pp. 28815-28822. doi: 10.1074/jbc.M704602200.

Grundler, T., et al. (2013). 'The surface proteins InlA and InlB are interdependently required for polar basolateral invasion by Listeria monocytogenes in a human model of the blood-cerebrospinal fluid barrier' *Microbes Infect*, 15 (4), pp. 291-301. doi: 10.1016/j.micinf.2012.12.005.

Grundling, A., Gonzalez, M. D. & Higgins, D. E. (2003). 'Requirement of the Listeria monocytogenes broad-range phospholipase PC-PLC during infection of human epithelial cells' *J Bacteriol*, 185 (21), pp. 6295-307. doi: 10.1128/JB.185.21.6295-6307.2003.

Guariglia-Oropeza, V., et al. (2018). 'The Listeria monocytogenes Bile Stimulon under Acidic Conditions Is Characterized by Strain-Specific Patterns and the Upregulation of Motility, Cell Wall Modification Functions, and the PrfA Regulon' *Front Microbiol*, 9 p. 120. doi: 10.3389/fmicb.2018.00120.

Guerreiro, D. N., Arcari, T. & O'Byrne, C. P. (2020). 'The sigma(B)-Mediated General Stress Response of Listeria monocytogenes: Life and Death Decision Making in a Pathogen' *Front Microbiol*, 11 p. 1505. doi: 10.3389/fmicb.2020.01505.

Guerreiro, D. N., et al. (2022). 'Acid stress signals are integrated into the sigmaB-dependent general stress response pathway via the stressosome in the food-borne pathogen Listeria monocytogenes' *PLoS Pathog*, 18 (3), p. e1010213. doi: 10.1371/journal.ppat.1010213.

Guldimann, C., et al. (2017). 'Stochastic and Differential Activation of sigma(B) and PrfA in Listeria monocytogenes at the Single Cell Level under Different Environmental Stress Conditions' *Front Microbiol*, 8 p. 348. doi: 10.3389/fmicb.2017.00348.

Guleria, I. & Pollard, J. W. (2001). 'Aberrant macrophage and neutrophil population dynamics and impaired Th1 response to Listeria monocytogenes in colony-stimulating factor 1-deficient mice' *Infect Immun*, 69 (3), pp. 1795-807. doi: 10.1128/IAI.69.3.1795-1807.2001.

Hall, M., et al. (2016). 'Structural basis for glutathione-mediated activation of the virulence regulatory protein PrfA in Listeria' *Proc Natl Acad Sci U S A*, 113 (51), pp. 14733-14738. doi: 10.1073/pnas.1614028114.

Hammer, N. D. & Skaar, E. P. (2011). 'Molecular mechanisms of Staphylococcus aureus iron acquisition' *Annu Rev Microbiol*, 65 pp. 129-47. doi: 10.1146/annurev-micro-090110-102851.
Hamon, M., Bierne, H. & Cossart, P. (2006). 'Listeria monocytogenes: a multifaceted model' *Nat Rev Microbiol*, 4 (6), pp. 423-34. doi: 10.1038/nrmicro1413.
Hanahan, D. (1983). 'Studies on transformation of Escherichia coli with plasmids' *J Mol Biol*, 166 (4), pp. 557-80. doi: 10.1016/s0022-2836(83)80284-8.
Harty, J. T. & Badovinac, V. P. (2002). 'Influence of effector molecules on the CD8(+) T cell response to infection' *Curr Opin Immunol*, 14 (3), pp. 360-5. doi: 10.1016/s0952-7915(02)00333-3.
Hathout, Y. (2007). 'Approaches to the study of the cell secretome' *Expert Rev Proteomics*, 4 (2), pp. 239-48. doi: 10.1586/14789450.4.2.239.
Henry, R., et al. (2006). 'Cytolysin-dependent delay of vacuole maturation in macrophages infected with Listeria monocytogenes' *Cell Microbiol*, 8 (1), pp. 107-19. doi: 10.1111/j.1462-5822.2005.00604.x.
Hingston, P., et al. (2017). 'Strand specific RNA-sequencing and membrane lipid profiling reveals growth phase-dependent cold stress response mechanisms in Listeria monocytogenes' *PLoS One*, 12 (6), p. e0180123. doi: 10.1371/journal.pone.0180123.
Hof, H. (2017). 'Listeria infections of the eye' *Eur J Ophthalmol*, 27 (2), pp. 115-121. doi: 10.5301/ejo.5000884.
Inohara, N., et al. (2003). 'Host recognition of bacterial muramyl dipeptide mediated through NOD2. Implications for Crohn's disease' *J Biol Chem*, 278 (8), pp. 5509-12. doi: 10.1074/jbc.C200673200.
Iwai, H., et al. (2007). 'A bacterial effector targets Mad2L2, an APC inhibitor, to modulate host cell cycling' *Cell*, 130 (4), pp. 611-23. doi: 10.1016/j.cell.2007.06.043.
Johansson, J. (2009). 'RNA thermosensors in bacterial pathogens' *Contrib Microbiol*, 16 pp. 150-160. doi: 10.1159/000219378.
Johansson, J. & Freitag, N. E. (2019). 'Regulation of Listeria monocytogenes Virulence' *Microbiol Spectr*, 7 (4). doi: 10.1128/microbiolspec.GPP3-0064-2019.
Johansson, J., et al. (2002). 'An RNA thermosensor controls expression of virulence genes in Listeria monocytogenes' *Cell*, 110 (5), pp. 551-61. doi: 10.1016/s0092-8674(02)00905-4.
Jones, A., Jonsson, A. B. & Aro, H. (2007). 'Neisseria gonorrhoeae infection causes a G1 arrest in human epithelial cells' *FASEB J*, 21 (2), pp. 345-55. doi: 10.1096/fj.06-6675com.
Jonquieres, R., et al. (1999). 'Interaction between the protein InlB of Listeria monocytogenes and lipoteichoic acid: a novel mechanism of protein association at the surface of gram-positive bacteria' *Mol Microbiol*, 34 (5), pp. 902-14. doi: 10.1046/j.1365-2958.1999.01652.x.
Joseph, B., et al. (2008). 'Glycerol metabolism and PrfA activity in Listeria monocytogenes' *J Bacteriol*, 190 (15), pp. 5412-30. doi: 10.1128/JB.00259-08.
Kallipolitis, B. H., et al. (2003). 'CesRK, a two-component signal transduction system in Listeria monocytogenes, responds to the presence of cell wall-acting

antibiotics and affects beta-lactam resistance' *Antimicrob Agents Chemother*, 47 (11), pp. 3421-9. doi: 10.1128/AAC.47.11.3421-3429.2003.
Kang, J., et al. (2015). 'VirR-Mediated Resistance of Listeria monocytogenes against Food Antimicrobials and Cross-Protection Induced by Exposure to Organic Acid Salts' *Appl Environ Microbiol*, 81 (13), pp. 4553-62. doi: 10.1128/AEM.00648-15.
Kellogg, R. A., et al. (2017). 'Cellular Decision Making by Non-Integrative Processing of TLR Inputs' *Cell Rep*, 19 (1), pp. 125-135. doi: 10.1016/j.celrep.2017.03.027.
Kocks, C., et al. (1992). 'L. monocytogenes-induced actin assembly requires the actA gene product, a surface protein' *Cell*, 68 (3), pp. 521-31. doi: 10.1016/0092-8674(92)90188-i.
Kortebi, M., et al. (2017). 'Listeria monocytogenes switches from dissemination to persistence by adopting a vacuolar lifestyle in epithelial cells' *PLoS Pathog*, 13 (11), p. e1006734. doi: 10.1371/journal.ppat.1006734.
Kyei, G. B., et al. (2006). 'Rab14 is critical for maintenance of Mycobacterium tuberculosis phagosome maturation arrest' *EMBO J*, 25 (22), pp. 5250-9. doi: 10.1038/sj.emboj.7601407.
Lasa, I., et al. (1997). 'Identification of two regions in the N-terminal domain of ActA involved in the actin comet tail formation by Listeria monocytogenes' *EMBO J*, 16 (7), pp. 1531-40. doi: 10.1093/emboj/16.7.1531.
Latunde-Dada, G. O. (2009). 'Iron metabolism: microbes, mouse, and man' *Bioessays*, 31 (12), pp. 1309-17. doi: 10.1002/bies.200900101.
Lechowicz, J. & Krawczyk-Balska, A. (2015). 'An update on the transport and metabolism of iron in Listeria monocytogenes: the role of proteins involved in pathogenicity' *Biometals*, 28 (4), pp. 587-603. doi: 10.1007/s10534-015-9849-5.
Leimeister-Wachter, M., Domann, E. & Chakraborty, T. (1992). 'The expression of virulence genes in Listeria monocytogenes is thermoregulated' *J Bacteriol*, 174 (3), pp. 947-52. doi: 10.1128/jb.174.3.947-952.1992.
Leitao, E., et al. (2014). 'Listeria monocytogenes induces host DNA damage and delays the host cell cycle to promote infection' *Cell Cycle*, 13 (6), pp. 928-40. doi: 10.4161/cc.27780.
Lepanto, P., et al. (2011). 'Pseudomonas aeruginosa interacts with epithelial cells rapidly forming aggregates that are internalized by a Lyn-dependent mechanism' *Cell Microbiol*, 13 (8), pp. 1212-22. doi: 10.1111/j.1462-5822.2011.01611.x.
Li, W., et al. (2019). 'Induction of MET Receptor Tyrosine Kinase Down-regulation through Antibody-mediated Receptor Clustering' *Sci Rep*, 9 (1), p. 1988. doi: 10.1038/s41598-018-36963-3.
Liao, Y., Smyth, G. K. & Shi, W. (2014). 'featureCounts: an efficient general purpose program for assigning sequence reads to genomic features' *Bioinformatics*, 30 (7), pp. 923-30. doi: 10.1093/bioinformatics/btt656.
Liu, S. I., et al. (1997). 'Effect of hepatocyte growth factor on cell cycle and c-met expression in human gastric cancer cells' *Anticancer Res*, 17 (5A), pp. 3575-80. Available at: https://www.ncbi.nlm.nih.gov/pubmed/9413205.

Liu, Y., et al. (2019). 'Systematic review of the Listeria monocytogenes sigma(B) regulon supports a role in stress response, virulence and metabolism' *Future Microbiol*, 14 pp. 801-828. doi: 10.2217/fmb-2019-0072.

Lobel, L. & Herskovits, A. A. (2016). 'Systems Level Analyses Reveal Multiple Regulatory Activities of CodY Controlling Metabolism, Motility and Virulence in Listeria monocytogenes' *PLoS Genet*, 12 (2), p. e1005870. doi: 10.1371/journal.pgen.1005870.

Lobel, L., et al. (2015). 'The metabolic regulator CodY links Listeria monocytogenes metabolism to virulence by directly activating the virulence regulatory gene prfA' *Mol Microbiol*, 95 (4), pp. 624-44. doi: 10.1111/mmi.12890.

Lobel, L., et al. (2012). 'Integrative genomic analysis identifies isoleucine and CodY as regulators of Listeria monocytogenes virulence' *PLoS Genet*, 8 (9), p. e1002887. doi: 10.1371/journal.pgen.1002887.

Loessner, M. J., et al. (2002). 'C-terminal domains of Listeria monocytogenes bacteriophage murein hydrolases determine specific recognition and high-affinity binding to bacterial cell wall carbohydrates' *Mol Microbiol*, 44 (2), pp. 335-49. doi: 10.1046/j.1365-2958.2002.02889.x.

Loh, E., et al. (2009). 'A trans-acting riboswitch controls expression of the virulence regulator PrfA in Listeria monocytogenes' *Cell*, 139 (4), pp. 770-9. doi: 10.1016/j.cell.2009.08.046.

Love, M. I., Huber, W. & Anders, S. (2014). 'Moderated estimation of fold change and dispersion for RNA-seq data with DESeq2' *Genome Biol*, 15 (12), p. 550. doi: 10.1186/s13059-014-0550-8.

Machado, H., et al. (2013). 'The Tat pathway is prevalent in Listeria monocytogenes lineage II and is not required for infection and spread in host cells' *J Mol Microbiol Biotechnol*, 23 (3), pp. 209-18. doi: 10.1159/000348245.

Malmirchegini, G. R., et al. (2014). 'Novel mechanism of hemin capture by Hbp2, the hemoglobin-binding hemophore from Listeria monocytogenes' *J Biol Chem*, 289 (50), pp. 34886-99. doi: 10.1074/jbc.M114.583013.

Mandin, P., et al. (2005). 'VirR, a response regulator critical for Listeria monocytogenes virulence' *Mol Microbiol*, 57 (5), pp. 1367-80. doi: 10.1111/j.1365-2958.2005.04776.x.

May, R. C., et al. (1999). 'The Arp2/3 complex is essential for the actin-based motility of Listeria monocytogenes' *Curr Biol*, 9 (14), pp. 759-62. doi: 10.1016/s0960-9822(99)80337-6.

McIntrye, J., Rowley, D. & Jenkin, C. R. (1967). 'The functional heterogeneity of macrophages at the single cell level' *Aust J Exp Biol Med Sci*, 45 (6), pp. 675-80. doi: 10.1038/icb.1967.67.

McLauchlin, J. & Low, J. C. (1994). 'Primary cutaneous listeriosis in adults: an occupational disease of veterinarians and farmers' *Vet Rec*, 135 (26), pp. 615-7. Available at: https://www.ncbi.nlm.nih.gov/pubmed/7716869.

Melton-Witt, J. A., et al. (2012). 'Oral infection with signature-tagged Listeria monocytogenes reveals organ-specific growth and dissemination routes in guinea pigs' *Infect Immun*, 80 (2), pp. 720-32. doi: 10.1128/IAI.05958-11.

Milenbachs, A. A., et al. (1997). 'Carbon-source regulation of virulence gene expression in Listeria monocytogenes' *Mol Microbiol*, 23 (5), pp. 1075-85. doi: 10.1046/j.1365-2958.1997.2711634.x.

Milohanic, E., et al. (2003). 'Transcriptome analysis of Listeria monocytogenes identifies three groups of genes differently regulated by PrfA' *Mol Microbiol*, 47 (6), pp. 1613-25. doi: 10.1046/j.1365-2958.2003.03413.x.

Monniot, C., et al. (2012). 'Novel listerial glycerol dehydrogenase- and phosphoenolpyruvate-dependent dihydroxyacetone kinase system connected to the pentose phosphate pathway' *J Bacteriol*, 194 (18), pp. 4972-82. doi: 10.1128/JB.00801-12.

Moran, J., et al. (2022). 'Single-cell imaging reveals non-cooperative and cooperative infection strategies of *Listeria monocytogenes* in macrophages' *bioRxiv*, p. 2022.06.04.493993. doi: 10.1101/2022.06.04.493993.

Moreno-Letelier, A., et al. (2011). 'Parallel Evolution and Horizontal Gene Transfer of the pst Operon in Firmicutes from Oligotrophic Environments' *Int J Evol Biol*, 2011 p. 781642. doi: 10.4061/2011/781642.

Murray, E. G. D., Webb, R. A. & Swann, M. B. R. (1926). ' A disease of rabbits characterised by a large mononuclear leucocytosis, caused by a hitherto undescribed bacillus Bacterium monocytogenes (n. sp.).' *The Journal of Pathology and Bacteriology*, 29 (4), pp. 407-439.

Mylonakis, E., Hohmann, E. L. & Calderwood, S. B. (1998). 'Central nervous system infection with Listeria monocytogenes. 33 years' experience at a general hospital and review of 776 episodes from the literature' *Medicine (Baltimore)*, 77 (5), pp. 313-36. doi: 10.1097/00005792-199809000-00002.

Mylonakis, E., et al. (2002). 'Listeriosis during pregnancy: a case series and review of 222 cases' *Medicine (Baltimore)*, 81 (4), pp. 260-9. doi: 10.1097/00005792-200207000-00002.

Newton, S. M., et al. (2005). 'The svpA-srtB locus of Listeria monocytogenes: fur-mediated iron regulation and effect on virulence' *Mol Microbiol*, 55 (3), pp. 927-40. doi: 10.1111/j.1365-2958.2004.04436.x.

Nguyen, B. N., Peterson, B. N. & Portnoy, D. A. (2019). 'Listeriolysin O: A phagosome-specific cytolysin revisited' *Cell Microbiol*, 21 (3), p. e12988. doi: 10.1111/cmi.12988.

NicAogain, K. & O'Byrne, C. P. (2016). 'The Role of Stress and Stress Adaptations in Determining the Fate of the Bacterial Pathogen Listeria monocytogenes in the Food Chain' *Front Microbiol*, 7 p. 1865. doi: 10.3389/fmicb.2016.01865.

Nielsen, P. K., et al. (2012). 'Genome-wide transcriptional profiling of the cell envelope stress response and the role of LisRK and CesRK in Listeria monocytogenes' *Microbiology (Reading)*, 158 (Pt 4), pp. 963-974. doi: 10.1099/mic.0.055467-0.

Nikitas, G., et al. (2011). 'Transcytosis of Listeria monocytogenes across the intestinal barrier upon specific targeting of goblet cell accessible E-cadherin' *J Exp Med*, 208 (11), pp. 2263-77. doi: 10.1084/jem.20110560.

Norman, T. M., et al. (2015). 'Stochastic Switching of Cell Fate in Microbes' *Annu Rev Microbiol*, 69 pp. 381-403. doi: 10.1146/annurev-micro-091213-112852.

Oevermann, A., Zurbriggen, A. & Vandevelde, M. (2010). 'Rhombencephalitis Caused by Listeria monocytogenes in Humans and Ruminants: A Zoonosis on the Rise?' *Interdiscip Perspect Infect Dis*, 2010 p. 632513. doi: 10.1155/2010/632513.

Ofer, A., et al. (2011). 'Implications of the inability of Listeria monocytogenes EGD-e to grow anaerobically due to a deletion in the class III NrdD ribonucleotide reductase for its use as a model laboratory strain' *J Bacteriol*, 193 (12), pp. 2931-40. doi: 10.1128/JB.01405-10.

Ollinger, J., Wiedmann, M. & Boor, K. J. (2008). 'SigmaB- and PrfA-dependent transcription of genes previously classified as putative constituents of the Listeria monocytogenes PrfA regulon' *Foodborne Pathog Dis*, 5 (3), pp. 281-93. doi: 10.1089/fpd.2008.0079.

Ooi, S. T. & Lorber, B. (2005). 'Gastroenteritis due to Listeria monocytogenes' *Clin Infect Dis*, 40 (9), pp. 1327-32. doi: 10.1086/429324.

Ortega, F. E., Koslover, E. F. & Theriot, J. A. (2019). 'Listeria monocytogenes cell-to-cell spread in epithelia is heterogeneous and dominated by rare pioneer bacteria' *Elife*, 8. doi: 10.7554/eLife.40032.

Pagelow, D., et al. (2018). 'The olfactory epithelium as a port of entry in neonatal neurolisteriosis' *Nat Commun*, 9 (1), p. 4269. doi: 10.1038/s41467-018-06668-2.

Parida, S. K., et al. (1998). 'Internalin B is essential for adhesion and mediates the invasion of Listeria monocytogenes into human endothelial cells' *Mol Microbiol*, 28 (1), pp. 81-93. doi: 10.1046/j.1365-2958.1998.00776.x.

Pentecost, M., et al. (2010). 'Listeria monocytogenes internalin B activates junctional endocytosis to accelerate intestinal invasion' *PLoS Pathog*, 6 (5), p. e1000900. doi: 10.1371/journal.ppat.1000900.

Pentecost, M., et al. (2006). 'Listeria monocytogenes invades the epithelial junctions at sites of cell extrusion' *PLoS Pathog*, 2 (1), p. e3. doi: 10.1371/journal.ppat.0020003.

Peron-Cane, C., et al. (2020). 'Fluorescent secreted bacterial effectors reveal active intravacuolar proliferation of Listeria monocytogenes in epithelial cells' *PLoS Pathog*, 16 (10), p. e1009001. doi: 10.1371/journal.ppat.1009001.

Peterson, B. N., et al. (2020). 'Secondary structure of the mRNA encoding listeriolysin O is essential to establish the replicative niche of L. monocytogenes' *Proc Natl Acad Sci U S A*, 117 (38), pp. 23774-23781. doi: 10.1073/pnas.2004129117.

Pillich, H., Puri, M. & Chakraborty, T. (2017). 'ActA of Listeria monocytogenes and Its Manifold Activities as an Important Listerial Virulence Factor' *Curr Top Microbiol Immunol*, 399 pp. 113-132. doi: 10.1007/82_2016_30.

Pistor, S., et al. (1995). 'The bacterial actin nucleator protein ActA of Listeria monocytogenes contains multiple binding sites for host microfilament proteins' *Curr Biol*, 5 (5), pp. 517-25. doi: 10.1016/s0960-9822(95)00104-7.

Portman, J. L., et al. (2017). 'Activity of the Pore-Forming Virulence Factor Listeriolysin O Is Reversibly Inhibited by Naturally Occurring S-Glutathionylation' *Infect Immun*, 85 (4). doi: 10.1128/IAI.00959-16.

Pouillot, R., et al. (2016). 'Infectious Dose of Listeria monocytogenes in Outbreak Linked to Ice Cream, United States, 2015' *Emerg Infect Dis*, 22 (12), pp. 2113-2119. doi: 10.3201/eid2212.160165.

Prokop, A., et al. (2017). 'OrfX, a Nucleomodulin Required for Listeria monocytogenes Virulence' *mBio*, 8 (5). doi: 10.1128/mBio.01550-17.

Quereda, J. J., et al. (2016). 'Bacteriocin from epidemic Listeria strains alters the host intestinal microbiota to favor infection' *Proc Natl Acad Sci U S A*, 113 (20), pp. 5706-11. doi: 10.1073/pnas.1523899113.
Quereda, J. J., et al. (2022). 'A Role for Taok2 in Listeria monocytogenes Vacuolar Escape' *J Infect Dis*, 225 (6), pp. 1005-1010. doi: 10.1093/infdis/jiaa367.
Quereda, J. J., et al. (2021). 'Pathogenicity and virulence of Listeria monocytogenes: A trip from environmental to medical microbiology' *Virulence*, 12 (1), pp. 2509-2545. doi: 10.1080/21505594.2021.1975526.
Quereda, J. J., et al. (2019). 'Reassessing the role of internalin B in Listeria monocytogenes virulence using the epidemic strain F2365' *Clin Microbiol Infect*, 25 (2), pp. 252 e1-252 e4. doi: 10.1016/j.cmi.2018.08.022.
Radoshevich, L. & Cossart, P. (2018). 'Listeria monocytogenes: towards a complete picture of its physiology and pathogenesis' *Nat Rev Microbiol*, 16 (1), pp. 32-46. doi: 10.1038/nrmicro.2017.126.
Rajabian, T., et al. (2009). 'The bacterial virulence factor InlC perturbs apical cell junctions and promotes cell-to-cell spread of Listeria' *Nat Cell Biol*, 11 (10), pp. 1212-8. doi: 10.1038/ncb1964.
Rengarajan, M. & Theriot, J. A. (2020). 'Rapidly dynamic host cell heterogeneity in bacterial adhesion governs susceptibility to infection by Listeria monocytogenes' *Mol Biol Cell*, 31 (19), pp. 2097-2106. doi: 10.1091/mbc.E19-08-0454.
Reniere, M. L., et al. (2015). 'Glutathione activates virulence gene expression of an intracellular pathogen' *Nature*, 517 (7533), pp. 170-3. doi: 10.1038/nature14029.
Rey, C., et al. (2020). 'Transcytosis subversion by M cell-to-enterocyte spread promotes Shigella flexneri and Listeria monocytogenes intracellular bacterial dissemination' *PLoS Pathog*, 16 (4), p. e1008446. doi: 10.1371/journal.ppat.1008446.
Rolhion, N. & Chassaing, B. (2016). 'When pathogenic bacteria meet the intestinal microbiota' *Philos Trans R Soc Lond B Biol Sci*, 371 (1707). doi: 10.1098/rstb.2015.0504.
Rolhion, N. & Cossart, P. (2017). 'How the study of Listeria monocytogenes has led to new concepts in biology' *Future Microbiol*, 12 pp. 621-638. doi: 10.2217/fmb-2016-0221.
Rousset, C., Fontecave, M. & Ollagnier de Choudens, S. (2008). 'The [4Fe-4S] cluster of quinolinate synthase from Escherichia coli: investigation of cluster ligands' *FEBS Lett*, 582 (19), pp. 2937-44. doi: 10.1016/j.febslet.2008.07.032.
Samant, S., et al. (2022). 'Listerial Spontaneous Bacterial Peritonitis' *Cureus*, 14 (2), p. e22051. doi: 10.7759/cureus.22051.
Samba-Louaka, A., et al. (2014). 'Listeria monocytogenes dampens the DNA damage response' *PLoS Pathog*, 10 (10), p. e1004470. doi: 10.1371/journal.ppat.1004470.
Santos-Lopez, A., et al. (2021). 'Experimental evolution to identify undescribed mechanisms of resistance to a novel cationic peptide antibiotic' *bioRxiv*, https://doi.org/10.1101/2020.12.16.423161 pp. 2020-12.

Schindelin, J., et al. (2012). 'Fiji: an open-source platform for biological-image analysis' *Nat Methods*, 9 (7), pp. 676-82. doi: 10.1038/nmeth.2019.
Schlech, W. F. (2019). 'Epidemiology and Clinical Manifestations of Listeria monocytogenes Infection' *Microbiol Spectr*, 7 (3). doi: 10.1128/microbiolspec.GPP3-0014-2018.
Scortti, M., et al. (2007). 'The PrfA virulence regulon' *Microbes Infect*, 9 (10), pp. 1196-207. doi: 10.1016/j.micinf.2007.05.007.
Seki, E., et al. (2002). 'Critical roles of myeloid differentiation factor 88-dependent proinflammatory cytokine release in early phase clearance of Listeria monocytogenes in mice' *J Immunol*, 169 (7), pp. 3863-8. doi: 10.4049/jimmunol.169.7.3863.
Shen, A. & Higgins, D. E. (2006). 'The MogR transcriptional repressor regulates nonhierarchal expression of flagellar motility genes and virulence in Listeria monocytogenes' *PLoS Pathog*, 2 (4), p. e30. doi: 10.1371/journal.ppat.0020030.
Silk, B. J., et al. (2012). 'Invasive listeriosis in the Foodborne Diseases Active Surveillance Network (FoodNet), 2004-2009: further targeted prevention needed for higher-risk groups' *Clin Infect Dis*, 54 Suppl 5 pp. S396-404. doi: 10.1093/cid/cis268.
Sirobhushanam, S., et al. (2017). 'Utilization of multiple substrates by butyrate kinase from Listeria monocytogenes' *Biochim Biophys Acta Mol Cell Biol Lipids*, 1862 (3), pp. 283-290. doi: 10.1016/j.bbalip.2016.12.001.
Sleator, R. D., et al. (2005). 'A PrfA-regulated bile exclusion system (BilE) is a novel virulence factor in Listeria monocytogenes' *Mol Microbiol*, 55 (4), pp. 1183-95. doi: 10.1111/j.1365-2958.2004.04454.x.
Smith, J. L., Liu, Y. & Paoli, G. C. (2013). 'How does Listeria monocytogenes combat acid conditions?' *Can J Microbiol*, 59 (3), pp. 141-52. doi: 10.1139/cjm-2012-0392.
Stapels, D. A. C., et al. (2018). 'Salmonella persisters undermine host immune defenses during antibiotic treatment' *Science*, 362 (6419), pp. 1156-1160. doi: 10.1126/science.aat7148.
Stasiewicz, M. J., Wiedmann, M. & Bergholz, T. M. (2011). 'The transcriptional response of Listeria monocytogenes during adaptation to growth on lactate and diacetate includes synergistic changes that increase fermentative acetoin production' *Appl Environ Microbiol*, 77 (15), pp. 5294-306. doi: 10.1128/AEM.02976-10.
Stavru, F., et al. (2013). 'Atypical mitochondrial fission upon bacterial infection' *Proc Natl Acad Sci U S A*, 110 (40), pp. 16003-8. doi: 10.1073/pnas.1315784110.
Suarez, M., et al. (2001). 'A role for ActA in epithelial cell invasion by Listeria monocytogenes' *Cell Microbiol*, 3 (12), pp. 853-64. doi: 10.1046/j.1462-5822.2001.00160.x.
Tattoli, I., et al. (2013). 'Listeria phospholipases subvert host autophagic defenses by stalling pre-autophagosomal structures' *EMBO J*, 32 (23), pp. 3066-78. doi: 10.1038/emboj.2013.234.
Thedieck, K., et al. (2006). 'The MprF protein is required for lysinylation of phospholipids in listerial membranes and confers resistance to cationic

antimicrobial peptides (CAMPs) on Listeria monocytogenes' *Mol Microbiol*, 62 (5), pp. 1325-39. doi: 10.1111/j.1365-2958.2006.05452.x.
Theriot, J. A., et al. (1994). 'Involvement of profilin in the actin-based motility of L. monocytogenes in cells and in cell-free extracts' *Cell*, 76 (3), pp. 505-17. doi: 10.1016/0092-8674(94)90114-7.
Tiensuu, T., et al. (2019). 'Flick of a switch: regulatory mechanisms allowing Listeria monocytogenes to transition from a saprophyte to a killer' *Microbiology (Reading)*, 165 (8), pp. 819-833. doi: 10.1099/mic.0.000808.
Toledo-Arana, A., et al. (2009). 'The Listeria transcriptional landscape from saprophytism to virulence' *Nature*, 459 (7249), pp. 950-6. doi: 10.1038/nature08080.
Travier, L., et al. (2013). 'ActA promotes Listeria monocytogenes aggregation, intestinal colonization and carriage' *PLoS Pathog*, 9 (1), p. e1003131. doi: 10.1371/journal.ppat.1003131.
Travier, L. & Lecuit, M. (2014). 'Listeria monocytogenes ActA: a new function for a 'classic' virulence factor' *Curr Opin Microbiol*, 17 pp. 53-60. doi: 10.1016/j.mib.2013.11.007.
Tripp, C. S., Wolf, S. F. & Unanue, E. R. (1993). 'Interleukin 12 and tumor necrosis factor alpha are costimulators of interferon gamma production by natural killer cells in severe combined immunodeficiency mice with listeriosis, and interleukin 10 is a physiologic antagonist' *Proc Natl Acad Sci U S A*, 90 (8), pp. 3725-9. doi: 10.1073/pnas.90.8.3725.
van der Veen, S. & Abee, T. (2010). 'Importance of SigB for Listeria monocytogenes static and continuous-flow biofilm formation and disinfectant resistance' *Appl Environ Microbiol*, 76 (23), pp. 7854-60. doi: 10.1128/AEM.01519-10.
Vazquez-Boland, J. A., Krypotou, E. & Scortti, M. (2017). 'Listeria Placental Infection' *mBio*, 8 (3). doi: 10.1128/mBio.00949-17.
Veiga, E. & Cossart, P. (2005). 'Listeria hijacks the clathrin-dependent endocytic machinery to invade mammalian cells' *Nat Cell Biol*, 7 (9), pp. 894-900. doi: 10.1038/ncb1292.
Veiga, E., et al. (2007). 'Invasive and adherent bacterial pathogens co-Opt host clathrin for infection' *Cell Host Microbe*, 2 (5), pp. 340-51. doi: 10.1016/j.chom.2007.10.001.
Vessey, C. J., et al. (1995). 'Altered expression and function of E-cadherin in cervical intraepithelial neoplasia and invasive squamous cell carcinoma' *J Pathol*, 176 (2), pp. 151-9. doi: 10.1002/path.1711760208.
Wampler, J. L., et al. (2004). 'Heat shock protein 60 acts as a receptor for the Listeria adhesion protein in Caco-2 cells' *Infect Immun*, 72 (2), pp. 931-6. doi: 10.1128/IAI.72.2.931-936.2004.
Wang, J., et al. (2015). 'Lamellipodin Is Important for Cell-to-Cell Spread and Actin-Based Motility in Listeria monocytogenes' *Infect Immun*, 83 (9), pp. 3740-8. doi: 10.1128/IAI.00193-15.
Wang, Y., et al. (2017). 'Structural insights into glutathione-mediated activation of the master regulator PrfA in Listeria monocytogenes' *Protein Cell*, 8 (4), pp. 308-312. doi: 10.1007/s13238-017-0390-x.
Weiglein, I., et al. (1997). 'Listeria monocytogenes infection of HeLa cells results in listeriolysin O-mediated transient activation of the Raf-MEK-MAP kinase

pathway' *FEMS Microbiol Lett*, 148 (2), pp. 189-95. doi: 10.1111/j.1574-6968.1997.tb10287.x.
Welch, M. D., Iwamatsu, A. & Mitchison, T. J. (1997). 'Actin polymerization is induced by Arp2/3 protein complex at the surface of Listeria monocytogenes' *Nature*, 385 (6613), pp. 265-9. doi: 10.1038/385265a0.
Whitfield, M. L., et al. (2002). 'Identification of genes periodically expressed in the human cell cycle and their expression in tumors' *Mol Biol Cell*, 13 (6), pp. 1977-2000. doi: 10.1091/mbc.02-02-0030.
Williams, J. R., Thayyullathil, C. & Freitag, N. E. (2000). 'Sequence variations within PrfA DNA binding sites and effects on Listeria monocytogenes virulence gene expression' *J Bacteriol*, 182 (3), pp. 837-41. doi: 10.1128/JB.182.3.837-841.2000.
Witte, C. E., et al. (2012). 'Innate immune pathways triggered by Listeria monocytogenes and their role in the induction of cell-mediated immunity' *Adv Immunol*, 113 pp. 135-56. doi: 10.1016/B978-0-12-394590-7.00002-6.
Witter, A. R., Okunnu, B. M. & Berg, R. E. (2016). 'The Essential Role of Neutrophils during Infection with the Intracellular Bacterial Pathogen Listeria monocytogenes' *J Immunol*, 197 (5), pp. 1557-65. doi: 10.4049/jimmunol.1600599.
Wollert, T., et al. (2007). 'Extending the host range of Listeria monocytogenes by rational protein design' *Cell*, 129 (5), pp. 891-902. doi: 10.1016/j.cell.2007.03.049.
Xiao, Q., et al. (2011). 'Sortase independent and dependent systems for acquisition of haem and haemoglobin in Listeria monocytogenes' *Mol Microbiol*, 80 (6), pp. 1581-97. doi: 10.1111/j.1365-2958.2011.07667.x.
Zenewicz, L. A. & Shen, H. (2007). 'Innate and adaptive immune responses to Listeria monocytogenes: a short overview' *Microbes Infect*, 9 (10), pp. 1208-15. doi: 10.1016/j.micinf.2007.05.008.
Zhang, T., Bae, D. & Wang, C. (2015). 'Listeriolysin O mediates cytotoxicity against human brain microvascular endothelial cells' *FEMS Microbiol Lett*, 362 (12), p. fnv084. doi: 10.1093/femsle/fnv084.

9. Appendix

9.1 Supplementary Videos

Supplementary videos are available on the University of Manchester's data sharing repository FigShare. Their unique Digital Object Identifiers (DOI) are shared here.

DOI: 10.48420/21217784

Supplementary Video 1. Formation of aggregates and upregulation of virulence genes. Representative confocal microscopy video of 3 biological replicates of HeLa cells infected with Lm-dsRed-*PactA*-GFP MOI=20 for 2 hours. Video show the formation of bacterial aggregates and upregulation of virulence gene expression as shown by increased GFP expression. Scale bar 5 µm.

DOI: 10.48420/21217796

Supplementary Video 2. Multiple bacteria may successfully invade the host cell from a single aggregate Representative confocal microscopy video of 3 biological replicates of HeLa cells infected with Lm-dsRed-*PactA*-GFP MOI=20 for 2 hours. Video shows an aggregate of 4 bacteria invading a HeLa cell and establishing a successful replicative invasion. Scale bar 10 µm

DOI: 10.48420/21217808

Supplementary Video 3. *L. monocytogenes* exposed to spent host cell media. x 10^7 Lm-dsRed-P*actA*-GFP was incubated for 2 hours at 37°C in spent media (bottom) (retrieved as described in Section 2.6.1). Representative video of 3 biological replicate experiment show upregulation of PrfA-regulated virulence genes via *PactA*-GFP (green) expression and the formation of aggregates occurs when exposed to spent media, but not fresh media. Scale bar 10 µm.

DOI: 10.48420/22010378

Supplementary Video 4. *L. monocytogenes* exposed to fresh media. 1.0 x 10^7 Lm-dsRed-P*actA*-GFP was incubated for 2 hours at 37°C in fresh media (bottom). Representative video of 3 biological replicate experiment show upregulation of PrfA-regulated virulence genes via *PactA*-GFP (green) expression but no aggregation occurs when exposed to fresh media. Scale bar 20 µm.